Oxidative status and genomic damage in an obesity model

Oxidativer Status und Genom-Schäden in einem Adipositas-Modell

Doctoral thesis for a doctoral degree

at the Graduate School of Life Sciences,

Julius-Maximilians-Universität Würzburg,

Section Biomedicine

submitted by

Ezgi Eylül Bankoglu

from Samsun, Turkey

Würzburg, 2016

Submitted on: _____

Members of the *Promotionskomitee*:

Chairperson:	Prof. Dr. Jörg Schultz
Primary Supervisor:	Prof. Dr. Helga Stopper
Supervisor (Second):	Prof. Dr. Tcholpon Djuzenova
Supervisor (Third):	Prof. Dr. Ute Hentschel Humeida
Supervisor (Fourth):	Prof. Dr. Jörg Vienken

Date of Public Defence: _____

Date of Receipt of Certificates: _____

Table of Contents

LIST OF ABBREVIATIONS

8-oxodG	8-hydroxydeoxyguanosine
8-oxoGua	8-hydroxyguanine
8-oxoGua	8-oxo-7, 8-dihydroguanine
8-oxoGuo	8-hydroxyguanosine
8-SH-G	8-mercaptoguanosine
A	adenine
ABC	avidin biotin complex
ADP	adenosine diphosphate
Akt	protein kinase B/PKB
ANOVA	analysis of variance
AS160	AKT substrate 160
ATP	adenosine triphosphate
BER	base excision repair
BMI	body mass index
BN	Binucleated
BPD-DS	biliopancreatic diversion with a duodenal switch
C	cytosin
CAT	catalase
CBMN	cytokinesis-block micronucleus
CBPI	cytokinesis block proliferation index
CE	collision energy
CR	caloric restriction
CXP	collision cell exit potential

DAB	diaminobenzidin
DABCO	diazobicyclo octane
DDR	DNA damage response
DHE	Dihydroethidium
DMEM	Dulbecco`s Modified Eagle Medium
DNA	deoxyribonucleic acid
DP	declustering potential
DSBs	double strand breaks
ETC	electron transport chain
FAD	Flavin adenine dinucleotide
FapyGua	2, 6-diamino-4-hydroxy-5-formamidopyrimidine
FBS	fetal bovine serum
FDA	fluorescein diacetate
FOXO1	forkhead box O1
FP	focusing potential
G	guanine
G6Pase	glucose-6-phosphatase
GB	gastric banding
GLUT4	glucosetransporter type 4
GPXs	glutathione peroxidase
GR	glutathione reductase
GSH	glutathione
GSK3β	glycogen synthase 3β
GYS1	glycogen synthase

HO-1	hemeoxygenase 1
HPLC	high performance liquid chromatography
HRP	horseradish peroxidase
HSP70	heat shock protein 70
IGF-1	insulin-like growth factor 1
IHH	immortalized human hepatocytes
IR	insulin receptor
IRS1/2	insulin receptor substrate ½
LC/MS/MS	liquid chromatography tandem mass spectrometry
LPO	lipid peroxidation
MDA	malondialdehyde
ME1	malic enzyme 1
MeOH	methanol
MN	micronucleus
MP	mobile phase
MRM	multiple reaction monitoring
mTORC1	mammalian target of rapamycin complex 1
mTORC1	the mammalian target of rapamycin complex 1
mTORC2	mammalian target of rapamycin complex 2
NAD	nicotinamoide adenine dinucleotide
NADPH oxidase	nicotinamide adenine dinucleotide phosphate-oxidase
NADPH	nicotinamide adenine dinucleotide phosphate oxidase
NAFLD	non-alcoholic fatty liver disease
NER	nucleotide excision repair

NOX	NADPH oxidase
OGTT	oral glucose tolerance test
PBS	phosphate buffered saline
PDK1	3-phosphoinositide-dependent protein kinase-1
PEPCK	phosphoenolpyruvate carboxykinase 1
PGC1α	peroxisome proliferator-activated receptor gamma coactivator 1α
PI3K	phosphoinositide-3-kinase
PIP2	phosphatidylinositol-4,5-biphosphate
PIP3	phosphatidylinositol-3,4,5-triphosphate
PKCλ/ζ	protein kinase Cλ/ζ
PP2A	protein phosphatase 2A
PPARγ	peroxisome proliferator-activatedreceptor g
Pten	phosphatase and tensin homolog
PTP1B	protein tyrosine kinase phosphatase non-receptor type 1
PTPs	protein tyrosine phosphatases
PVDF membrane	polyvinylidene difluoride membranes
RIPA	radio immune-precipitation assay
RNA	ribonucleic acid
ROS	reactive oxygen species
RYGB	Roux-en-Y gastric bypass
S6	ribosomal protein S6
S6K	ribosomal protein S6 kinase
SCD	stearoly-CoA desaturase
SDH	succinate dehydrogenase

SEM	standard error of the mean
SODs	superoxide dismutase
SREBP1-c	sterol regulatoryelement binding transcription factor 1
SSBs	single strand breaks
STAT3	signal transducer and activatorsof transcripton 3
T	thymine
T2DM	type 2 diabetes mellitus
TBA	thiobarbituric acid
TBARS	thiobarbituric acid reactive substances
TBS	tris buffered saline
TCA	tricarboxylic acid cycle
TRIB3	tribbles homologue 3
Tris	trishydroxymethylaminomethane
TSC1/2	tuberous sclerosis complex ½
ULK1	unc-51-like kinase 1
VSG	vertical sleeve gastrectomy
WAT	white adipose tissue
WHO	World Health Organization
γ-H2AX	phosphorylated histone 2AX

1 INTRODUCTION

1.1 Obesity and its prevalence

Obesity can be viewed as a disease with multiple risk factors that are due to the extreme fat accumulation [1]. In biological terms, obesity is the expansion of white adipose tissue (WAT) by hyperplasia and hypertrophy [2]. The accepted classification of obesity is generated according to body mass index (BMI), calculated as body weight (kg) divided by the square of body height (m) (**Table 1**) [1]. BMI measurement does not require any specialized equipment, therefore it is a widely accepted, easy and robust method to classify large populations [3].

Table 1: Classification of obesity according to WHO [4].

Classification	BMI (kg/ m^2)
Underweight	< 18.50
Normal range	18.50-24-99
Overweight	≥ 25.00
Pre-obese	25.00-29.99
Obese	≥ 30.00
Obese class I	30.00-34.99
Obese class II	35.00-39.99
Obese class III	≥ 40.00

Obesity has become a global challenge and one of the most concerning health problems of the future [5]. According to WHO data, more than 1.9 billion adults (18 years and older) were overweight in 2014 and of these, over 600 million were obese [6]. **Figure 1** and **Figure 2** show the global prevalence of obesity.

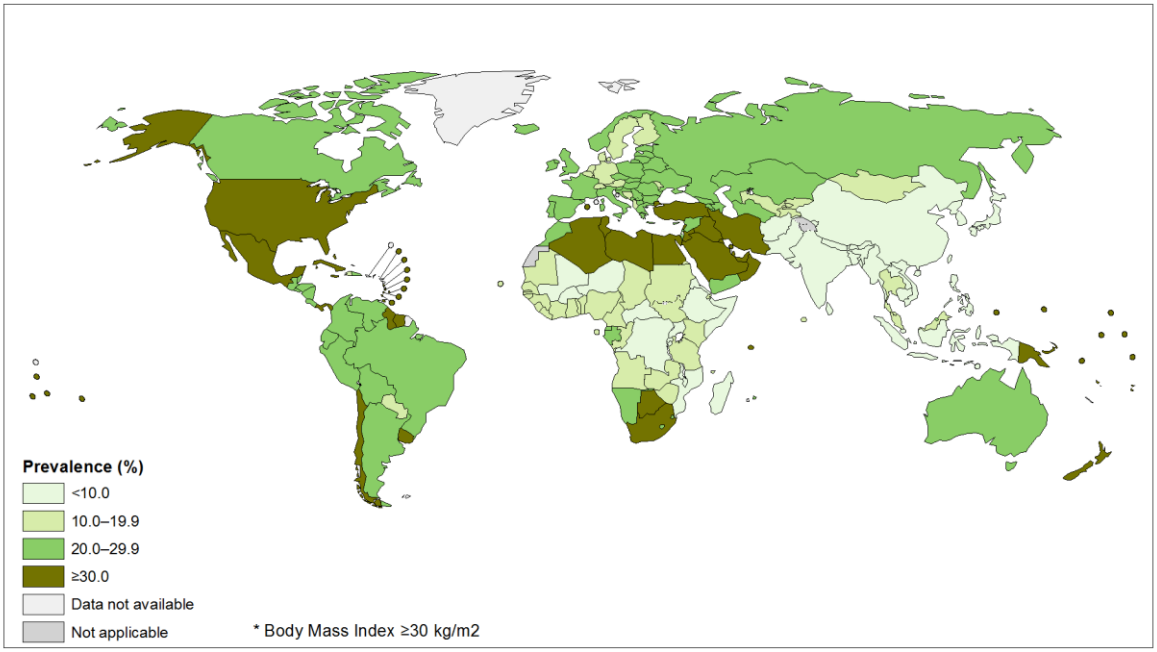

Figure 1: Global prevalence of obesity among females above 18 years old in 2014 (reprinted from WHO with permission) [7].

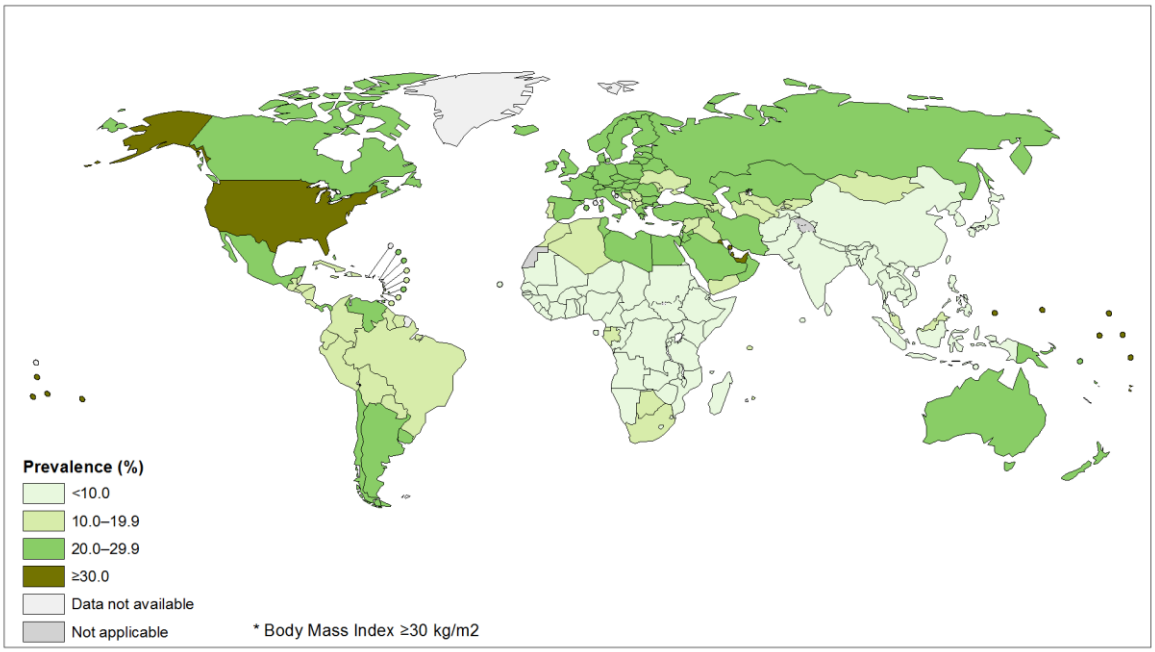

Figure 2: Global prevalence of obesity among males above the 18 years old in 2014 (reprinted from WHO with permission) [8].

Obesity is not only a threat for adults, but also for children. The 2013 WHO report showed that 42 million children under the age of 5 were overweight or obese worldwide [6]. Obesity leads to an increased incidence of several chronic diseases such as hypertension, type 2 diabetes mellitus (T2DM), heart disease, non-alcoholic fatty liver disease, certain forms of cancer and other health problems, which overall results in increased mortality [1]. The rising prevalence of obesity among children causes a dramatic increase in obesity related diseases and premature mortality in early adulthood [9, 10].

Obesity is an important risk factor for many related disease; however, T2DM may be nominated as the most deleterious one [11]. Obese people have a 7 times higher risk of T2DM than normal weight people [12] and among the people with T2DM 80% are overweight or obese [13]. Co-occurrence of obesity and T2DM might further increase the related health problems such as cardiovascular disease, hypertension and non-alcoholic fatty liver disease.

1.2 Oxidative stress and genomic damage in obesity

It has been shown that obesity is associated with profound metabolic and metabonomic changes but is also linked with elevated oxidative stress, which is defined as an imbalance between the generation of reactive oxygen species (ROS) and antioxidant reactions. Oxidative stress shows association with insulin resistance, hyperinsulinemia, high blood pressure and inflammation, which are some of the many risk factors related to obesity [14]. Some of the important endogenous ROS sources are NADPH oxidase, mitochondria, endoplasmic reticulum, xanthine oxidase and cytochrome P450s [15, 16]. The NADPH oxidase and mitochondria are discussed further in detail in section 1.3, since they are the most important known endogenous ROS sources.

Under normal physiological conditions, ROS have an important role in the regulation of physiological functions by activating signaling pathways. Antioxidant defense systems such as glutathione (GSH), glutathione peroxidase (GPXs), glutathione reductase, catalase (CAT), superoxide dismutase (SODs) and heme oxygenase-1 help to preserve redox homeostasis [17, 18]. In the context of obesity, elevated ROS production could be explained by mitochondrial dysfunction, reduced antioxidant capacity, enhanced NADPH oxidase

activity, and chronic inflammation [16, 17, 19]. The antioxidant defense mechanisms may be overwhelmed and remaining ROS may attack cellular macromolecules such as proteins and DNA, in the latter case leading to mutations and genomic instability.

Oxidative DNA damage has been suggested as a main player in carcinogenesis [20]. Some studies showed that ROS could contribute to the initiation or progression of cancer either by direct oxidation of macromolecules or by over-activation of signaling pathways, which could alter the expression of proliferation-associated genes or tumor suppressor [21-23]. Petros et al., [24] showed that increased ROS production due to mtDNA mutations contribute to prostate cancer. Vincent et al., [25], showed the vulnerability of obese older women compared to the non-obese individuals in an exercise associated oxidative challenge. Oxidized purines and pyrimidines, single strand breaks (SSBs) and double strand breaks (DSBs) are common types of DNA damages, which are caused by reactive oxygen species (ROS). Of these, 8-oxo-7,8-dihydroguanine (8-oxoGua) and 2, 6-diamino-4-hydroxy-5-formamidopyrimidine (FapyGua) are derived from reaction of guanine with the hydroxyl radical [26]. The oxidized guanine base is an important link between oxidative stress and DNA damage. Among the many DNA oxidation products, the modified guanine base is one of the most investigated. Another reason for the focused attention on the modified guanine base is that it has mutagenic potential. Oxidative modifications of the guanine base may cause loss of its base pairing specificity and lead to GC to AT transversion in case of inefficient repair [27]. The FapydG formation increases the conformational flexibility compared to the original guanine base and this may reduce the genomic stability of DNA [28]. Al-Aubaidy et al. [29] showed a positive correlation between serum 8-oxodG and BMI.

1.3 Endogenous reactive oxygen species (ROS) sources

Here, the possible endogenous sources of reactive oxygen species (ROS) are briefly discussed. Mitochondria and NADPH oxidase enzyme family were the focus of our work, since they are the major contributors to cellular ROS formation. There are also many other enzymes and organelles that contribute cellular ROS production beside mitochondria and NADPH oxidase enzyme family. These possible contributors are xanthine oxidase, nitric oxide synthase, cyclooxygenase, lipoxygenase and cytochrome P450 enzymes. Besides, peroxisome and the endoplasmic reticulum are organelles, which can produce ROS [30].

1.3.1 Mitochondria

It is assumed that approximately 2 billion years ago the mitochondrion was enveloped by an archezoan cell and formed the first eukaryote. ATP generation by oxidative phosphorylation was a benefit for the host and besides the protected environment inside the cell a nutrient rich environment was a positive side for the mitochondrion. This symbiotic relationship succeeded and has developed into a more complex interrelationship. Mitochondria take part in the biosynthesis of haem and iron-sulphur centers, regulation of cytosolic calcium ions, genesis of substrate for lipid and protein synthesis, and facilitation of cellular stress responses (response to hypoxia and activation of programmed cell death) [31].

Mitochondria play a key role in energy metabolism. ATP generation is based on electron transfer through the electron transfer chain (ETC), which belongs to the respiratory chain complex I-IV, from oxygen down to water. Tricarboxylic acid cycle (TCA) enzymes form the electron carriers NADH and FADH2, which are energy rich molecules that donate an electron to the ETC during ATP production. The respiratory chain complex machinery pumps protons from mitochondrial matrix to the intermembrane space [32].

Complex I (NADH dehydrogenase) is the largest molecule of the mitochondrial respiratory complexes. Complex I is responsible for the transfer of electrons from NADH to coenzyme Q. Complex II (succinate dehydrogenase, SDH) are placed in the inner membrane facing to the mitochondrial matrix. Complex II regulates the oxidation of succinate to fumarate, enables the reduction of the FAD cofactor and passes the electrons to ubiquinone. Complex III (ubiquinol cytochrome c reductase) is localized in the mitochondrial inner membrane and transfers the electrons from reduced coenzyme Q to cytochrome c. Complex IV (cytochrome c oxidase) is engaged with the transfer of the protons from the matrix to the innermembrane space. In complex IV, the electrons are removed from cytochrome c and transferred to molecular oxygen [33]. The proton motive force, which is generated by a proton gradient trough the ETC, gives rise to ADP phosphorylation via ATP synthase (ATPase-complex V) [34]. The ETC from mitochondria can be seen in **Figure 3**.

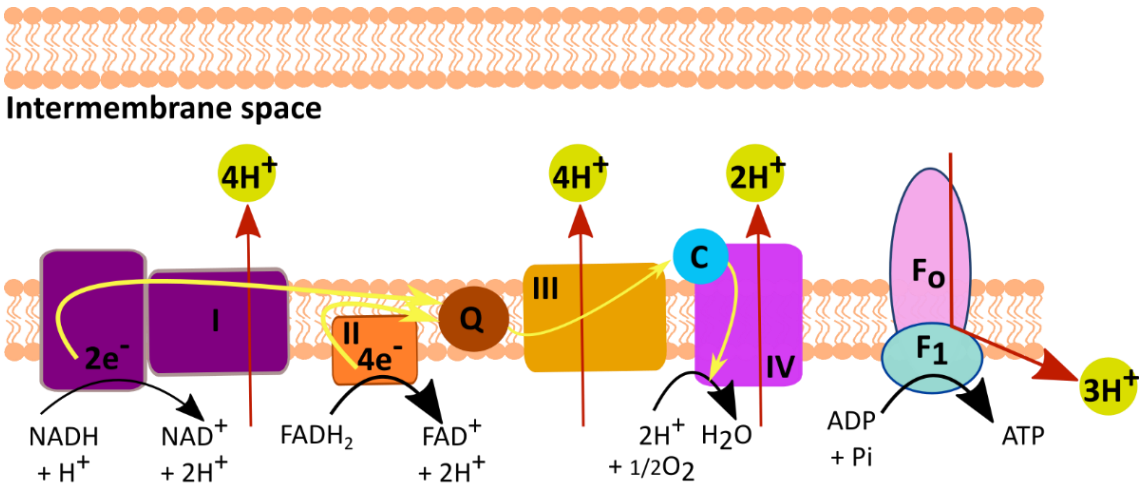

Figure 3: Electron transfer chain (ETC) of mitochondria. Complex I transfers electrons from electron carrier nicotinamide adenine di nucleotide (NADH) to coenzyme Q. Coenzyme Q accepts also electrons from complex II and transfers all electrons to complex III and cytochrome c. Cytochrome c sends electrons to complex IV, which reduces molecular oxygen to water. This proton gradient helps to ATP synthase to produce ATP from ADP. Modified from [35].

Mitochondria generate roughly 90% of the total ROS in the cell and the mitochondrial electron transport chain is the central source of ROS formation. This fact makes the mitochondria also a primary target for oxidative stress. A small percent of electrons (prematurely reduced oxygen, which forms ROS) leaks from ETC regardless of the efficiency of the oxidative phosphorylation process in the mitochondria [32]. Under normal condition, the antioxidant machinery can eliminate the ROS and protect the cell. However, ROS scavenging may be unsuccessful under overwhelming conditions.

Depending on where ROS form, they can reach different cellular compartments. If the ROS generation takes place at the inner mitochondrial membrane, the strong electric field in the membrane drives the ROS to the intermembrane space. ROS generation from prosthetic groups of matrix-oriented subunits can reach to the matrix compartment. The antioxidant systems in matrix can neutralize the ROS. However, high levels of ROS can escape from the matrix to the intermembrane space and cytosol. The ROS in the intermembrane space and cytosol can lead to oxidative damage and take part in redox signaling. The mitochondrial DNA (mtDNA) can become a target for mitochondrial ROS generated in the matrix [31]. Mitochondrial DNA is necessary for coding of several

components from the mitochondrial respiratory complexes and mutation in mtDNA can cause mitochondrial dysfunction and disease. Besides, mutations in mtDNA are associated with different pathologies like diabetes, neurodegenerative disease, cardiovascular disease and cancer [36].

Mitochondrial ROS can attack nuclear DNA as well. Samper et al., [37], demonstrated elevated double strand breaks and chromosomal translocation in mitochondrial superoxide dismutase deficient primary mouse embryonic fibroblasts. Even though excessive ROS formation can cause damage, a moderate amount of mitochondrial ROS is important for signaling and protein function.

During active ATP production in mitochondria, electron carriers are oxidized, the proton motive force is low and the respiration rate is high. Under these conditions, mitochondrial superoxide production rate is low [38]. In contrast, the resting mitochondrial state is associated with low ATP demand, low respiration rate and high proton motive force due to the reduction of ETC components. The resting state of mitochondria produces higher superoxide than the active state [39]. Superoxide itself is particularly reactive and cannot pass through membranes. However, superoxide is rapidly converted to the H_2O_2 in mitochondria and H_2O_2 can pass through the membranes and diffuse to the cell cytosol [40].

The modern world offers us plenty of food and demands limited physical activity. As a result, the development of obesity, metabolic syndrome and related disease is rising. Since mitochondria have a central role in energy metabolism, mitochondria become a possible therapeutic target and origin for obesity and metabolic syndrome [40].

1.3.2 NADPH oxidase (NOX) enzyme family

Until the discovery of the NADPH oxidase enzyme complex, which produces ROS as its primary function, ROS formation was thought to be coincidental and undesirable in cells [41]. The NADPH oxidase was originally found in phagocytes and it became known with its host defense role. However, in recent years non-phagocytic NADPH oxidase enzymes are found in different cells such as fibroblasts, vascular smooth muscle cells and renal tubular cells [42]. This enzyme family is known as NOX enzymes as well. The NOX family has 7

isoform: NOX1, NOX2, NOX3, NOX4, NOX5, DUOX1 and DUOX2. These isoforms have slightly different physiological functions according to their distribution in tissues. For example, NOX1 is mainly expressed in colon tissue and NOX4 is in kidney and vascular cells [43]. When the NADPH oxidase enzyme complex is inactive (in resting cells), its components are distributed between cytosol and membranes. The $gp91^{phox}$ and $p22^{phox}$ subunits are localized in the plasma membrane and together build up the flavocytochrome b_{558}. The cytosolic components of NADPH oxidase are $p47^{phox}$, $p67^{phox}$, $p40^{phox}$ and Rac1/2. For the ROS production by NADPH oxidase, clustering of all components is essential. The activation of the NADPH enzyme complex can take place by stimulation through various factors, which triggers the phosphorylation of cytosolic components and their translocation to the plasma membrane to interact with flavocytochrome b_{558} [44]. A representative scheme of NADPH oxidase can be seen in **Figure 4**.

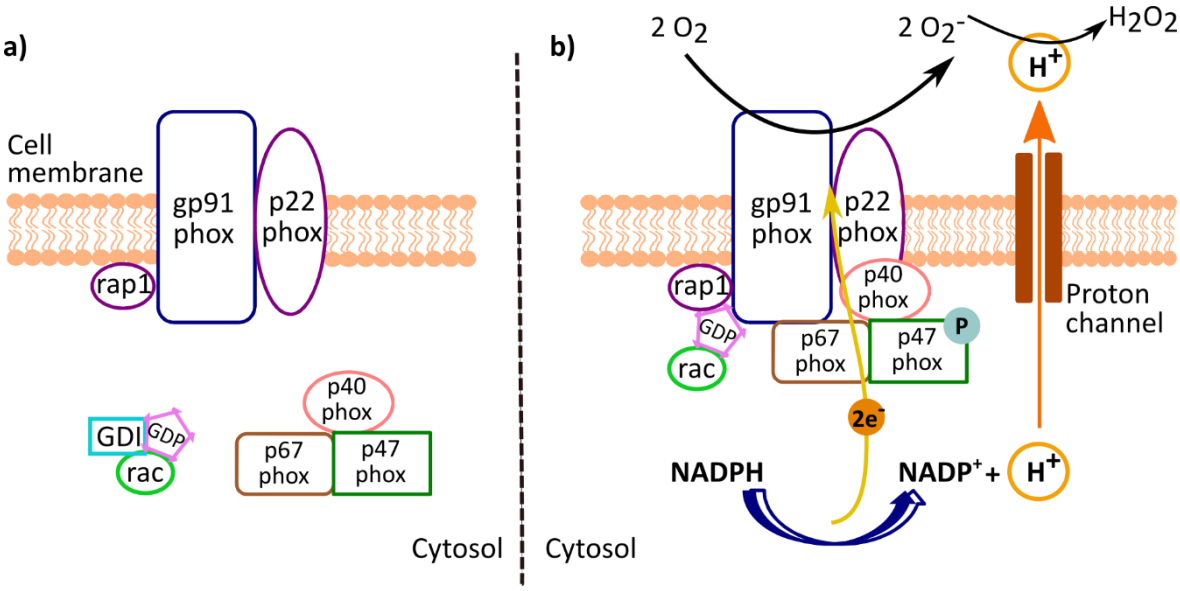

Figure 4: Representation of the NADPH oxidase enzyme. **a)** NADPH oxidase in resting form and **b)** NADPH oxidase in active form. The activation of NADPH oxidase enzyme is accomplished by translocation of cytosolic subunits p40phox, p47phox, p67phox and Rac to the membrane in order to form a complex with flavocytochrome b558 (consisting of gp91phox and p22phox), the membrane subunit. Modified after www.caymanchem.com/app/template/Article.vm/article/2126/figure/1.

Though the activation mechanism for NOX1, NOX2 and NOX3 is similar, the rest of NOX isoforms have different mechanisms. NOX4 can be active in cells that do not express cytoplasmic subunits. NOX4 activation might be regulated at the mRNA level [45]. NOX5, DUOX1 and DUOX2 are regulated by Ca^{2+} levels [43].

NOX enzyme- derived ROS contribute various physiological function like host defense, regulation of cell signaling (inhibition of phosphatases, activation of kinases and regulation of ion channels) and regulation of cell growth etc. NOX enzymes are widely expressed in many tissues [46]. Besides the contribution in many physiological functions, hyperactivity of NOX enzyme family members might contribute to the pathology of many diseases by impairment of redox sensitive signaling pathways. Since there are some evidences about the role of oxidative stress in insulin resistance, steatosis, fibrosis and obesity etc., the relevance of hyperactivation of NOX enzymes is considered in the progression of NAFLD, metabolic syndrome and obesity [44].

It has been suggested that insulin induced ROS play an important role in the insulin-signaling cascade as second messenger. However, among the signaling enzymes the protein-tyrosine phosphatase (PTPs) have themselves found to be sensitive to inhibition by oxidation (other signaling regulators might be sensitive too!). Additionally to PTPs, there are many other potential enzymes (such as MAP kinase and Pten), which are susceptible to ROS induced inhibition. NOX4 has been suggested as potential source for insulin-stimulated ROS generation. Besides in the kidney tissue, NOX4 is dominantly expressed in insulin sensitive tissues like liver, muscle and adipose [47]. Mahadev et al., [48], demonstrated the role of NOX4 generated ROS production in insulin signaling by adenovirus mediated NOX4 deletion in 3T3-L1 adipocyte cells. Their data proved that a reduced amount of ROS formation (due to NOX4 deletion) caused mitigated phosphorylation of insulin receptor (IR), insulin receptor substrate-1 (IRS-1), downstream mediator of insulin signaling and glucose uptake. Upregulation of NOX2 and increased NOX4 mRNA expression has been reported in diabetic nephropathy. Though it is not clear yet which NOX isoform has the main role, it has been accepted that NOX has a role in diabetic nephropathy [46].

The findings in literature suggested an association between insulin resistance and NOX4. However, the role of different NOX isoforms and regulatory components have not been well described as well as the possible contribution of NADPH enzymes in metabolism.

It is still an interesting question whether elements of the NADPH enzyme family might be a target for possible pharmaceutical therapy.

1.4 Obesity and cancer incidence

Obesity has been identified as cancer risk factor by the World Cancer Research Fund and American Institute for Cancer Research [49]. According to some epidemiological studies, overweight and obese individuals are at an increased risk for developing certain forms of cancer, especially of the colon, kidney, liver, breast, endometrium, thyroid and pancreas [50-52]. The risk ratio of some of the cancer types in obesity can be found in **Table 2**.

Table 2: Cancer risk ratio per 5 kg/ m^2 BMI in men and women [53].

Cancer Type	Risk Ratio for Men (95% CI)	Risk Ratio for Women (95% CI)
Esophageal adenocarcinoma	1.52 (1.33 - 1.74)	1.51 (1.31 - 1.74)
Thyroid	1.33 (1.04 - 1.70)	1.14 (1.06 - 1.23)
Colon	1.24 (1.20 - 1.28)	1.09 (1.05 - 1.13)
Renal	1.24 (1.15 - 1.34)	1.34 (1.25 - 1.43)
Liver	1.24 (0.95 - 1.63)	1.07 (0.55 - 2.08)
Rectum	1.09 (1.06 - 1.12)	1.02 (1.00 - 1.05)
Gallbladder	1.09 (0.99 - 1.21)	1.59 (1.02 - 2.47)
Pancreas	1.07 (0.93 - 1.23)	1.12 (1.02 - 1.22)
Prostate	1.03 (1.00 - 1.07)	–
Endometrium	–	1.59 (1.50 - 1.68)

Obesity is not just a risk factor for various cancers, but also a reason for weak response to possible therapies (chemo and radiotherapy) [53]. The finding from Incio et al., [54], demonstrated in a diet-induced obese mouse breast cancer model that resistance to anti-VEGF therapy develops under obesity.

There are several proposed mechanisms by which obesity may be linked to cancer development, including fat tissue alterations, chronic inflammation, hyperinsulinemia (elevated insulin and IGF) and oxidative stress [2, 50, 55, 56].

Adipose tissue is an endocrine organ and secretes adipokines, which have an important role in metabolism. Among them, leptin and adiponectin are known for their involvement in cancer [55, 57]. WAT includes different cell types such as fibroblasts, pre-adipocytes, mature adipocytes and macrophages. According to the location of WAT (visceral or subcutaneous) the amount of the different cell types may differ [19]. In the case of obesity, there is a reduction in maturation of pre-adipocytes which results in increased circulating proinflammatory cytokines [57]. Together with elevated insulin and IGF-1, the adipokines and proinflammatory factors induce activation of several signaling pathways like PI3K/Akt, MAPK and STAT3 (**Figure 5**) [58]. Activation of mitogen-activated protein kinase (MAPK) regulates cell proliferation, differentiation, apoptosis, mitosis, gene expressions and metabolism [59]. STAT3 takes part in the regulation of several physiological factors such as development, proliferation and metabolism. Additionally, STAT3 is mainly phosphorylated in neoplastic cells [60].

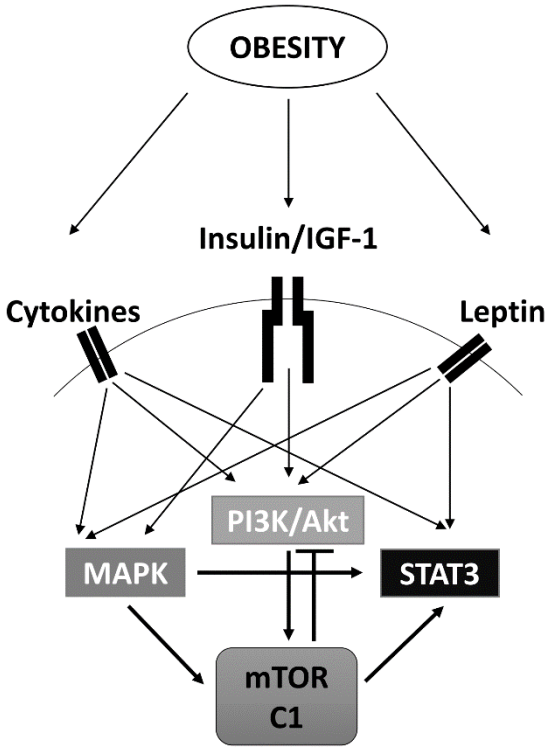

Figure 5: Possible signaling pathways, which can be altered in obesity (modified from [58]).

Insulin and IGFs have regulatory roles, which is relevant at the whole organism level and this increases the importance of both peptides in cancer [61]. Elevated insulin can bind to the insulin receptor as well as to the insulin like growth factor-1 (IGF-1) receptor and lead to the activation of PI3K/Akt and mitogen-activated protein kinase (MAPK) pathways [62]. Additionally, the Akt pathway causes the activation of mTOR C1 that promotes protein translation and contributes to the growth of many sporadic cancers [63].

1.5 Insulin signaling and type 2 diabetes mellitus (T2DM)

During evolution, due to limited food sources, the caloric demand was one of the biggest problem for organisms and they developed dietary energy storage together with insulin signaling 600 million years ago. However, humans have altered the environment, developed technology and have achieved a high caloric supply, which is readily available at least in industrialized countries. This gave rise to metabolic problems, which puts the insulin signaling in the center of attention [64]. T2DM is often associated with obesity and since both, T2DM as well as obesity have reached epidemic dimensions, it became

important to understand insulin signaling and to investigate the relations between chronic diseases and insulin resistance [65].

Insulin is a peptide hormone, which is secreted by Beta cells of the pancreas and which sustains glucose homeostasis, carbohydrate, lipid and protein metabolism, and tissue growth and development [65, 66]. Insulin stimulates PI3K/Akt signaling, which is necessary for regulation of insulin dependent systemic and cellular metabolism. PI3K/Akt signaling activation takes place following to IR to IRS1/2 binding, which activates PI3K. Activated PI3K leads to the phosphorylation of phosphatidylinositol-3,4,5-biphosphate (PIP2) to phosphatidylinositol,-3,4,5- triphosphate (PIP3) at plasma membrane and generates the activation and translocation of Akt by PIP3 promoted upstream kinases like 3-phophoinositide-dependent protein kinase-1 (PDK1) and mammalian target of rapamycin complex 2 (mTORC2). PDK1 and mTORC2 lead to activation of Akt by phophorylation on threonine 308 in the catalytic domain and serine 473 in the regulatory domain. The activation of Akt facilitates its translocation from plasma membrane to cellular compartments (cytoplasm, mitochondria and nucleus) and stimulates the phosphorylation of its downstream substrates, which play roles in the regulation of metabolism [67-69]. Insulin stimulated changes in PI3K/Akt signaling pathway can be seen in **Figure 6**.

Malfunction of the insulin action in skeletal muscle, liver and adipose tissue may cause systemic insulin resistance. This is defined as a situation in which the response to insulin is reduced or below the normal range or lost [70].

In skeletal muscle, insulin resistance means a decrease in glucose transport and a decline in muscle glycogen synthesis. In liver, insulin resistance results in failure of gluconeogenesis suppression, but stimulates fatty acid synthesis. Adipose tissue shows altered glucose transport (insulin stimulated) and lipolysis [71]. Insulin resistance is a good marker to predict the possible future risk of T2DM for an individual [72]. Though obesity provokes peripheral insulin resistance, not all insulin signaling is diminished. For example, in liver tissue the gluconeogenic pathway becomes insulin resistant, however insulin dependent lipogenesis stays sensitive [73].

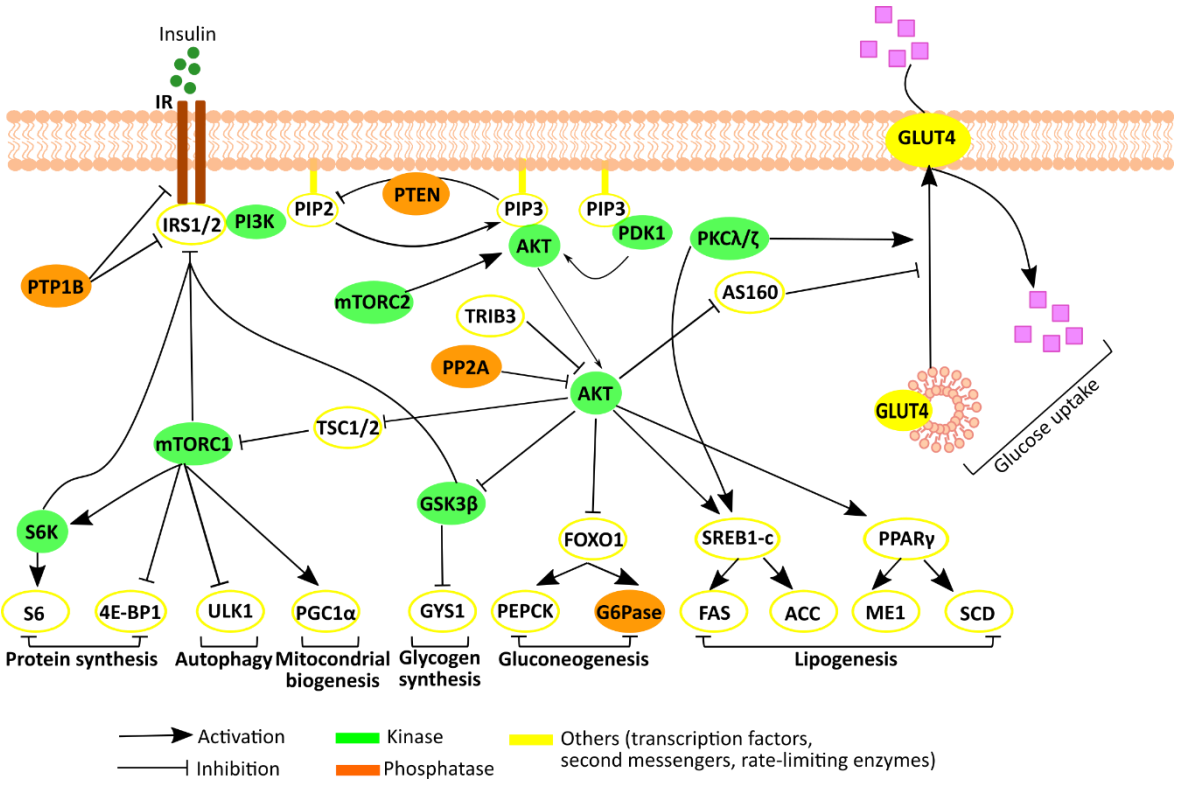

Figure 6: Insulin stimulated PI3K/Akt signaling and related downstream substrates. Abbreviations: Forkhead box O1, FOXO1; glucose-6-phosphatase, G6Pase; glycogen synthase kinase 3β, GSK3β; glycogen synthase, GYS1; insulin receptor, IR; insulin receptor substrates 1/2, IRS1/2; malic enzyme 1, ME1; mammalian target of rapamycin complex 1, mTORC1; mammalian target of rapamycin complex 2, mTORC2; 3-phosphoinositide-dependent protein kinase-1, PDK1; peroxisome proliferator-activated receptor gamma coactivator 1α, PGC1α; phosphoinositide-3-kinase, PI3K; protein kinase B, Akt; phosphatidylinositol-4,5-biphosphate, PIP2; phosphatidylinositol-3,4,5-triphosphate, PIP3; phosphoenolpyruvate carboxykinase 1, PEPCK; protein kinase Cλ/ζ, PKCλ/ζ; peroxisome proliferator-activatedreceptor g, PPARγ; protein phosphatase 2A, PP2A; protein tyrosine kinase phosphatase non-receptor type 1, PTP1B; ribosomal protein S6, S6; stearoly-CoA desaturase, SCD; ribosomal protein S6 kinase, S6K; glucosetransporter type 4, GLUT4; sterol regulatoryelement binding transcription factor 1, SREBP1-c; AKT substrate 160, AS160; tribbles homologue 3, TRIB3; tuberous sclerosis complex 1/2, TSC1/2; unc-51-like kinase 1, ULK1. Modified from [68].

Other tissues, which may not adapt to the increased insulin output by the pancreas under this condition, may be harmed. Alterations in insulin signaling might be caused by oxidative stress and adipose tissue modifications, - or - the altered insulin signaling might itself be the reason for oxidative stress and adipose tissue modifications. The link between oxidative

stress, insulin signaling and adipose tissue is like the chicken-egg situation. Any kind of modification might cause the induction of a vicious cycle.

1.6 DNA damage and cancer

DNA carries the genetic information, which is essential for life. Several lesions can accumulate in the DNA over time and maintaining the integrity of DNA is important to sustain cellular functions [74].

DNA integrity can be insulted by exogenous sources (such as ionizing radiation, various chemicals) and endogenous sources (such as reactive oxygen and nitrogen species, lipid peroxidation products due to cellular metabolism). DNA bases are susceptible to chemical modifications that end up with various lesions. Reactive oxygen and nitrogen species alone may lead to 70 or more different oxidative base and sugar modifications [74, 75].

DNA damage can manifest itself as base modification or strand breaks (single or double). During DNA replication, modified bases may be repaired and are then no damage will be inherited to the next generation. However, if such an unrepaired modification succeeds to be passed on to daughter cells, it may lead to permanent differences in the genetic information, manifesting as mutations or chromosomal aberrations [74, 76].

The outcome of DNA damage is variable according to the type of the lesion. Lesions might be mutagenic, cytotoxic or cytostatic. In the first place, DNA damage may induce the cellular DNA damage response (DDR) machinery and trigger a cell cycle arrest, which can result in cell death or senescence. In the long term, because of the irreversibility of mutations, DNA damage contributes to carcinogenesis [77]. For example, 8-oxoguanine is one of the most investigated oxidative mutagenic lesion, which can lead to GC→TA transversion during DNA replication [74].

Mutation is involved in the loss of tumor-suppressor genes or the activation of oncogenes, contributing to transformation of a cell into a cancer cell. All cancers are characterized by genomic instability, which is mostly detectable as modifications in chromosome number and structure, and/or DNA nucleotide insertion or deletion [74, 78]. For example, Ras activation by either overexpression or by mutation is a common share in various human

cancer. Ras oncogene activation leads to increase in ROS production and Ras oncogenic signal is known for its influence of cell survival regulators like PI3K/Akt. Another example is *c-Myc* protooncogene. *c-Myc* activation causes increase in H_2O_2 generation and DNA double strand breaks. These kind of changes might help to the adaptation process and transformation to malignant cell [79].

DDR is closely related to cell-cycle checkpoints and the chromosome segregation machinery to assure that only intact correct DNA material is transferred to next generation cells. There are known examples which indicate that altered DDR function is linked to neoplastic lesions [78]. The activation and inactivation of DDR are found in sporadic cancers such as colon, kidney, pancreatic and prostate. For example, elevated expression of Chk1 was found in liver and colorectal cancers, increased phosphorylation of Chk2 was observed in colon and lung cancers. Moreover, in lung, colon and kidney cancers inactivation of ATM in DDR was demonstrated and inactivation of p53 was demonstrated in many solid tumors [80]. Gorgoulis et al., [81], analysed precancerous and cancer lesions and determine the activation of DDR and genomic instability. Their findings suggested that elevation in cell proliferation leads to DNA replication stress and this stress activates DDR. Tort et al., [82], investigated the DDR in human tumorigenesis and showed the correlation between DDR activation and cyclin E elevation.

Besides, they found greater DDR activation in the colorectal adenomas with a higher risk of malignancy (with grade 3) and only moderate or no DDR activation in colorectal adenomas with grade 1 and 2.

Activated DDR response in precancerous lesions might restrict the progression, contribute long latency or prevent early lesions to turn into malignant lesions. In this respect, it is possible to refer to DDR as tumor-suppressor. However, long-term selective pressure can lead to the inactivation of several DDR factors and can allow the cells to escape from senescence or apoptosis. Furthermore, the cells might end up in a tumor [81, 83, 84]. Overall, genetic stability and cancer development are strongly associated with the involvement of DNA repair and of the overall quality of cellular DDR.

There are other sources as well that contribute to DNA damage and DDR activation in early stages of cancer development. One of them is elevated ROS formation, which can react either directly or through stimulation of various signaling pathways. ROS are important signaling molecules for cellular proliferation too and can contribute DNA replication stress by stimulating the proliferation [75].

1.7 Impact of weight change in cancer

Human studies and animal experiments showed that quality and the quantity of the diet has a great impact on health status and cancer progression [52]. Increased caloric consumption might have an impact on the genes engaged with DNA repair, cell proliferation, differentiation and apoptosis by the modification of hormones and growth factors [85]. Reduced caloric intake has been known to lower cancer incidence and increase longevity in rodents [86]. The correlation between weight and tumor development from epidemiological studies suggests that cancer is a preventable disease and diet is one of the contributing factor [85]. Many different rodent studies proved that caloric restriction can lower the tumor incidence and increase the life span. All these studies showed anti-aging and anti-tumor activity of caloric restriction (CR). Qiu et al., [87], demonstrated the ability of CR to reduce oxidative stress. Since elevated ROS are able to damage the cellular macromolecules and lead to the accumulation of cellular damage, oxidative stress may increase the risk of tumorigenesis. The anti-tumor effect of CR might be partly due to its anti-oxidative outcome.

Another suggested anti-tumor mechanism of CR is the IGF-1. It is known that elevated IGF-1 involved increased cancer risk including colon cancer. Some rodent studies proved that CR regulates the IGF-1 level.

Beside the regulation of oxidative stress, DNA damage and metabolic pathways, the regulation of oncogenes and tumor suppressors might be other mechanism for anti-tumor activity of CR. [85]. Different studies showed that CR modulate the expression of oncogenes and tumor suppressors by regulating DNA methylation and/or histone modification [85, 88].

Though there are many rodent studies, CR in humans has not been well defined. The situation in humans is much more complex and not as easily applicable as in rodent studies. There are some observational studies that show positive effects of CR in humans. One of them is about the Okinawa community who has a traditionally lower caloric diet. Willcox et al., [89], demonstrated that various cancer types such as lymphoma, prostate, breast and colon are lower among the Okinawan population than among age-matched Japanese and Americans. However, it is not thoroughly understood whether caloric restriction and weight loss may help to reduce the damage, which has been already done. There are still lots of open questions to answer such as the mechanism under lying CR and reduction of cancer risk, how much of the effect is coming from insulin and IGF-1, whether the cancer risk is only related to proliferation induction or other mechanisms are relevant too and at last what is the role of genomic damage.

1.8 Bariatric surgery as therapeutic option for weight control and obesity related diseases

Since we are living in an obesogenic environment, increasing the awareness and addressing obesity as a disease is important to solve the problem [90]. Achieving weight loss is essential to prevent related diseases, pre-mature mortality and to reduce the healthcare costs. There are non-surgical treatment options and bariatric surgery techniques.

Non-surgical treatments aim towards a reduction of energy intake and an increase of physical activity in combination with pharmacotherapy [91]. However, it is known that life style modifications on an individual level are very difficult and in most cases, those who did succeed to lost weight, will regain it over time [92]. The National Institute of Health stated that bariatric surgery might be a choice for severely obese adults with a BMI over 40 or over 35 and suffering from obesity related health problem (T2DM, heart disease and sleep apnea) [93].

Conventional therapies like diet, sports and pharmacological supplements are not efficient in the long term, notably for morbid obesity [94]. In severely obese individuals who are not able to reduce their weight by conventional options, bariatric surgery has become the therapeutic option of choice [95]. Bariatric surgery helps to reduce weight and to maintain

this reduction by the combination of restrictive and malabsorptive aspects. There are various different surgical procedures, of which gastric banding (GB), vertical sleeve gastrectomy (VSG), biliopancreatic diversion with a duodenal switch (BPD-DS) and gastric bypass (Roux-en-Y) are the most often applied ones [96]. Due to its positive impact on metabolic disorders such as insulin resistance, bariatric surgery is now sometimes even called metabolic surgery [97, 98].

1.8.1 Gastric banding

Gastric banding works with restrictive principles. There is an adjustable form of this procedure, which gives the possibility to change the diameter of the gastric band noninvasively by the help of a subcutaneous reservoir that can be enlarged or shrunk with a saline injection [99-101]. Mortality rate is low, reversibility of the surgery is easy and it is less invasive compared to other methods [90]. Weight loss with gastric banding has been reported as less persistent compared to the other methods [99].

1.8.2 Vertical sleeve gastrectomy

In vertical sleeve gastrectomy (VSG), a gastric sleeve, which continues with the esophagus and duodenum, is constructed by removing 80% of the stomach. In VSG, the restriction of food intake by artificial construction of the stomach supplies the weight loss [102].

The reduction of stomach volume may lower the ghrelin amount and has an impact on appetite [93]. VSG helps to achieve weight loss and to improve glucose tolerance [103]. In spite of the successful weight loss, many patients regain a significant amount of their weight back in the long term [100].

1.8.3 Biliopancreatic diversion with a duodenal switch

Biliopancreatic diversion with a duodenal switch (BPD-DS) is a combination of removing the big part of the stomach and altering the absorption and bile flow. BPD-DS modifies the route of the food through the upper small bowel [104]. A constructed gastric sleeve, which helps to reduce food intake, is linked directly to the lower part of the intestine to reduce the absorption. There is very small part of duodenum left to allow the absorption of vitamins and minerals. However, reduction of the absorption process causes malnutrition

in the long-term and leads to health problems such as anemia and osteoporosis [93]. It is not very popular, because of its severe metabolic alterations and limited weight loss [90].

1.8.4 Roux-en-Y gastric bypass surgery

Roux-en-Y gastric bypass (RYGB) is one of the most often performed bariatric surgery types and can be considered the gold standard method [105, 106]. RYGB leads to anatomical and physiological changes such as stomach size reduction, bypass of the stomach and proximal small bowel (first 30-50 cm) and bile flow [97]. RYGB leads to a significant weight reduction by decreased appetite and food consumption, increased energy expenditure, enterohormonal changes, bile flow alterations and gut microbiota changes, although the mechanism are not fully understood. [107].

Overall, the mechanisms underlying the therapeutic effect of bariatric surgery and the possible differences compared to the weight loss by diet (caloric restriction) are not well defined. Moreover, the association among the cancer risk, obesity and weight loss has not been clearly shown. Contributing factors to cancer risk are still hypothetical. The role of proliferation, genomic damage and oxidative stress in pathologies of obesity is not adequately explained.

2 OBJECTIVES

Obesity is becoming an epidemic and one of the biggest health concerns of the future. It leads to an increase in pre-mature morbidity and mortality. Related health problems like type 2 diabetes mellitus and nonalcoholic fatty liver disease play an important role in the health consequences of obesity as well. Cohort studies showed that obesity as well as the related diseases have a strong association with several kinds of cancer. However, it is still not clear which mechanisms lead to this increased cancer incidence. Hypotheses usually focus on the involvement of oxidative stress.

Therefore, we investigated the link between obesity, oxidative stress and genomic damage as early biomarker for elevated cancer risk in a rat model of obesity. Since kidney, liver and colon are among the organs with the highest increase in cancer risk due to obesity, we focused on these three organs in our research. The main question was whether weight reduction is associated with a reduction of oxidative stress and genomic damage, which would indicate the possibility of cancer risk reduction by weight loss. As potential mechanistic factor, insulin resistance was considered. As methods for weight loss, dietary restriction as well as bariatric surgery were applied. Among the bariatric surgeries, Roux-en-Y gastric bypass surgery has become the gold standard and therapeutic choice to achieve a sustained weight loss in obesity and improvement of the metabolic state, but its consequences for cancer risk are discussed controversially. There is still a lack of information about the impact of bariatric surgery induced weight loss on cancer risk.

To better understand the role of insulin signaling in induction of oxidative stress and genomic damage, we used a whole-body Pten haplodeficient mouse model. With Pten, as a protein in the pathway of insulin-mediated signaling and negative regulator, its deficiency gave the opportunity to observe the association between insulin signaling, oxidative stress and genome integrity under physiological insulin level. Pten haplodeficient mouse model in which we focused on the liver, as well as cell culture with a pharmacological Pten inhibitor. In addition, the whole-body Pten haplodeficient mice were also lacking Akt2 enabling their use to investigate the involvement of Akt signaling in elevated oxidative stress and genomic damage.

3 MATERIALS AND METHODS

3.1 Materials

3.1.1 Cell line and cell culture reagents

Immortalized human hepatocytes (IHH) were used to investigate the genotoxicity of insulin. IHH cells were supplied from Prof. Dr. Folkert Kuipers, Department of Pediatrics, University Hospital Groningen, Groningen, Netherlands. William`s Medium E (W1878) and dexamethasone (D4902) were obtained from Sigma Aldrich (Steinheim, Germany or St. Louis, USA). The cell culture reagents were obtained from PAA Laboratories GmbH (Pasching, Austria) and Invitrogen Life Technologies (Carlbad, USA). Fetal bovine serum (FBS) was from Biochrom (Berlin, Germany). Human insulin solution was purchased from Santa Cruz Biotechnology (Santa Cruz, CA, USA). Pten inhibitor (VO-OHpic, Trihydrate) was obtained from BioVison, Inc. (Milpitas, CA, USA).

3.1.2 Animals

Zucker$^{fa/fa}$ rats (male) and Zucker$^{fa/+}$ rats (male) were purchased from Charles River, Research Models and Services, Germany GmbH (Sulzfeld, Germany).

C57BL/6 whole-body Pten haplodeficient mice were provided from Dr. Pier P. Pandolfi, Beth Israel Medical Center.

3.1.3 Chemicals and reagents

Dihydroethidium (DHE) was purchased from Merck Biosciences GmbH (Schwalbach, Germany). PVDF membranes were obtained from BIO-RAD (Hercules, USA). Normal donkey serum was obtained from Milipore (Temecula, USA). Peroxidase Substrate kit (SK-4100) and Vectastain ABC kit (PK-6100) were purchased from Vector Laboratories, Inc. (Burlingame, USA). Malondialdehyde tetrabutylammonium salt and 2-thiobarbituric acid were obtained from Sigma-Aldrich (Steinheim, Germany). 8-oxoGua and 8-oxoguo were purchased from Cayman (Ann Arbor, USA). 8-oxodG was obtained from Wako (Neuss, Germany). Gel Red and Gel Green were purchased from Biotrend (Köln, Germany).

3.1.4 Antibodies

The antibodies against beta-actin (3700s) and p-histone H2A.X (S139) (20E3) were obtained from Cell Signaling Technology Inc. (Beverly, USA). The antibody against Hsp70 (sc-24) was obtained from Santa Cruz Biotechnology (Santa Cruz, CA, USA) and HO-1 (ab68477) was obtained from Abcam (Cambridge, UK). The secondary antibodies HRP-conjugated goat anti-mouse IgG (sc-2005) and biotin-conjugated antibody donkey anti-rabbit IgG-B (sc-2089) were purchased from Santa Cruz Biotechnology (Santa Cruz, CA, USA). The secondary antibody HRP-conjugated anti-rabbit IgG (7074s) was purchased from Cell Signaling Technology Inc. (Beverly, USA).

3.2 Methods

3.2.1 Experimental design I

The rodent obesity model was used in collaboration with the Department of General, Visceral, Vascular and Paediatric Surgery, University Hospital of Würzburg. Gastric bypass surgery and the sham surgery were performed (as described in section 3.2.1.2) by Dr. Florian Seyfried (Surgical Department). Additionally, an oral glucose tolerance test (OGTT) was performed by our collaborators as described in section 3.2.1.3. Our collaboration partners focused further on gut microbial flora, gut hormones and pancreas, while we obtained kidney, liver and colon tissue as well as aliquots of the urine samples from four different time points. Preparation and analysis of the herein described tissues was performed entirely by the author of this thesis.

3.2.1.1 Rodent obesity model

Thirty-two male Zucker$^{fa/fa}$ rats and twelve male Zucker$^{fa/+}$ rats were purchased from Charles River, France at 6 weeks of age. Animals were housed under ambient humidity and temperature for 22 ^{o}C in a 12h light/dark cycle and had free access to tap water and Purina 5008 Lab diet (Purina Mills, USA, 16.7% of calories from fat) unless stated otherwise.

At 12 weeks of age, Zucker$^{fa/fa}$ rats were randomly divided into 2 different groups: gastric bypass surgery group (n=15) or sham surgery group (n=17).

After surgery, all RYGB and 12 sham-operated (obese) animals were fed ad libitum. Five sham operated Zucker$^{fa/fa}$ rats (CR group) received caloric restriction yielding the amount of calories necessary to achieve the same body weight as the RYGB group. Twelve Zucker$^{fa/+}$ rats were used as lean controls and five of them also underwent sham surgery. Food intake and body weight were measured daily. As regulation of glucose control and the secretion of the gastrointestinal peptide hormones are under circadian rhythm food intake was measured every 2 hours in lean control, sham ad libitum, and RYGB rats. Based on these results, 33% of the daily food intake was administered to the CR group during the light phase, and 66% at the beginning of the dark phase. All metabolic measurements were performed by our collaborators at the beginning of the dark phase in order to avoid possible confounders related to the circadian rhythm. Urine collection was achieved before surgery and at 3 different time points after surgery (postoperative days 14, 21 and 27). Collected urine samples were immediately frozen and kept at -80 ^{o}C. The overall design of the animal experiment is displayed in **Figure 7**.

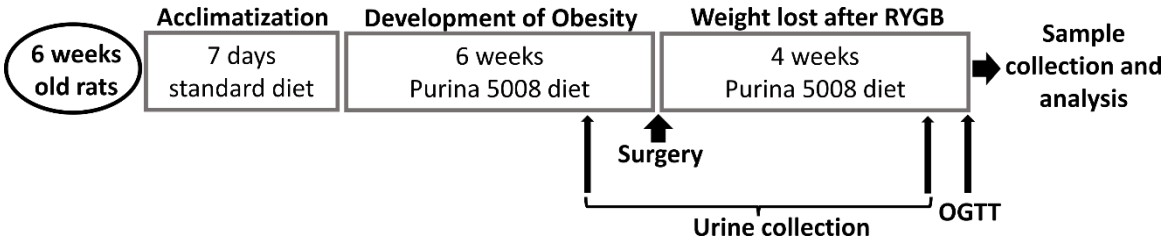

Figure 7: Scheme of animal experiment design.

At the end of the 10 weeks experimental period, animals were sacrificed 45 minutes after a fixed meal of 3g Purina 5008 diet. On the final day, there were four main experimental groups of animals:

- **Lean** (healthy control group *ad libitum*, Zucker$^{fa/+}$)
- **Obese** (sham surgery *ad libitum*, Zucker$^{fa/fa}$)
- **RYGB** (gastric bypass surgery *ad libitum*, Zucker$^{fa/fa}$)
- **CR** (caloric restriction group, Zucker$^{fa/fa}$)

For tissue harvesting a midline laparotomy was performed by surgeons from the University Hospital of Würzburg and the pancreas was removed within two minutes in order to avoid tissue degeneration. Kidney, liver and colon were removed for further investigation. After taking the organs (kidney, liver and colon) out, they were subdivided into four pieces. One small piece from each organ was immediately used for primary cell isolation in order to execute the comet assay (see section 3.2.1.6.1). The parts for protein isolation, cyrosections and paraffin sections were snap frozen and stored at -80 ^{o}C until the experiments were performed. One of the frozen parts was immersed in 10% neutral buffered formalin for overnight prior to embedding in paraffin for immunohistochemistry.

The animal experiments were approved by the Veterinary Office of the Government of Unterfranken, Germany, with licence number of 55.2-2531.01-72/12. All animal experiments were performed according to the European Community guidelines for the use of experimental animals and the German law for the protection of animals.

3.2.1.2 Surgery and perioperative care

Rats were food deprived for 6 hours pre-operatively. Surgical anesthesia was induced and maintained with isoflurane/O_2 mixture. Animals were placed on a warm pad during surgery. Prior to surgery 5mg/kg caprofen were applied to the animals subcutaneously. The abdomen was opened using a midline laparotomy and closed using continuous suturing.

3.2.1.2.1 RYGB surgery

Surgery was performed according to a standardized protocol which has been shown to result in weight loss and its long term maintenance [108]. Briefly, the jejunum was transected 16cm aboral to the pylorus to create the biliopancreatic limb. The stomach was divided 3mm below the gastro-esophageal junction to create a small pouch. The stomach remnant was subsequently closed. The aboral jejunum was anastomosed end-to-side to the small pouch. At the level of the lower jejunum, a 7mm side-to-side jejuno-jejunostomy between the biliopancreatic limb and the alimentary limb was performed creating a common channel of ~25cm in length. Roux-en-Y gastric bypass anatomy can be seen in **Figure 8**.

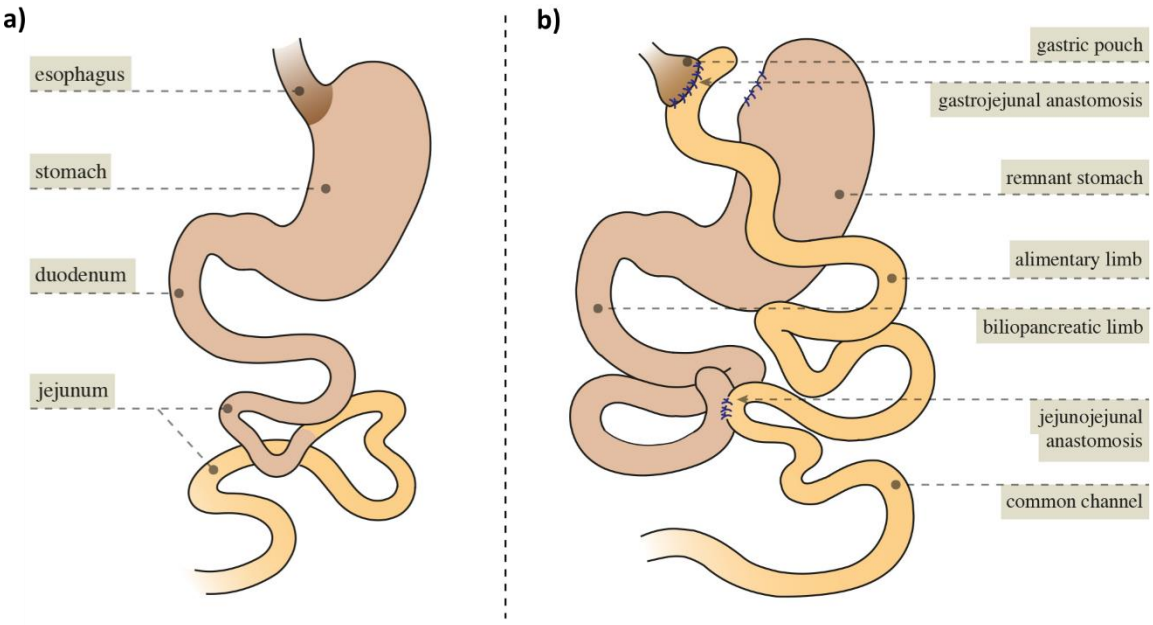

Figure 8: Anatomy of Roux-en-Y gastric bypass. **a)** Gastric tract before Roux-en-Y gastric bypass surgery. **b)** Gastric tract after Roux-en-Y gastric bypass surgery. Created by Laura Rotzinger and used with her permission.

3.2.1.2.2 Sham surgery

The small bowel and gastro-esophageal junction were mobilized and a gastrostomy on the anterior wall of the stomach and a jejunostomy with subsequent closure were performed.

3.2.1.3 Metabolic measurement

An oral glucose tolerance test (OGTT) was performed at the beginning of the dark cycle on postoperative day 27 in all animals. In order to avoid oral gavage and therefore to reduce discomfort and pressure on the upper anastomosis, animals were trained to drink 10 ml/kg body weight of a 25% glucose solution within 10 min after an overnight fast on two occasions before the OGTT was performed. After an 8 hour overnight fast, blood glucose was measured (Breeze 2® glucometer, Bayer, Zurich, Switzerland) in conscious rats at baseline, and 15, 30, 60 and 120 minutes after glucose ingestion. Blood was obtained from the tail vein by a small incision. A drop of blood was applied directly to a glucometer and 100 µl were collected at each time point in tubes containing EDTA and a dipeptidyl peptidase-4 inhibitor. The plasma fraction was separated by centrifugation at 4°C and stored at -80 °C. Total insulin was measured using the Ultrasensitive Rat Insulin ELISA (Merodia AB, Sweden 10-1251-10) from EMD Millipore (www.merck.millipore.com).

3.2.1.4 Detection of ROS on cryosections by DHE staining

Five µm cryosections from snap-frozen kidney, liver and colon tissues were prepared with a Leica CM3050 cryostat (Leica, Wetzlar, Germany). The sections were stained immediately after the preparation with 10 µM DHE for 30 min in the dark at room temperature. After staining, sections were washed 3 times with PBS and covered with a cover glass. Pictures were taken with an Eclipse 55i microscope (Nikon GmbH, Düsseldorf, Germany) and a Fluoro Pro MP 5000 camera (Intas Science Imaging Instruments GmbH, Göttingen, Germany) at 400-fold magnification. Quantification was done by analyzing 200 cells per animal by using Image j software (http://rsbweb.nih.gov/ij).

3.2.1.5 Western Blot analysis

A part of snap-frozen kidney, liver and colon tissue was homogenized by using an ultra-turrax in ice-cold radio immune-precipitation assay (RIPA) lysis buffer (50 mM Tris-HCl, 150 mM NaCL, 1 mM EDTA, 0.25% sodium desoxycholate, 1% Nonidet P-40 substitute in deionized water, adjustment of pH to 7.4 with HCl), which contains freshly added protease inhibitor cocktail (5 mg/ml), sodium orthovanadate (200 mM) and sodium fluoride (200 mM) to inhibit protease and phosphatase activity. After homogenization of tissue, samples were centrifuged at 14,000 rpm and 4 ^{o}C for 15 min. The protein lysate was stored at -20 ^{o}C until the performance of western blot analysis. The protein concentration of samples was determined by using Bio-Rad protein assay (based on Bradford`s method). Fifty µg of protein per sample were loaded on SDS gels and electrophoresis was performed in order to separate proteins. The separated proteins were transferred from gel to PVDF membrane (polyvinylidene difluoride membranes, 0.2 µ). The membrane was blocked at least for 2 hours in 5% (w/v) of skim milk powder in TBS-T buffer (5 mM TRIS, 150 mM NaCl, 0.05% (w/v) Tween-20). After blocking, the membrane was incubated with primary antibody (heat shock protein 70 (HSP70, 1:1000); heme oxygenase-1 (HO-1, 1:5000) and β-actin (1:5000)) overnight at 4 ^{o}C. On the next day, the membrane was incubated with horseradish peroxidase (HRP) - conjugated secondary antibody (1:5000) for 1 hour and then with HRP substrate (ECL substrate, BIO-RAD, Hercules, USA) for 5 min. The membrane was exposed to an x-ray sensitive film and the film was developed later on.

Quantification was done by analyzing the bands on each film by using Image j software (http://rsbweb.nih.gov/ij). The results were normalized to the endogenous control β-actin.

3.2.1.6 Genotoxicity tests

3.2.1.6.1 Isolation of primary cells for alkaline comet assay

A small piece cut from fresh kidney, liver or colon and washed with cold PBS. Organ pieces were minced in cold medium on ice. Dulbecco`s Modified Eagle Medium (DMEM) low glucose (1 g/L), supplemented with 10% (v/v) fetal bovine serum (FBS), 1% (w/v) L-glutamine, 2.5% (w/v) 4-(2-hydroxyethyl)-1-piperazineethanesulfonic acid (HEPES) and 0.4 % antibiotics (50 U/ml penicillin and 50 mg/ml streptomycin), was used for isolation of primary kidney cells. DMEM low glucose medium (1 g/L), supplemented with 10 % (v/v) FBS, 1% (w/v) L-glutamine, 0.4% antibiotics (50 U/ml penicillin and 50 mg/ml streptomycin) and 1 % sodium pyruvate, was used for isolation of primary liver cells. DMEM high glucose (4.5 g/L), supplemented with 10 % (v/v) fetal bovine serum, 1% (w/v) L-glutamine and 0.4% antibiotics (50 U/ml penicillin and 50 mg/ml streptomycin), was used for isolation primary colon cells. After mincing the tissue, the mixture was put through a nylon cell strainer with a pore size of 100 µm (BD, Heidelberg, Germany) and centrifuged at 1000 rpm, 4 ^{o}C for 5 min. The cell pellet was re-suspended in 1 ml cold medium and kept on ice until the experiment was performed. Viability of cells was monitored by trypan blue staining. The cell pellet was diluted with 0.2% (w/v) trypan blue 1:1 and counting was performed with a Neubauer chamber.

3.2.1.6.2 Alkaline comet assay

The alkaline comet assay is a single gel electrophoresis assay, which can detect single and double strand breaks, and it is one of the standard methods to determine DNA damage. The comet assay is a simple, cheap and sensitive application, which is based on the lysis of agarose embedded cells. Embedding is required in order to immobilize the cellular DNA for the following electrophoresis step that results in the formation of a comet [109].

After isolation, 20 µl of cell suspension was mixed with 180 µl of 0.5% low melting point agarose at 37 ^{o}C. The rest of the cell pellet was kept on ice for vitality tests. 45 µl of cell-agarose mixture was placed on a fully frosted slide that was coated with 1.5% of high

melting point agarose. The cell suspension was covered with a cover glass and the slides were kept at 4 ^{o}C for 5 min to solidify the mixture. After gentle removal of the cover-glass, slides were kept in a lysis solution (1% Triton X-100, 10% dimethyl sulfoxide, and 89% lysis buffer containing 10mM Tris, pH 10; 1% Na-sarcosine; 2.5M NaCl; and 100mM Na_2EDTA) for 1 hour in dark at 4 ^{o}C. After the lysis step, to allow DNA unwinding, the slides were placed in an electrophoresis chamber that was filled with fresh electrophoresis buffer (300mM NaOH and 1mM Na_2EDTA, pH 13) for 20 min at 4 ^{o}C in dark. Then the electrophoresis was performed for 20 min at 25 V (1.1 V/cm) and 300 mA. To neutralize the slides they were immersed in 0.4 M Tris buffer (pH 7.5) for 5 min and then to dehydrate in methanol for 5 min at −20 ^{o}C. The slides were left to dry under a fume hood and stained with 20 µl of Gel red/Dabco solution. Following all these steps, damaged DNA migrates and forms a comet-like structure, an example for which can be seen in **Figure 9**.

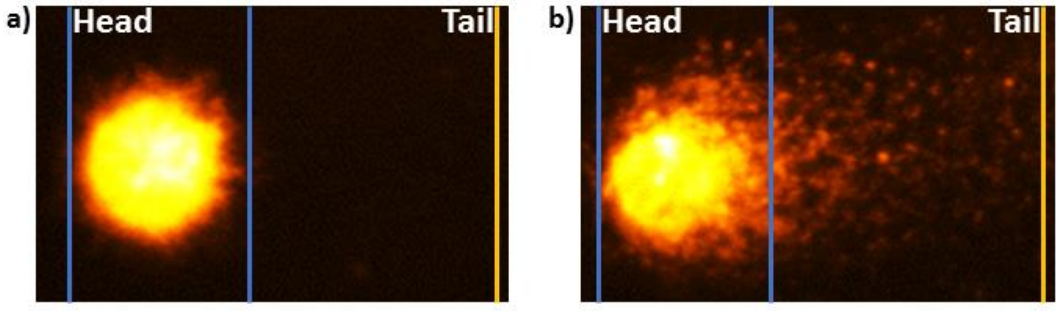

Figure 9: Representative pictures of agarose embedded cells under microscope. An example for a cell with intact nuclear DNA (**a**) and an example for a cell with DNA damage (**b**). The comet assay is based on the migration of small DNA fragments (single or double strand breaks) in an electric field. DNA damage is quantified with a specialized software and expressed as percent of DNA in tail.

Evaluations of the slides were done with a fluorescence microscope (Labophot 2; Nikon) at 200-fold magnification and image analysis software (Komet 5, BFI Optilas, Germany). One hundred randomly selected cells (50 per replicate slide) for each treatment were analysed. The percentage of DNA in the tail was used to quantify DNA damage.

3.2.1.6.3 Detection of phosphorylated H2AX sites

Formation of DNA DSBs induces phosphorylation of histone 2A (H2AX) on Ser-139, which is referred to as γ- H2AX. Phosphorylation of H2AX is considered a key component in DNA

DSB repair. However, if repair fails, DNA DSBs might lead to mutation and chromosomal aberrations [110, 111].

Antibody staining was performed against phosphorylated Ser-139 at the C-terminus of histone H2AX in order to detect double strand breaks on paraffin sections of kidney, liver and colon. The paraffin sections (2 µm) were prepared with a microtome (LEICA RM 2165, Wetzlar, Germany) and mounted on positively charged slides. The sections were heated at 60 ^{o}C for 1 hour, deparaffinised (3 x 4 min Roti-Histol, 2 x 3 min 100% EtOH, 1 x 2 min 70% EtOH) and washed with PBS. Antigen retrieval was achieved by cooking the slides for 4 min in citrate buffer (10 mM sodium citrate, pH 6) on the highest level in a pressure cooker. To cool down, the slides were washed with PBS. The sections were blocked in 5% donkey serum for 1 hour at room temperature in the dark. To reduce background staining, endogenous peroxidase activity was depleted by incubation with 3% of H_2O_2 for 15 min at room temperature in the dark. Prior to the incubation with biotinylated antibody, slides were incubated successively with 0.001% avidin and biotin for 15 min at room temperature in the dark. Later on, primary antibody (phospho-Histone H2AX (Ser139, clone 20E3) rabbit mAb; 1:200) incubation was performed overnight at 4 ^{o}C in dark. Following the washing steps, biotin-conjugated secondary antibody (donkey anti rabbit IgGB, sc2089, Santa Cruz Biotechnology; 1:200) incubation was performed for 45 min, at room temperature in the dark. After washing the sections with PBS, they were incubated with the avidin biotin complex (ABC) reagent (Vectastin-Elite ABC reagent: two drops of reagent A and reagent B mixed with 10 mM sodium phosphate, 0.9% NaCl, pH 7.5) for 30 min at room temperature in the dark and washed again in PBS. Following that, the sections were incubated with diaminobenzidin (DAB) chromogen (Vector Laboratories) for 10 min at room temperature. DAB reacts with HRP in the presence of peroxide to yield an insoluble brown-colored product at locations where peroxidase-conjugated antibodies are bound to samples (**Figure 10**). Counterstaining was done with Ehrlich's haematoxylin (1 g haematoxylin, 48 mL 99.8% isopropanol, 51.9 mL H2O d, 50 mL glycerol, 1.5 g potassium alum, 5 mL acetic acid, 0.2 g potassium iodate) for three minutes and then the sections were washed for 10 min in pure water. Before mounting with Eukitt (Fluka), the sections were dehydrated (1 x 1 min 70% EtOH, 4 x 2 min 100% EtOH, 2 x 3 min Roti-Histol).

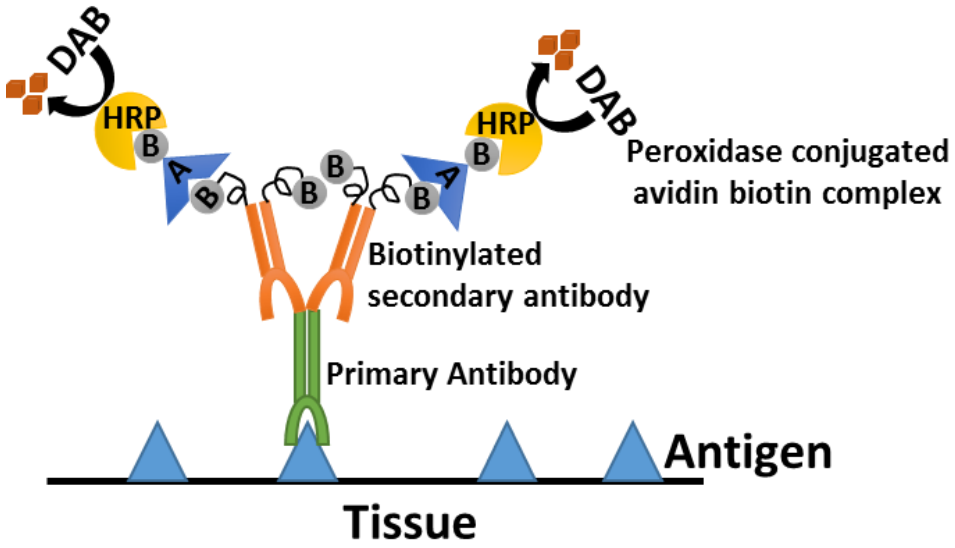

Figure 10: Schematic representation of the ABC-DAB reaction in immunohistochemistry.

Pictures were taken with a Keyence BZ-9000 microscope at 400-fold magnification. The positive cells was assessed by manually scoring 15 to 20 images per animal and total cell number was counted by automated image analysis (in the range of 6000 to 12000 cells for kidney and 3000 to 6000 for liver) in kidney and liver. The percentage of positive cells was evaluated by dividing the positive cell number by the total cell number. In colon sections, 50 crypts per sample were quantified and the results were expressed as positive cell number per crypt.

3.2.1.7 Urine analysis

3.2.1.7.1 TBARS assay

Free radical induced lipid oxidation (lipid peroxidation, LPO) associates with various alterations such as integrity, fluidity and functional loss of biologic membranes. Furthermore, LPO products have been suggested to be mutagenic and carcinogenic [112]. LPO was monitored by colorimetric measurements of the formation of thiobarbituric acid reactive substances (TBARS). The TBARS assay is based on the reaction between malondialdehyde (MDA) that is a secondary lipid peroxidation product and thiobarbituric acid (TBA) to form a colored MDA-TBA complex, which can be quantified at 532 nm [113, 114]. Several concentrations of malondialdehyde (MDA, 32-16-8-4-2-0 µM) were used as standard. A standard reaction mixture contained MDA and aqueous solution of thiobarbituric acid (1% TBA, pH 1.5) (1:1, v/v). The sample mixture contained 500 µl of

diluted urine samples (1:1, v/v) and 500 µl of TBA (1%, pH 1.5). The reaction between the lipid peroxidation products and TBA was induced by boiling the samples at 100 ^{o}C (water bath) for 30 min and samples were then cooled on ice. The absorbance from the standards and the samples was measured at 532 nm before and after boiling. The differences between the absorbances were used as net optic density in order to evaluate the lipid peroxidation products in urine as MDA equivalence. The results were normalized to the urinary creatinine level (analysis for creatinine performed by central laboratory of University Hospital, Würzburg).

3.2.1.7.2 Quantification of urinary DNA and RNA oxidation biomarkers in urine by LC/MS/MS

Oxidative damage to DNA is a contributing factor to carcinogenesis. Oxidation of guanine bases has received special attention, because of its high mutagenic potential [115]. Even though RNA oxidation has not been investigated much, oxidation of RNA has as well an important effect on disease pathology [116, 117].We used specific and sensitive HPLC tandem mass spectrometry methods in order to quantify the oxidation of DNA and RNA.

A standard stock mixture of 8-hydroxyguanine (8-oxoGua), 8-hydroxydeoxyguanosine (8-oxodG) and 8-hydroxyguanosine (8-oxoGuo) was prepared and used to develop serial dilutions for the standard curve. 8-mercaptoguanosine (8-SH-G) was used as internal standard (IS) at the concentration of 16 µM. Urine samples were thawed at room temperature and diluted with IS 1:1. The mixture of urine and IS was stirred vigorously and filtered by a simple nylon syringe filter (0.2 µm) (Phenomenex, Aschaffenburg, Germany).

Analysis was performed using an Agilent 1100 series HPLC with an auto sampler (Agilent Technologies, Böblingen, Germany). After the elution was performed on ODS AQ column (C18, 150x4.6 mm, 5 µm) (YMC, Dinslaken, Germany) with a combination of a C18 guard column (4x2 mm), the samples were introduced to the turbo ion spray source of an API 3000 triple-quadrupole mass spectrometer (Applied Biosystem). Detection of the biomarkers was operated under positive ion mode. The analyst Software 1.4.42 was used to control an automated valco valve (VICI, Switzerland), which directed the first 10 min and the last 5 min of elution to the waste for reducing the contamination in the ion source. The mobile phase contained 0.1% formic acid in de-ionized water (MPA) and 0.1% formic acid

in methanol (MPB). The concentration of MPA was started with 95% and reduced to 50% in 10 min. Fifty percent of MPA was held for 2 min and the next 3 min reduced further to 30%. The MPA concentration increased from 30% to 95% in 3 min and was held at 95% for 8 min in order to supply the initial conditions for next injection. Flow rate was 0.3 ml/min and injection volume was 25 µl. The running time per sample was 25 min. Nitrogen was used as curtain, nebulizer and collision gas. Multiple reaction monitoring (MRM) parameters for biomarkers are listed in **Table 3**. The results were normalized to the urinary creatinine level (analysis for creatinine performed by central laboratory of University Hospital, Würzburg).

Table 3: MRM parameters for quantification of urinary DNA and RNA oxidation biomarkers and IS

Analyte	Transition [m/z]	DP (V)	FP (V)	CE (V)	CXP (V)
8-oxoGua	168.00→140	20	200	30	15
8-oxodG	284.10→168	21	110	21	16
8-oxoguo	300.00→168	25	230	19	8.4
8-SH-G	315.98→184	31	200	26	4.0

DP: declustering potential, FP: focusing potential, CE: collision energy, CXP: collision cell exit potential, 8-oxoGua: 8-hydroxyguanine, 8-oxodG: 8-hydroxydeoxyguanosine, 8-oxoGuo: 8-hydroxyguanosine and 8-SH-G: 8-oxodG: 8-hydroxydeoxyguanosine

3.2.2 Experimental design II

We had the chance to access liver samples of a whole body Pten haplodeficient mouse model via a collaboration with the Hepatology Division of the University Hospital Würzburg. To develop a better understanding of the role of insulin signaling and Pten in oxidative stress and genomic damage, this whole body Pten haplodeficient mouse model, which is focused on liver, was used. Our collaboration partners were interested in the role of peripheral insulin sensitive tissues on Pten and Akt2 dependent hepatic lipid accumulation and they investigated hepatic lipid content, expression of hepatic multidrug-resistance transporters, cytokines and proliferation markers. Details about the animal experiment are

found in section 3.2.2.1. Additionally, an in vitro system was used to demonstrate the genotoxicity of insulin in liver cells.

3.2.2.1 Whole-body Pten haplodeficient mouse model

Mice were housed according to the Swiss Animal Protection Laws in groups with a 12-h dark-light cycle and free access to food and water. All animal experiments were performed according to the European Community guidelines for the use of experimental animals and the German law for the protection of animals. Male mice with whole-body targeted deletion of *Pten* and Akt2 were in a C57BL/6 background and Pten and Akt2 deletion was maintained after backcrosses as previously described [118, 119]. $Pten^{+/+}/Akt2^{+/+}$, $Pten^{+/-}/Akt2^{+/+}$ and $Pten^{+/-}/Akt2^{-/-}$ mice were obtained by crossing $Pten^{+/-}/Akt2^{+/-}$ mice. The heredity of targeted alleles was confirmed by PCR. Twelve weeks old mice were fed either with a standard diet (Kliba 3336, 5.5% fat content) or with a high fat diet (Kliba 2126, 23.6% fat content) for 20 weeks. Animals were sacrificed with 32 weeks age and liver tissue was collected for further analysis. We received snap frozen liver samples and paraffin-embedded liver sections of the following animal groups from our collaborators of the Hepatology Division:

Standard diet (SD) fed groups:

- **WT** (wild-type mice, $Pten^{+/+}/Akt2^{+/+}$, n=6)
- $\boldsymbol{Pten^{+/-}/Akt2^{+/+}}$ (whole-body Pten haplodeficient mice, n=9)
- $\boldsymbol{Pten^{+/-}/Akt2^{-/-}}$ (whole-body Pten haplodeficient mice lacking Akt2, n=8)

High fat diet (HFD) fed groups:

- **WT** (wild-type mice, $Pten^{+/+}/Akt2^{+/+}$, n=9)
- $\boldsymbol{Pten^{+/-}/Akt2^{+/+}}$ (whole-body Pten haplodeficient mice, n=9)
- $\boldsymbol{Pten^{+/-}/Akt2^{-/-}}$ (whole-body Pten haplodeficient mice lacking Akt2, n=9)

ROS formation and oxidative stress status level in liver tissue was investigated by DHE staining and western blot (expression of HSP70 and HO-1). DHE staining on liver cryosections and western blot were carried out respectively as described in section 3.2.1.4

and section 3.2.1.5. A γ-H2AX antibody staining was performed on paraffin embedded liver sections in order to determine the DNA DSBs according to section 3.2.1.6.3.

3.2.2.2 In vitro hepatocyte model to investigate the insulin-mediated genotoxicity

3.2.2.2.1 Cell culture and treatment conditions

The immortalized human hepatocyte cell line (IHH) was cultured in William`s Medium E with 10% (v/v) fetal bovine serum, 1% (w/v) L-glutamine, 1% (w/v) antibiotic (50 U/ml penicillin and 50 mg/ml streptomycin), 1 mU/ml human insulin and 50 nM/L dexamethasone in an incubator with 5% CO_2, 37 ^oC. IHH cells were sub-cultured two to three times per week.

One day prior to experiments, IHH cells ($8x10^4$ cells/ml) were inoculated in 6 well plates with 3 ml medium per well, which did not contain insulin and dexamethasone. On the following day, cells were pre-incubated with a vanadium complex that is a specific inhibitor of PTEN (VO-OHpic, 50 nM) for 15 min at 37 ^oC. After 15 min pre-incubation, cells were treated for an additional 30 min (for DHE staining), 2h (for comet assay) or 4h (for micronucleus test) with insulin (10 or 100 nM).

Insulin stock solution was prepared by solving 5.7 mg insulin in 1 ml sterile water and diluted further with 0.1 M HCl solution (1:1, v/v). Concentration of the stock solution was 0.5 mM and it was prepared as 15 µl aliquots for single use. Aliquots were stored at –20 ^oC. HCl solution (0.05 M) was used to dilute insulin and as solvent control.

3.2.2.2.2 Vitality test

In order to differentiate between cytotoxicity and genotoxicity of the applied concentrations of insulin in the comet assay, a vitality test was performed. Two different dyes (fluorescein diacetate and gel red) were used to assess vitality of cells. Seventy µl of cell suspension was mixed with 30 µl of staining solution (2µl Gel Red stock (Biotium, Hayward, CA) solution and 12µl fluorescein diacetate (FDA; 5mg/ml in acetone) in 2 ml PBS). Twenty µl of this mixture was applied on the slide and covered with a cover slip (21x26 mm2). In total 200 cells (red and green stained) were counted at 200-fold magnification with an Eclipse 55i microscope which was equipped with FITC filter (Nikon GmbH,

Düsseldorf, Germany). The proportion of green cells (vital) to red cells (dead) was evaluated.

FDA is a fluorogenic substrate, which can be hydrolysed intracellularly by cellular esterase activity and leads to accumulation of green fluorescent fluorescein [120]. Gel red has similar characteristics as ethidium bromide and works with the same principle. It enters the cells, which do not have an intact plasma membrane and binds to the DNA in order to exhibit a bright red fluorescent color. With this staining combination, it is possible to determine the plasma membrane integrity and cellular enzymatic activity.

3.2.2.2.3 Intracellular ROS analysis by DHE staining

The cell permeable fluorescent dye dihydroethidium (DHE) was used in order to detect intracellular ROS. The cells were split one day prior to the experiment and seeded on 24 mm cover slips. The next day, after pre-incubation with PTEN inhibitor, an additional 30 min incubation was performed with insulin (10 and 100 nM) and DHE (5 µM) at 37 ^{o}C in the dark. At the end of the incubation time, cells were washed with PBS and pictures of the cells were taken with an Eclipse 55i microscope (Nikon GmbH, Düsseldorf, Germany) and a Fluoro Pro MP 5000 camera (Intas Science Imaging Instruments GmbH, Göttingen, Germany) at 200-fold magnification. Two hundred fifty cells were analysed per group by using ImageJ software (http://rsbweb.nih.gov/ij).

3.2.2.2.4 Alkaline comet assay

After treatment, cells were harvested and 20 µl of cell suspension was used to carry out the alkaline comet assay as described in 3.2.1.6.2. One hundred randomly selected cells (50 per replicate slide) for each treatment were analysed. The percentage of DNA in the tail was quantified to investigate the DNA damage.

3.2.2.2.5 Cytokinesis-block micronucleus (CBMN) assay

A micronucleus (MN), which forms from acentric chromosome fragments (chromosome breaks lacking centromeres) or whole chromosome loss during mitosis, is a biomarker for genomic instability (**Figure 11**). The CBMN assay can determine both chromosome breakage and loss. Chromosomal abnormalities are an expression of DNA damage such as DNA double strand breaks. The MN frequency in human peripheral lymphocytes exhibits a

strong association with aging and cancer [121]. Micronucleus formation is one of the routine mutagenicity testing methods in the approval of substances. Here, IHH cells were prepared and treated as described 3.2.2.2.1.

After the treatment, the medium was replaced with fresh medium containing the cytokinesis inhibitor cytochalasin B (3 µg/ml) for 24 hours to block separation of daughter cells, yielding cells with two daughter nuclei, i.e. binucleated cells. After cytokinesis-block, cells were harvested, placed on a glass slide by cytospin centrifugation and fixed in methanol at –20 ^{o}C for at least 2 hours. Before counting, cells were stained with gel green (1:100 diluted in bidistilled water) and mounted with Dabco for microscopy. MN were counted with an Eclipse 55i fluorescence microscope (Nikon GmbH, Düsseldorf, Germany) at 400-fold magnification, using a long-pass FITC filter. For each treatment, two replicate slides were prepared and 1000 binucleated cells (BN) per slide were scored for the presence of MN. In addition, mitotic and apoptotic cells were registered. The cytokinesis block proliferation index (CBPI) as an indicator of cytostatic effects was determined by using the equation below:

$$\frac{(\mathbf{no.\ of\ mononucleated\ cells} + \mathbf{2xno.\ of\ binucleated\ cells} + \mathbf{3xno.\ of\ multinucleated\ cells})}{(\mathbf{sum\ of\ mononucleated, binucleated\ and\ multinucleated\ cells})}$$

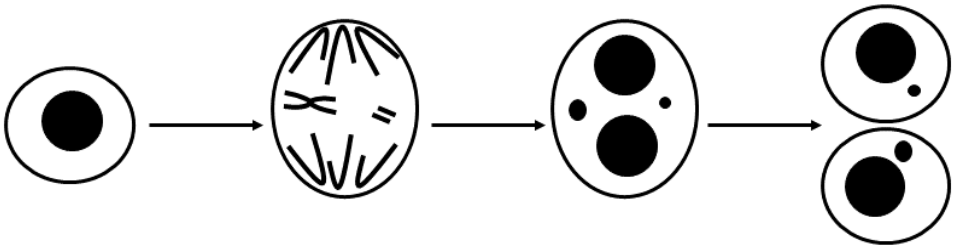

Figure 11: Mechanism of micronucleus formation. A micronucleus forms either from a lagging whole chromosome or lagging chromosome fragments during mitosis. Modified from [121].

3.2.3 Statistical analysis

Data are presented as mean ± SEM. Statistical analysis was performed with the SPSS 22 software. The Kruskal-Wallis test was used to determine significance between multiple groups and the Mann-Whitney U-test was used to determine the significance between two groups. The changes in body weight were compared with one way analysis of variance (ANOVA) followed by Bonferroni`s post hoc test for multiple comparison. The correlation between DNA damage and plasma insulin level was compared by Spearman correlation test. Results with p values of ≤ 0.05 were considered as significant.

4 RESULTS

4.1 Results of the Zucker$^{fa/fa}$ rat obesity model

4.1.1 Body weight, daily food intake and metabolic parameters

Gastric bypass surgery and the sham surgery were performed (as described in section 3.2.1.2) by our collaboration partners from the surgery department, University Hospital of Würzburg. They also monitored body weight and daily food intake during the 27-day postoperative period and performed an oral glucose tolerance test (as described in section 3.2.1.3) with the following groups:

- **Lean** (healthy control group *ad libitum*, Zucker$^{fa/+}$, n=12)
- **Obese** (sham surgery *ad libitum*, Zucker$^{fa/fa}$, n=12)
- **RYGB** (gastric bypass surgery *ad libitum*, Zucker$^{fa/fa}$, n=15)
- **CR** (caloric restriction group, Zucker$^{fa/fa}$, n=5)

At the beginning, body weight was similar in the Obese, RYGB and CR groups and significantly higher compared to the Lean group. During the 27 days, Obese rats gained weight, while the rats in CR and RYGB groups lost weight and in the end showed a significant reduction in body weight compared to the sham-operated Obese rats. On the 27th day, there was no significant difference between the Lean group and the groups with body weight reduction (RYGB and CR) (**Figure 12**).

The average daily food intake was significantly higher in sham-operated Obese rats compared to the Lean rats. Food intake in the gastric bypass group (RYGB) was significantly reduced compared to the sham-operated Obese rats. The CR group received the same amount of food as the RYGB group, intended to provide caloric restriction, which was significantly less food than that of the Lean group (**Figure 13**).

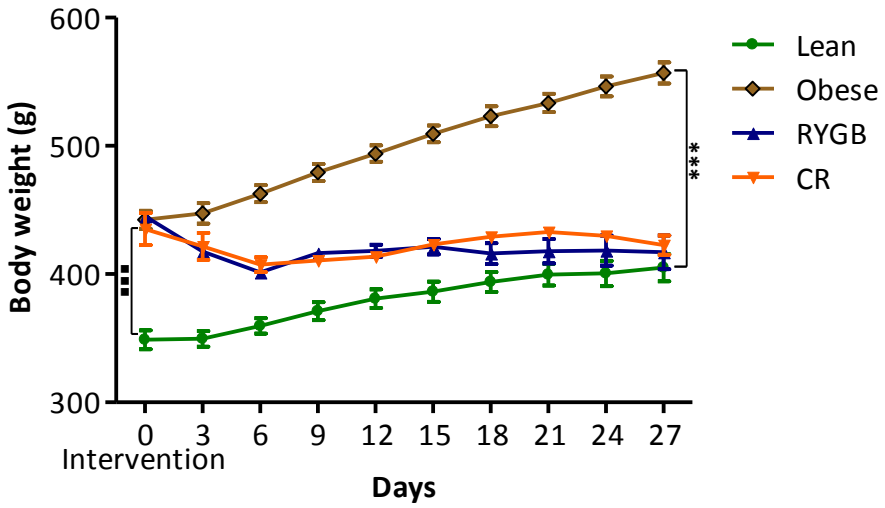

Figure 12: Body weight between postoperative days 0 and 27. Data are presented as mean ± SEM. ▪▪▪ p≤0.001 Lean vs. Obese rats (including RYGB and CR on day 0) and *** p≤0.001 Lean, RYGB and CR vs. Obese on day 27. Lean: Zucker$^{fa/+}$ rats (n=12), Obese: sham-operated Zucker$^{fa/fa}$ rats (n=12), RYGB: Roux-en-Y gastric bypass surgery operated Zucker$^{fa/fa}$ obese rats (n=15), CR: body weight matched to RYGB group with caloric restriction of Zucker $^{fa/fa}$ obese rats (n=5).

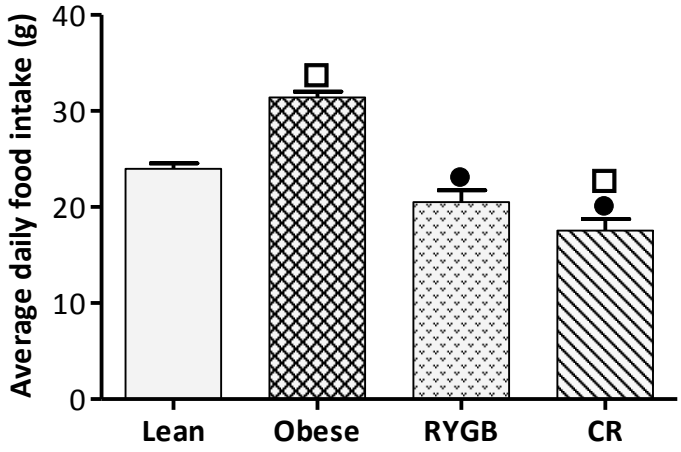

Figure 13: Average daily food intake between postoperative days 0 and 27. Data are presented as mean ± SEM. □ p≤0.01 vs. Lean, and ● p≤0.01 vs. Obese. Lean: Zucker$^{fa/+}$ rats (n=12), Obese: sham-operated Zucker$^{fa/fa}$ rats (n=12), RYGB: Roux-en-Y gastric bypass surgery operated Zucker$^{fa/fa}$ obese rats (n=15), CR: body weight matched to RYGB group with caloric restriction of Zucker$^{fa/fa}$ obese rats (n=5).

Blood glucose and plasma insulin levels were determined (performed by surgery department collaboration partners) at 0, 15, 30, 60 and 120 min after 25% of glucose solution ingestion subsequent to 8 hours overnight fasting. Sham-operated obese animals showed the highest blood glucose increase while the decrease was faster in the RYGB group. The Lean and CR animals were similar to each other in their response pattern but were at a lower glucose level than the Obese and RYGB groups (**Figure 14**).

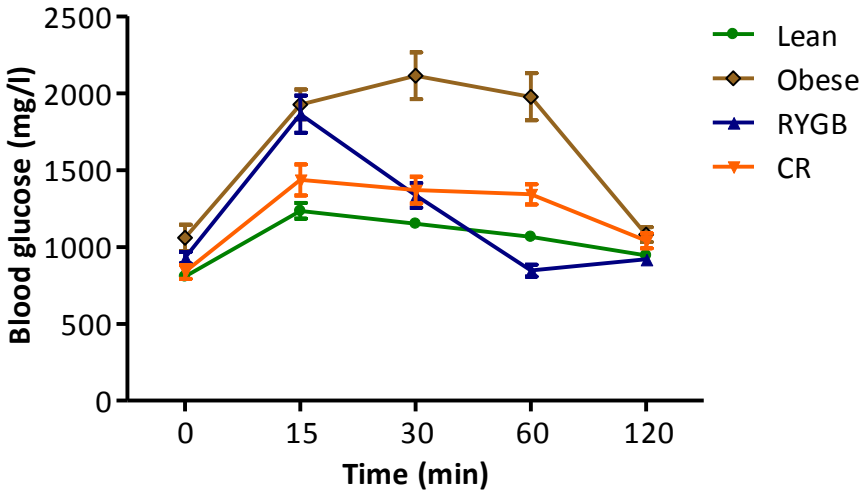

Figure 14: Blood glucose level at 0, 15, 30, 60 and 120 min after 25% glucose solution ingestion following 8 hours overnight fasting. Data are presented as mean ± SEM. Lean: Zucker$^{fa/+}$ rats (n=12), Obese: sham-operated Zucker$^{fa/fa}$ rats (n=12), RYGB: Roux-en-Y gastric bypass surgery operated Zucker$^{fa/fa}$ obese rats (n=15), CR: body weight matched to RYGB group with caloric restriction of Zucker$^{fa/fa}$ obese rats (n=5).

Blood insulin levels were higher in Obese, RYGB and CR than in the Lean rats. The pattern of insulin secretion was altered by loss of body weight, with an elevated secretion upon stimulation and a more effective reduction after glucose utilization (**Figure 15**).

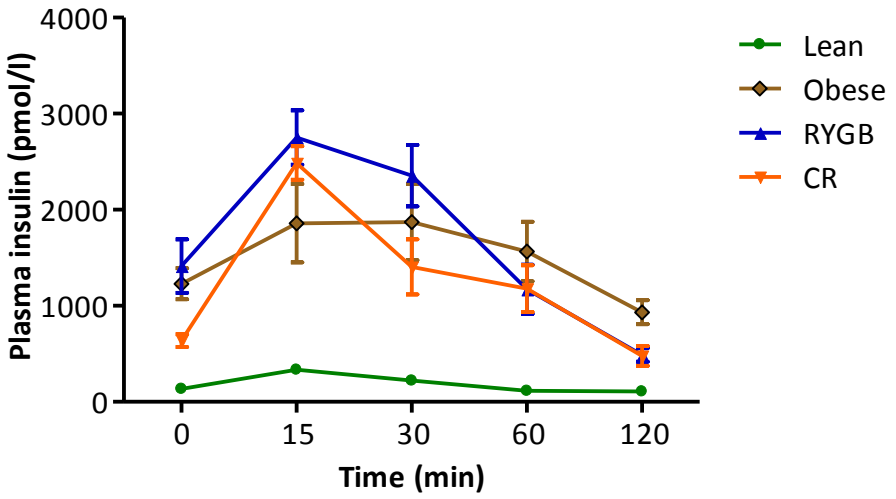

Figure 15: Plasma insulin level at 0, 15, 30, 60 and 120 min after 25% glucose solution ingestion following 8 hours overnight fasting. Data are presented as mean ± SEM. Lean: Zucker$^{fa/+}$ rats (n=12), Obese: sham-operated Zucker$^{fa/fa}$ rats (n=12), RYGB: Roux-en-Y gastric bypass surgery operated Zucker$^{fa/fa}$ obese rats (n=15), CR: body weight matched to RYGB group with caloric restriction of Zucker$^{fa/fa}$ obese rats (n=5).

Since there was a clear difference in the response pattern of the animals following the glucose solution ingestion, area under curve (AUC) was evaluated for blood glucose (**Figure 16**) and plasma insulin levels (**Figure 17**). The trapezoidal rule was used to evaluate the AUC. $AUC_{glucose}$ of Obese animals showed a significant increase compared to the Lean group. Weight loss either by gastric bypass (RYGB) or by caloric restriction (CR) sustained significant reduction in $AUC_{glucose}$. There was no significant difference between RYGB and CR group, however there was a significant difference in $AUC_{glucose}$ of CR group compared to the Lean.

$AUC_{insulin}$ was significantly higher in Obese, RYGB and CR groups compared to the Lean group (**Figure 17**). Weight loss (by gastric bypass nor by caloric restriction) did not lower the plasma insulin level or improve the hyperinsulinemia. However, glucose uptake and the basal insulin level were enhanced by weight loss either with RYGB or with CR.

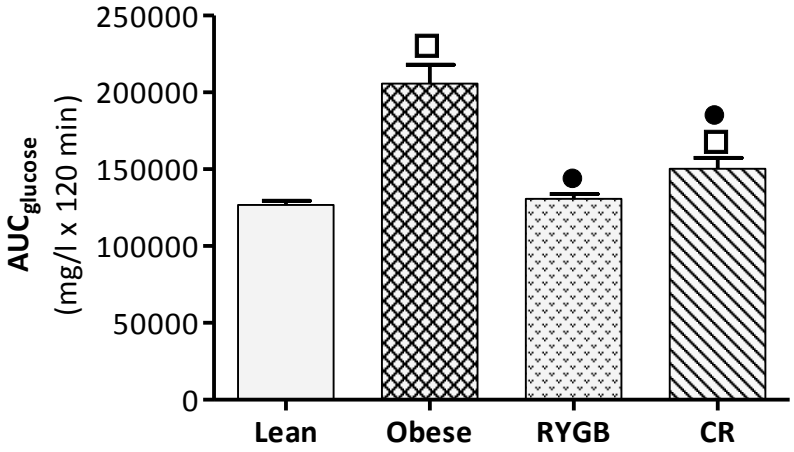

Figure 16: $AUC_{glucose}$ after 25% glucose solution ingestion following to 8 hours overnight fasting. The trapezoidal rule was used to calculate area under the curve. Data are presented as mean ± SEM. □ p≤0.01 vs. Lean and ● p≤0.01 vs. Obese. Lean: $Zucker^{fa/+}$ rats (n=12), Obese: sham-operated $Zucker^{fa/fa}$ rats (n=12), RYGB: Roux-en-Y gastric bypass surgery operated $Zucker^{fa/fa}$ obese rats (n=15), CR: body weight matched to RYGB group with caloric restriction of $Zucker^{fa/fa}$ obese rats (n=5).

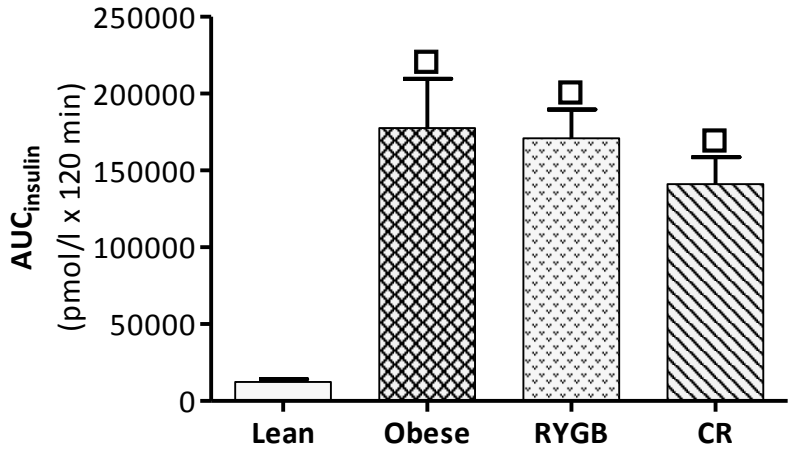

Figure 17: $AUC_{insulin}$ after 25% glucose solution ingestion following to 8 hours overnight fasting. The trapezoidal rule was used to calculate area under the curve. Data are presented as mean ± SEM. □ p≤0.01 vs. Lean. Lean: $Zucker^{fa/+}$ rats (n=12), Obese: sham-operated $Zucker^{fa/fa}$ rats (n=12), RYGB: Roux-en-Y gastric bypass surgery operated $Zucker^{fa/fa}$ obese rats (n=15), CR: body weight matched to RYGB group with caloric restriction of $Zucker^{fa/fa}$ obese rats (n=5).

4.1.2 Oxidative stress and genomic damage in kidneys of obese Zucker$^{fa/fa}$ rats

4.1.2.1 Oxidative stress

DHE staining on kidney cryosections was used to assess the oxidative stress status in different group of animals. The sham-operated Obese group exhibited significantly elevated oxidative stress compared to the Lean group. Weight loss either by gastric bypass surgery (RYGB group) or by caloric restriction (CR group) reduced the elevation of ROS production significantly compared to the Obese group. Representative pictures can be seen in **Figure 18**.

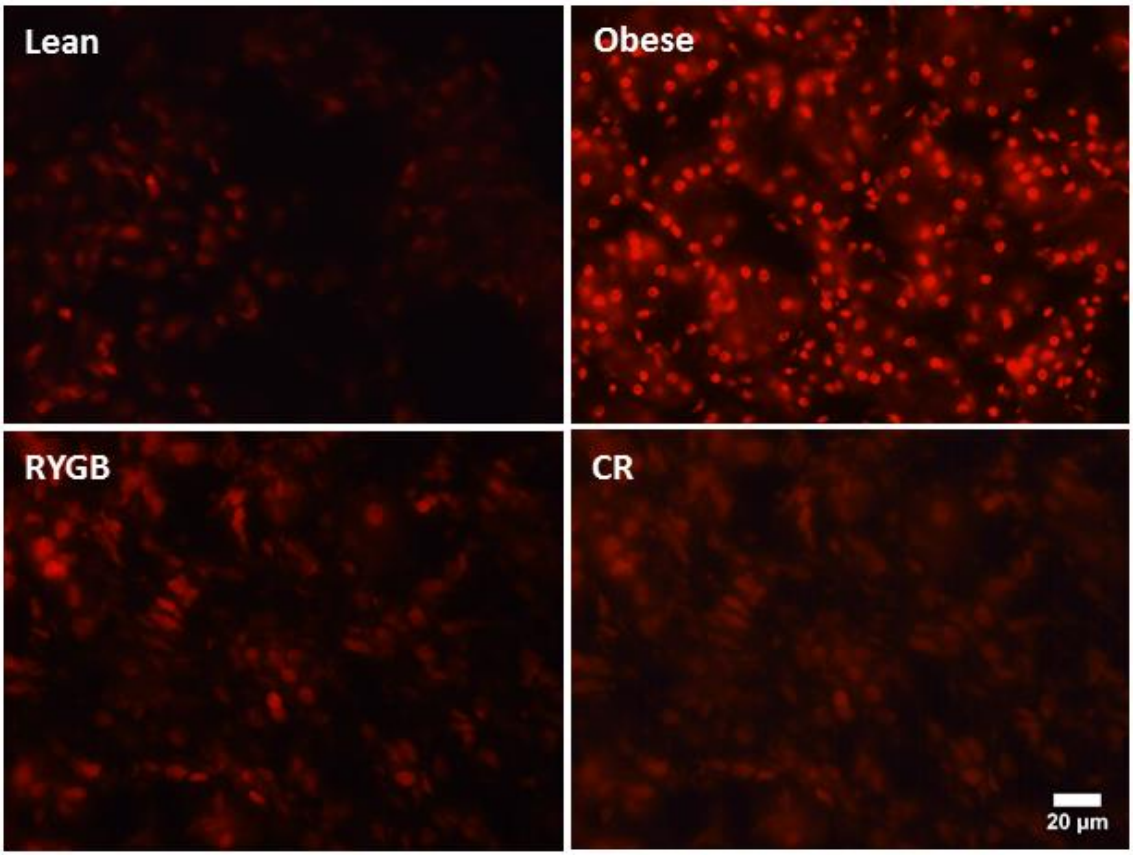

Figure 18: Representative pictures of DHE stained kidney sections are shown. ROS formation was visualized by staining 5 µm cryosections from kidney tissue of rats with the dye DHE.

The DHE fluorescence was quantified with imageJ and represented as mean grey value in **Figure 19**.

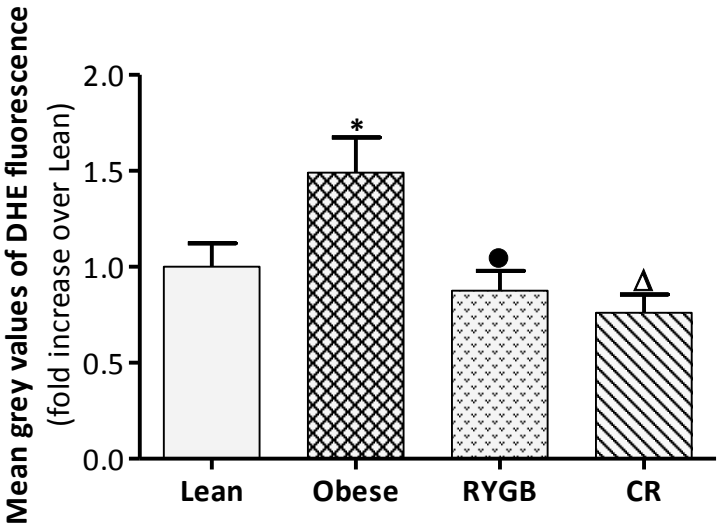

Figure 19: Detection of ROS in rat kidney by DHE staining. Quantification of DHE fluorescence was achieved by measuring the mean grey value of 200 cells using image j software. Data are presented as mean ± SEM. * p≤0.05 vs. Lean, Δ p≤0.05 vs. Obese and ● p≤0.01 vs. Obese. Lean: Zucker$^{fa/+}$ rats (n=12), Obese: sham-operated Zucker$^{fa/fa}$ rats (n=12), RYGB: Roux-en-Y gastric bypass surgery operated Zucker$^{fa/fa}$ obese rats (n=15), CR: body weight matched to RYGB group with caloric restriction of Zucker$^{fa/fa}$ obese rats (n=5).

4.1.2.2 Heat shock protein expression

Western blot analysis was performed to monitor the expression of heat shock protein 70 (HSP70) and heat shock protein 32 (also known as heme oxygenase-1; HO-1). HSP70 is considered as stress protein, and HO-1 is regarded as antioxidant enzyme (or stress response protein). Representative pictures of western blots can be seen in **Figure 20a** (HSP70) and **Figure 20b** (HO-1). Expression of HSP70 and HO-1 in kidneys of the sham-operated Obese rats was increased significantly compared to the Lean rats (**Figure 21**). Expression of HSP70 and HO-1 in the kidneys of the RYGB and the CR group were reduced compared to the Obese group.

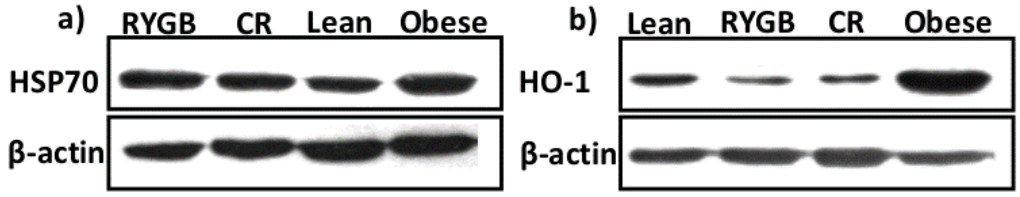

Figure 20: Photographs of representative western blots from HSP70 (**a**) and HO-1 (**b**) detection. Samples were applied to the gels in a coded manner; therefore, the sequence of the samples is not identical with the group sequence shown below in the quantification.

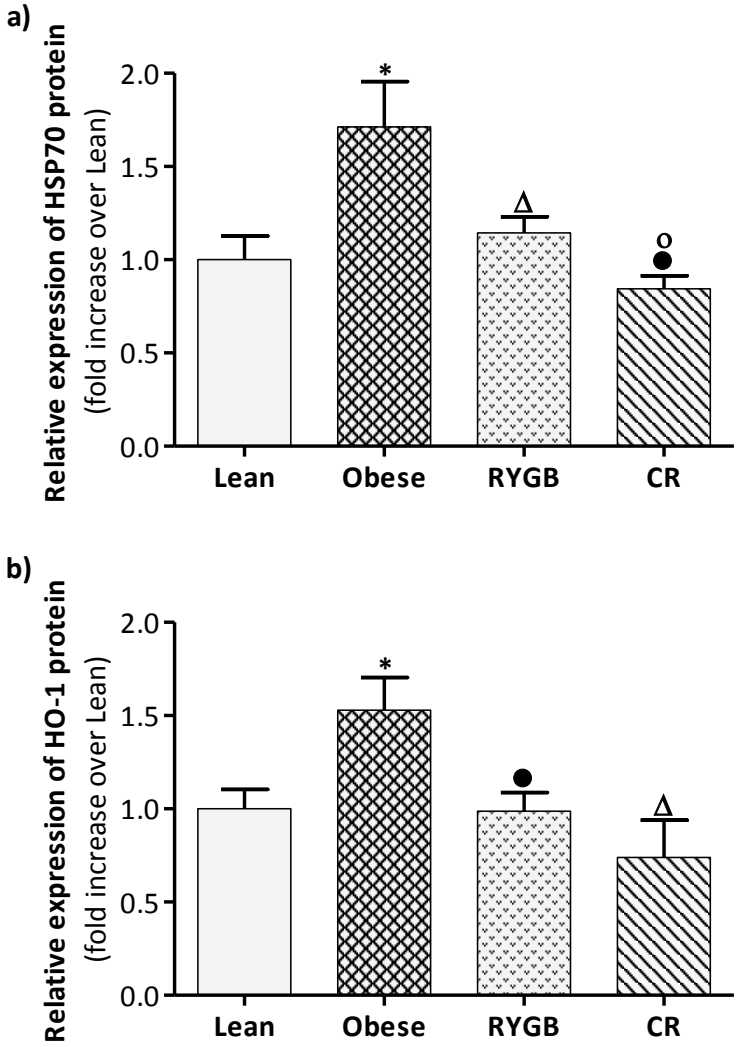

Figure 21: Expression of HSP70 (**a**) and antioxidant enzyme HO-1 (**b**) in rat kidney. Band intensity was quantified by image j and normalized to the endogenous control β-actin for HSP70 and HO-1. Data are presented as mean ± SEM. * p≤0.05 vs. Lean, ● p≤0.01 vs. Sham, Δ p≤0.05 vs. Sham and ○ p≤0.05 vs. RYGB. Lean: Zucker$^{fa/+}$ rats (n=12 for HSP70 and 11 for HO-1), Obese: sham-operated Zucker$^{fa/fa}$ rats (n=12 for HSP70 and 11 for HO-1), RYGB: Roux-en-Y gastric bypass surgery operated Zucker$^{fa/fa}$ obese rats (n=15), CR: body weight matched to RYGB group with caloric restriction of Zucker$^{fa/fa}$ obese rats (n=5).

4.1.2.3 DNA damage induction

Two different methods were used to monitor the genomic damage, the alkaline comet assay and γ-H2AX antibody staining.

The comet assay was used to investigate the DNA damage in freshly isolated primary kidney cells. There was no significant change in the percentage of viable cells among the groups (**Table 4**).

Table 4. Viability of the primary kidney cells after isolation.

Group	Viability (%)
Lean	90.53±3.062
Obese	86.17±4.12
RYGB	78.79±3.81
CR	78.60±3.83

Data are presented as mean viability ± SEM. Lean: Zucker$^{fa/+}$ rats (n=12), Obese: sham-operated Zucker$^{fa/fa}$ rats (n=12), RYGB: Roux-en-Y gastric bypass surgery operated Zucker$^{fa/fa}$ obese rats (n=14), CR: body weight matched to RYGB group with caloric restriction of Zucker$^{fa/fa}$ obese rats (n=5).

The sham-operated Obese rats showed an increase compared to the Lean group. Both weight reduction groups (RYGB and CR) exhibited a slight reduction in DNA damage compared to the Obese rats. However, the differences between the treatment groups were not significant due to the high standard deviation within the groups (**Figure 22**).

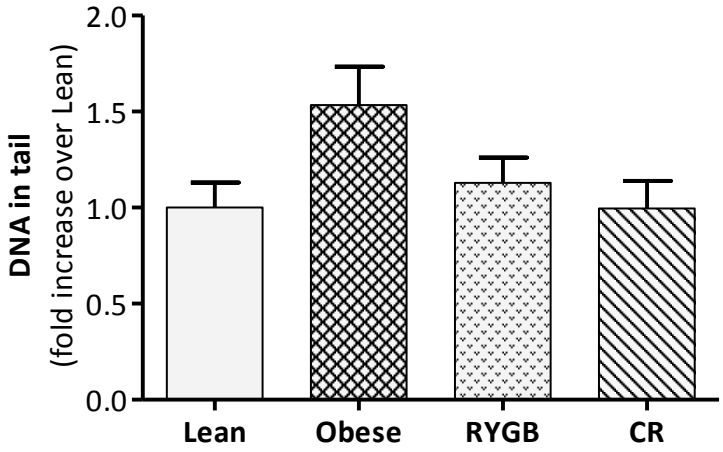

Figure 22: DNA damage in primary rat kidney cells measured by comet assay. Data are presented as mean of DNA damage as percentages of DNA in tail ± SEM. Lean: Zucker$^{fa/+}$ rats (n=12), Obese: sham-operated Zucker$^{fa/fa}$ rats (n=12), RYGB: Roux-en-Y gastric bypass surgery operated Zucker$^{fa/fa}$ obese rats (n=14), CR: body weight matched to RYGB group with caloric restriction of Zucker$^{fa/fa}$ obese rats (n=5).

An antibody staining was performed against γ-H2AX to monitor DNA double strand breaks in kidney sections. A representative picture of a γ-H2AX antibody staining can be seen in **Figure 23**.

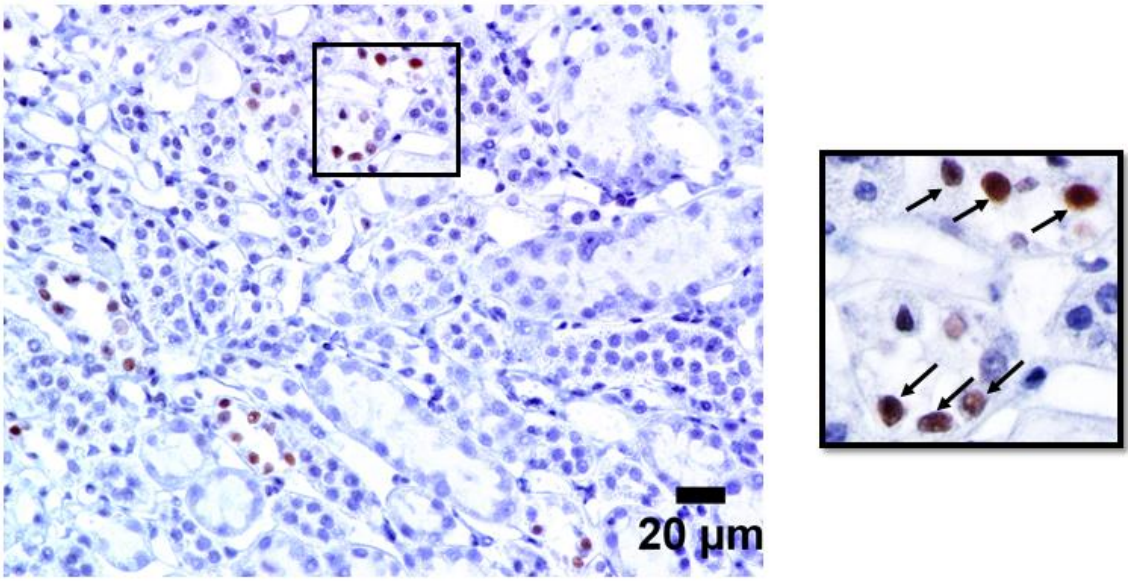

Figure 23: Representative picture of γ-H2AX antibody stained paraffin embedded kidney section of sham-operated obese rat. Brown colored cells, which are indicated by black arrows, represent γ-H2AX positive cells.

In the kidneys of the sham-operated Obese rats, a significant induction of DNA double strand breaks was observed compared to Lean rats and the weight loss (RYGB and CR groups) reduced the DNA double strand breaks to the level of the Lean group (**Figure 24**).

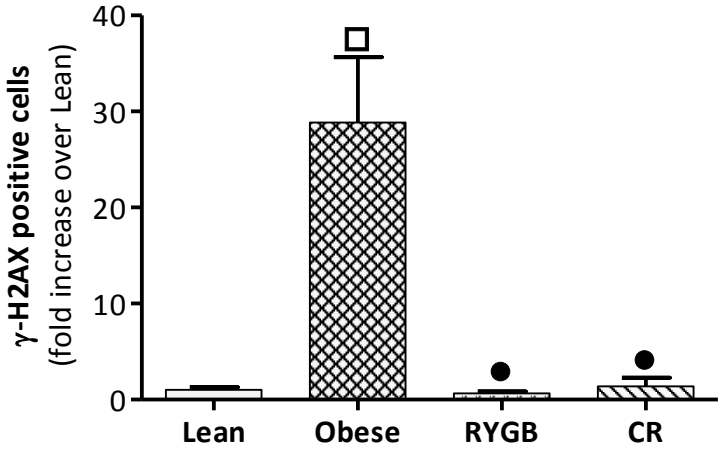

Figure 24: Detection of phosphorylated H2AX sites as DNA double strand break marker on paraffin embedded kidney sections. Quantification of kidney sections: total cell number in 15 to 20 photos were quantified per animal by image j. Data are presented as mean of γ-H2AX positive cells ± SEM. □ p≤0.01 vs. Lean and ● p≤0.01 vs. Obese. Lean: Zucker$^{fa/+}$ rats (n=12), Obese: sham-operated Zucker$^{fa/fa}$ rats (n=12), RYGB: Roux-en-Y gastric bypass surgery operated Zucker$^{fa/fa}$ obese rats (n=14) and CR: body weight matched to RYGB group with caloric restriction of Zucker$^{fa/fa}$ obese rats (n=4).

4.1.2.4 Correlation between DNA-damage and basal plasma insulin level

In the search for a possible connection between genomic damage and plasma insulin level, γ-H2AX positive cells were correlated with basal insulin levels (plasma insulin level at 120 min after beginning of OGTT, shortly before sacrificing the animals) for all Zucker$^{fa/fa}$ rats. The reason for including RYGB and CR was that even within these groups insulin levels were still higher than in healthy lean rats.

The DNA damage showed a positive correlation with the plasma insulin level in kidney with Spearman`s correlation coefficients of 0.525 ($p \leq 0.01$) (**Figure 25**).

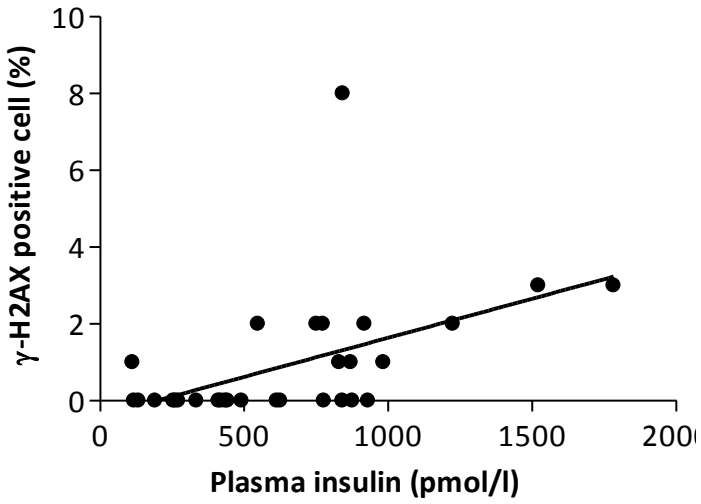

Figure 25: Correlation between the DNA damage marker γ-H2AX and the basal plasma insulin level (120 min of OGTT test, before sacrificing) in kidney. Data are presented as mean of γ-H2AX positive cell percentages ± SEM across all Zucker$^{fa/fa}$ rats (12 Obese, 14 RYGB and 4 CR).

4.1.3 Oxidative stress and genomic damage in livers of obese Zucker$^{fa/fa}$ rats

4.1.3.1 Oxidative stress

The level of oxidative stress was assessed by DHE staining in livers of Obese and Lean rats. Representative pictures can be seen in **Figure 26**.

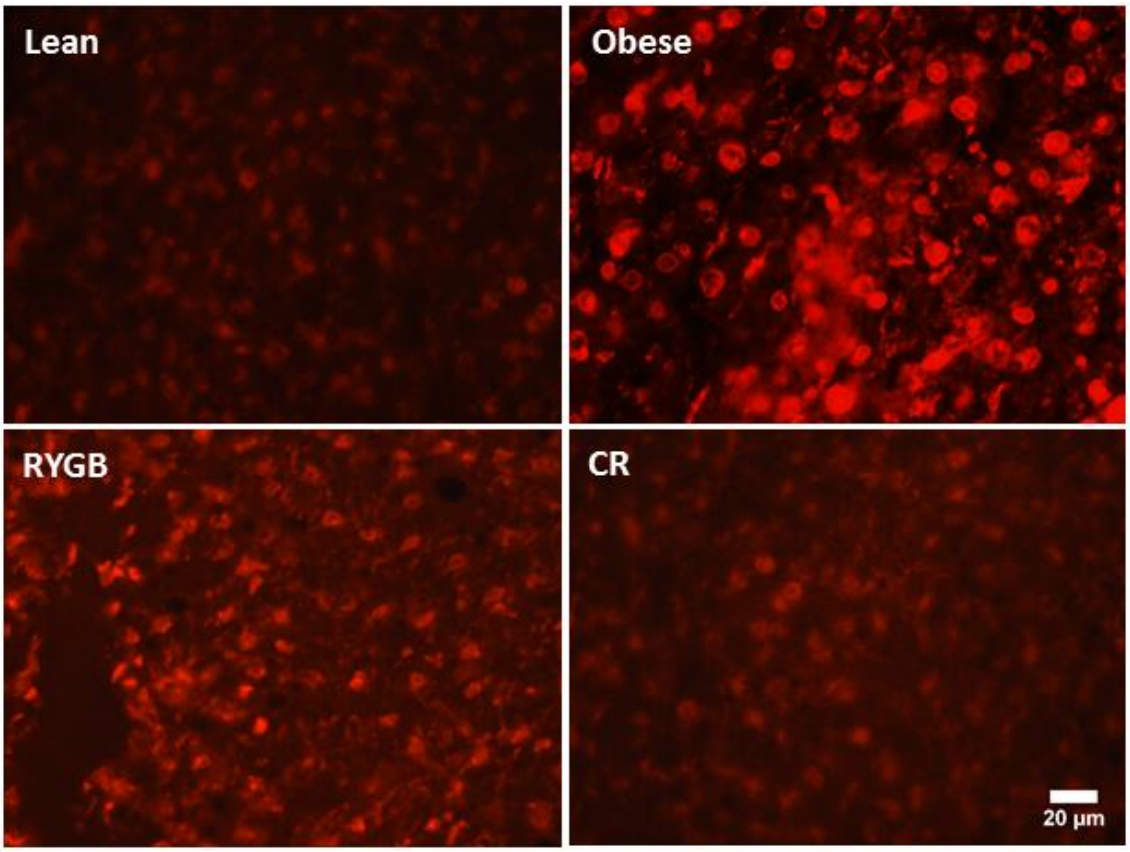

Figure 26: Representative pictures of DHE stained liver sections were shown. ROS formation was visualized by staining 5 µm cryosections from kidney tissue of rat with the dye DHE.

The DHE fluorescence was quantified with imageJ and represented as mean grey value in **Figure 27**. The sham-operated Obese group exhibited significantly elevated oxidative stress in liver compared to the Lean group. Weight loss either by gastric bypass surgery (RYGB group) or by caloric restriction (CR group) reduced the elevation of ROS production significantly compared to the Obese group.

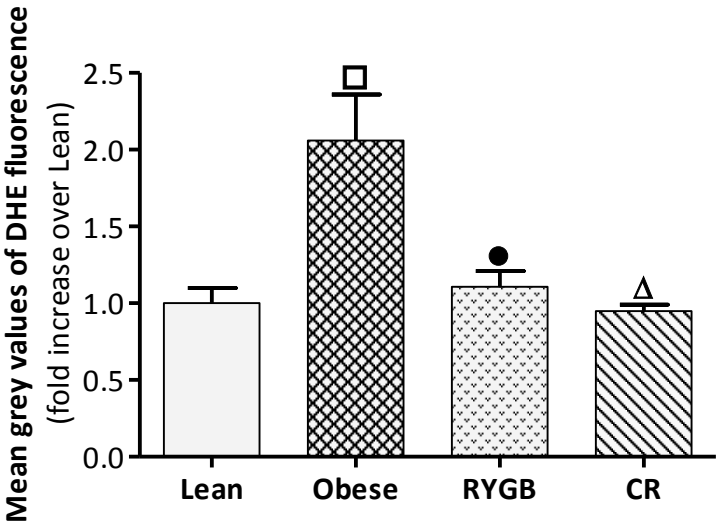

Figure 27: Detection of ROS in rat liver by DHE staining. Quantification of DHE fluorescence was achieved by measuring the mean grey value of 200 cells using image j software. Data are presented as mean ± SEM. □ p≤0.01 vs. Lean, Δ p≤0.05 vs. Obese and ● p≤0.01 vs. Obese. Lean: Zucker$^{fa/+}$ rats (n=12), Obese: sham-operated Zucker$^{fa/fa}$ rats (n=12), RYGB: Roux-en-Y gastric bypass surgery operated Zucker$^{fa/fa}$ obese rats (n=15), CR: body weight matched to RYGB group with caloric restriction of Zucker$^{fa/fa}$ obese rats (n=5).

4.1.3.2 Heat shock proteins expression

Western blot analysis was performed to monitor the expression of heat shock protein 70 (HSP70) and heat shock protein 32 (referred to as HO-1). Representative blots can be seen in **Figure 28a** and **b**.

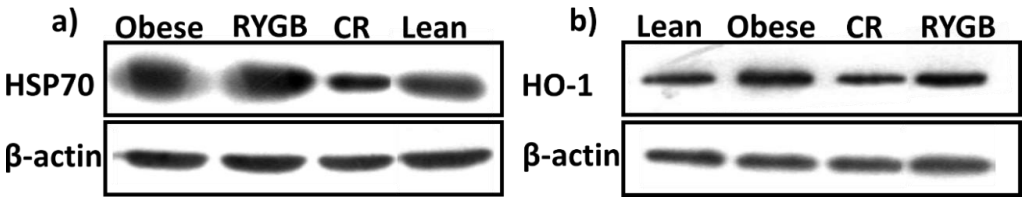

Figure 28: Photographs of representative western blots from HSP70 (**a**) and from HO-1 (**b**). Samples were applied to the gels in a coded manner; therefore, the sequence of the samples is not identical with the group sequence shown below in the quantification.

The expression of HSP70 in liver tissue did not show any significant difference (**Figure 29a**), but HO-1 expression exhibited a similar pattern to that of the kidneys (**Figure 29b**).

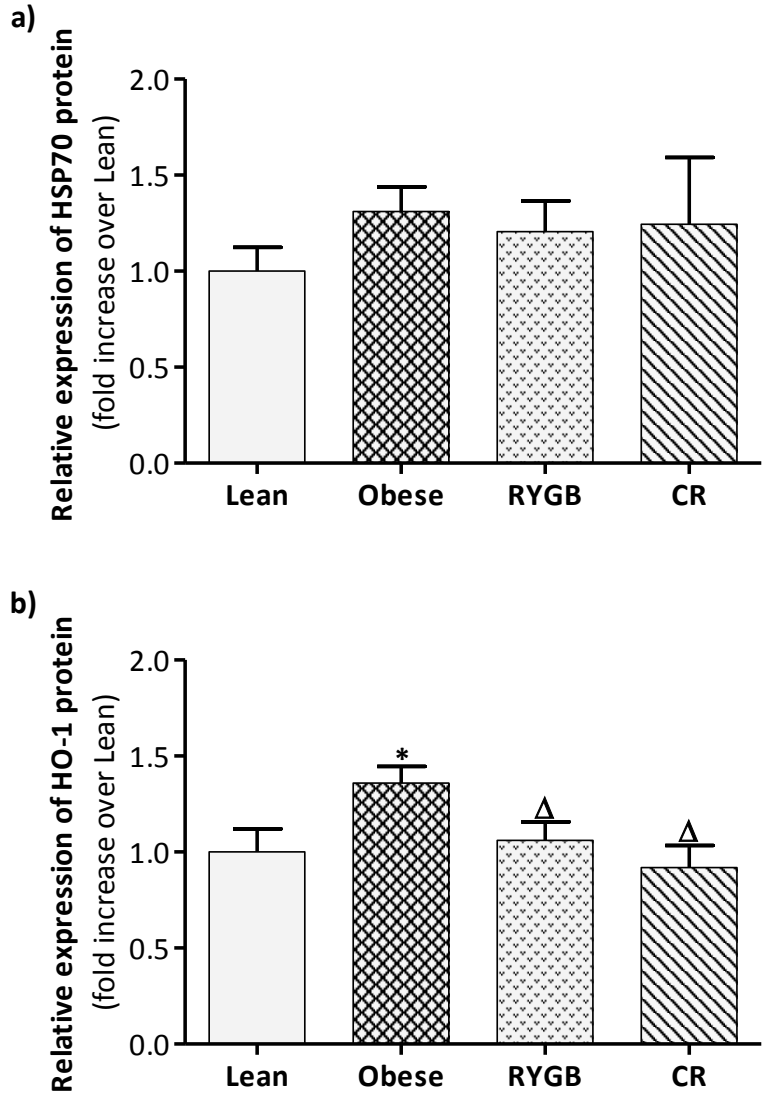

Figure 29: Expression of HSP70 (**a**) and antioxidant enzyme HO-1 (**b**) in rat liver. Band intensity was quantified by image j and normalized to the endogenous control β-actin for HSP70 and HO-1. Data are presented as mean ± SEM. * p≤0.05 vs. Lean and Δ p≤0.05 vs. Sham. Lean: Zucker$^{fa/+}$ rats (n=12), Obese: sham-operated Zucker$^{fa/fa}$ rats (n=12), RYGB: Roux-en-Y gastric bypass surgery operated Zucker$^{fa/fa}$ obese rats (n=15), CR: body weight matched to RYGB group with caloric restriction of Zucker$^{fa/fa}$ obese rats (n=5).

4.1.3.3 DNA damage induction

Two different methods were used to monitor the genomic instability, alkaline comet assay and γ-H2AX antibody staining.

The comet assay was used to investigate the DNA damage in freshly isolated primary liver cells. There was no significant change in the percentage of viable cell among the groups after isolation (**Table 5**).

Table 5. Viability of the primary liver cells after isolation.

Group	Viability (%)
Lean	92.33±2.09
Obese	89.05±3.00
RYGB	86.98±2.63
CR	85.20±3.75

Data are presented as mean viability ± SEM. Lean: Zucker$^{fa/+}$ rats (n=12), Obese: sham-operated Zucker$^{fa/fa}$ rats (n=12), RYGB: Roux-en-Y gastric bypass surgery operated Zucker$^{fa/fa}$ obese rats (n=14), CR: body weight matched to RYGB group with caloric restriction of Zucker$^{fa/fa}$ obese rats (n=5).

The sham-operated Obese rats showed a slight increase compared to the Lean group. Both weight reduction groups (RYGB and CR) exhibited a reduction in DNA damage compared to the Obese rats. However, the differences were not significant due to the high standard deviation within the groups (**Figure 30**).

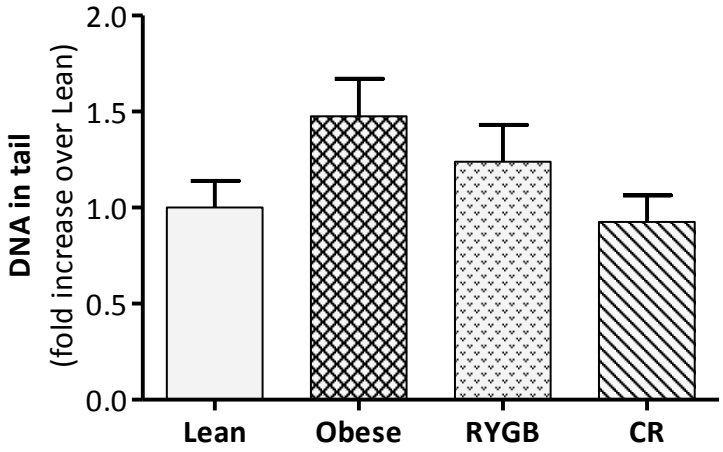

Figure 30: DNA damage in primary rat liver cells measured by comet assay. Data are presented as mean of DNA damage as percentages of DNA in tail ± SEM. Lean: Zucker$^{fa/+}$ rats (n=12), Obese: sham-operated Zucker$^{fa/fa}$ rats (n=12), RYGB: Roux-en-Y gastric bypass surgery operated Zucker$^{fa/fa}$ obese rats (n=14), CR: body weight matched to RYGB group with caloric restriction of Zucker$^{fa/fa}$ obese rats (n=5).

An antibody staining was performed against γ-H2AX to monitor DNA double strand breaks in liver sections. A representative picture of a γ-H2AX antibody staining can be seen in **Figure 31**.

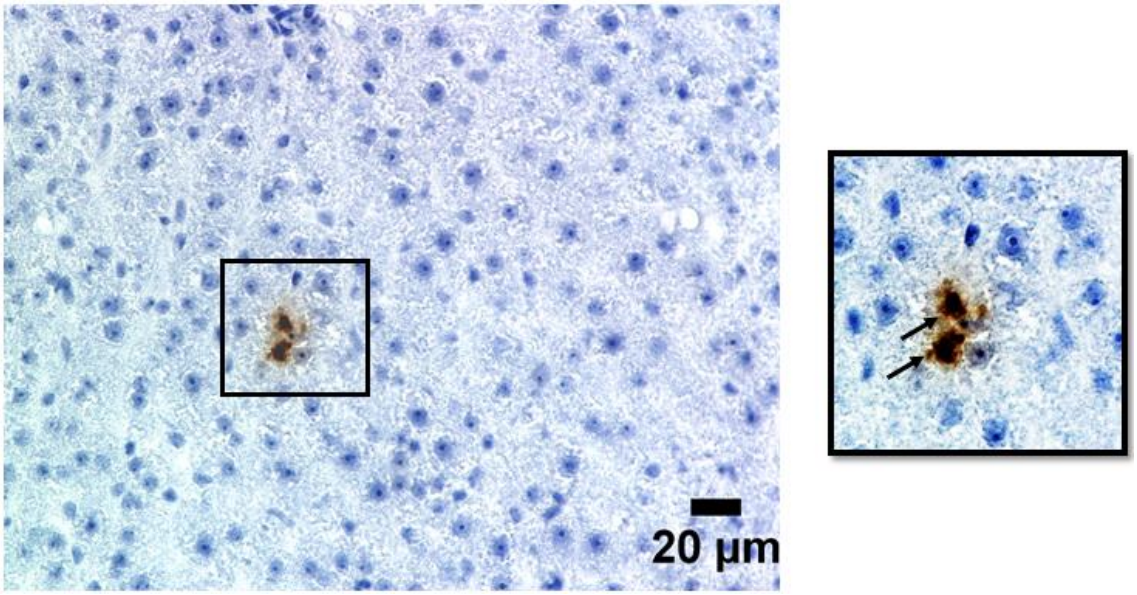

Figure 31: Representative picture of γ-H2AX antibody stained paraffin embedded liver section of sham-operated obese rat. Brown colored cells, which are indicated by black arrows, represent γ-H2AX positive cells.

In the livers of the sham-operated Obese rats, a significant induction of DNA double strand breaks was observed compared to Lean rats and weight loss (RYGB and CR groups) reduced the DNA double strand breaks to the level of the Lean group (**Figure 32**).

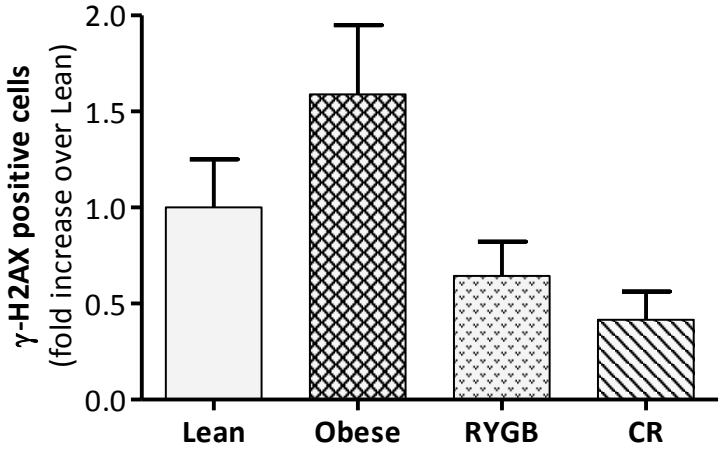

Figure 32: Detection of phosphorylated H2AX sites as DNA double strand break marker on paraffin embedded liver sections. Quantification of liver sections: 15 to 20 photos each were quantified per animal by image j. Data are presented as mean of γ-H2AX positive cells ± SEM. Lean: Zucker$^{fa/+}$ rats (n=12), Obese: sham-operated Zucker$^{fa/fa}$ rats (n=11), RYGB: Roux-en-Y gastric bypass surgery operated Zucker$^{fa/fa}$ obese rats (n=14) and CR: body weight matched to RYGB group with caloric restriction of Zucker$^{fa/fa}$ obese rats (n=5).

4.1.3.4 Correlation between DNA-damage and basal plasma insulin level

In the search for a possible connection between genomic damage and plasma insulin level, γ-H2AX positive cells were correlated with basal insulin levels (plasma insulin level at 120 min after beginning of OGTT, shortly before sacrificing the animals) for all Zucker$^{fa/fa}$ rats. The reason for including RYGB and CR was that even within these groups insulin levels were still higher than in healthy lean rats.

The DNA damage showed a positive correlation with the plasma insulin level in liver with a Spearman`s correlation coefficient of 0.475 ($p \leq 0.05$) (**Figure 33**).

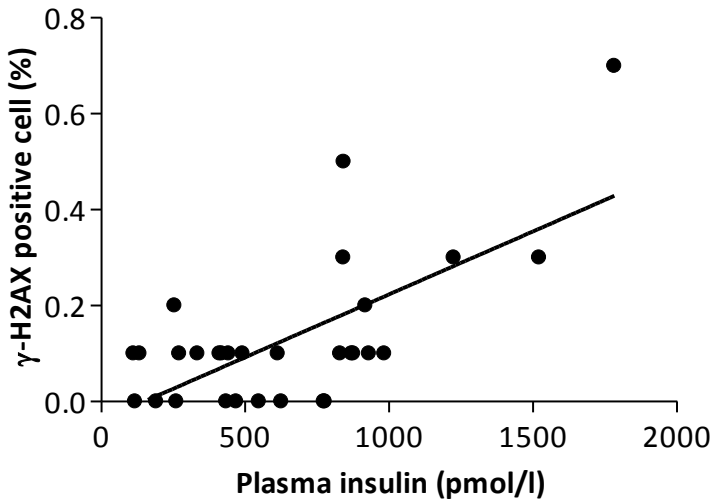

Figure 33: Correlation between the DNA damage marker γ-H2AX in liver and basal plasma insulin levels (120 min of OGTT test, before sacrificing). Data are presented as mean of γ-H2AX positive cell percentages ± SEM across all Zucker$^{fa/fa}$ rats (12 Obese, 14 RYGB and 4 CR).

4.1.4 Oxidative stress and genomic damage in colons of obese Zucker$^{fa/fa}$ rats

4.1.4.1 Oxidative stress

The level of oxidative stress was assessed by DHE staining of colon slices of Obese and Lean rats. Representative pictures of DHE stained cryosections from colon tissues can be found in **Figure 34**.

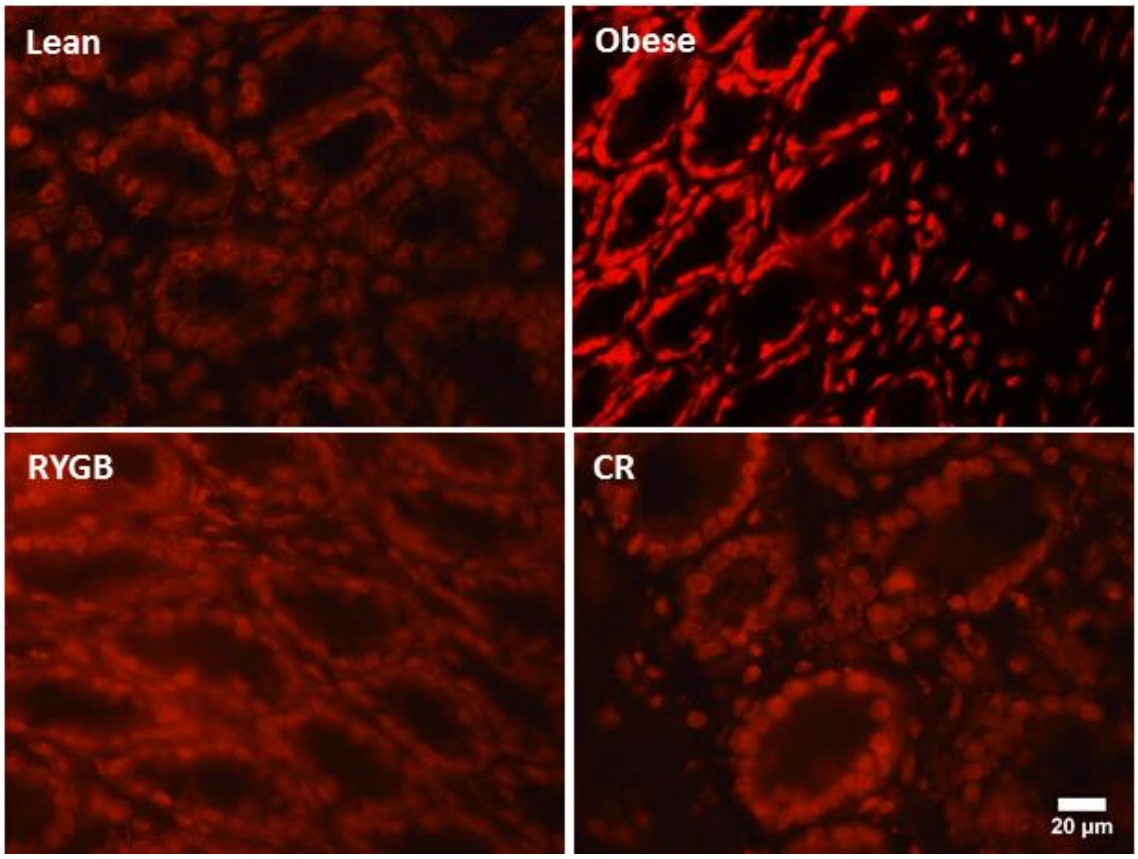

Figure 34: Representative pictures of DHE stained colon sections. ROS formation was visualized by staining 5 µm cryosections from colon tissue of rat with the dye DHE.

The sham-operated Obese group exhibited significantly elevated oxidative stress in colon compared to the Lean group. Weight loss either by gastric bypass surgery (RYGB group) or by caloric restriction (CR group) reduced the elevation of ROS production significantly compared to the Obese group (**Figure 35**).

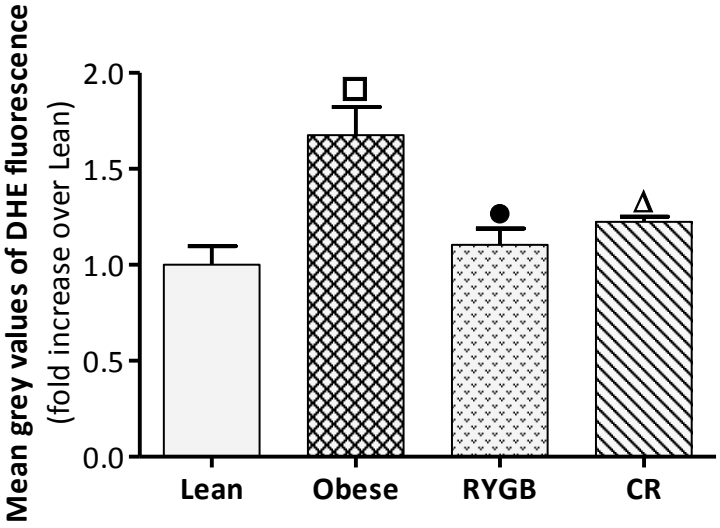

Figure 35: Detection of ROS in rat colon by DHE staining. Quantification of DHE fluorescence was achieved by measuring the mean grey value of 200 cells using image j software. Data are presented as mean ± SEM. □ p≤0.01 vs. Lean, Δ p≤0.05 vs. Obese and ● p≤0.01 vs. Obese. Lean: Zucker$^{fa/+}$ rats (n=12), Obese: sham-operated Zucker$^{fa/fa}$ rats (n=12), RYGB: Roux-en-Y gastric bypass surgery operated Zucker$^{fa/fa}$ obese rats (n=14), CR: body weight matched to RYGB group with caloric restriction of Zucker$^{fa/fa}$ obese rats (n=5).

4.1.4.2 Heat shock protein expression

Western blot analysis was performed to monitor the expression of heat shock protein 70 (HSP70) and heat shock protein 32, known as the antioxidant enzyme heme oxygenase-1 (HO-1). Representative blots can be seen in **Figure 36a** (HSP70) and **b** (HO-1).

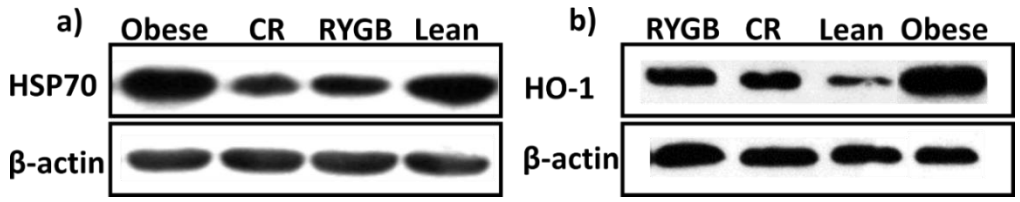

Figure 36: Photographs of representative western blots from HSP70 (**a**) and from HO-1 (**b**). Samples were applied to the gels in a coded manner; therefore, the sequence of the samples is not identical with the group sequence shown below in the quantification.

HSP70 expression in colon tissue showed a trend with a similar pattern to kidney, but no significant change (**Figure 37a**). HO-1 expression was altered significantly with a similar pattern to that observed in kidney and liver (**Figure 37b**).

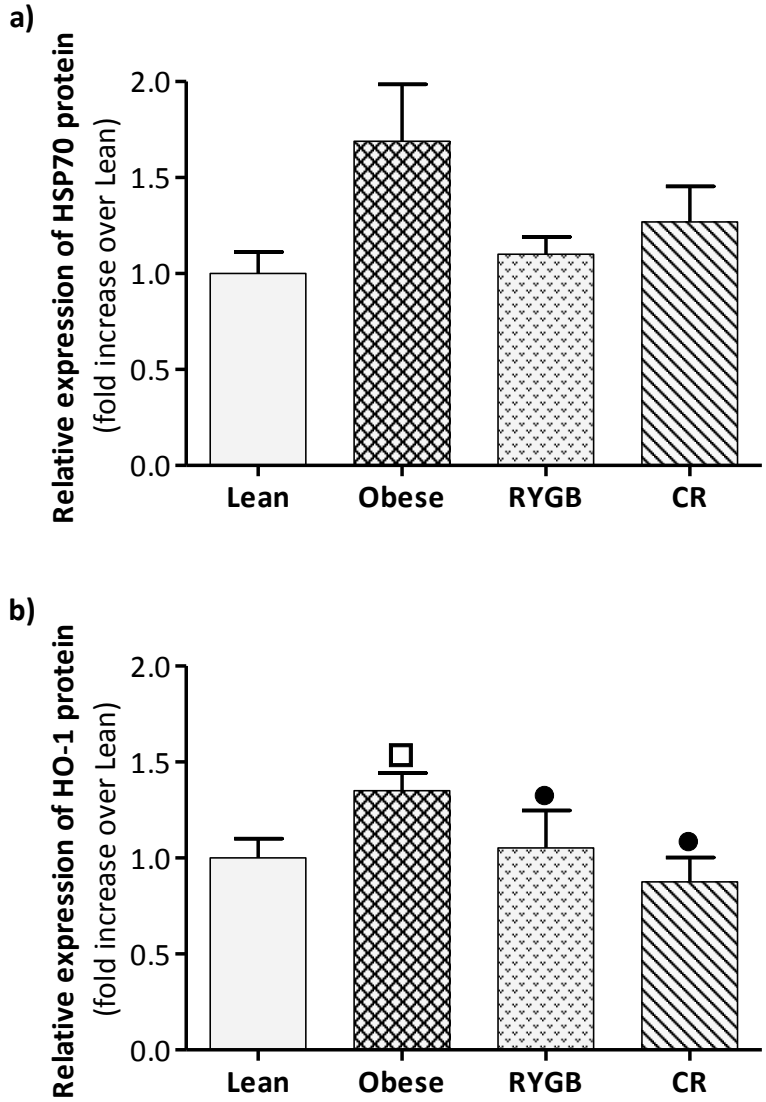

Figure 37: Expression of HSP70 (a) and antioxidant enzyme HO-1 (b) in rat colon. Band intensity was quantified by image j and normalized to the endogenous control β-actin for HSP70 and HO-1. Data are presented as mean ± SEM. □ p≤0.01 vs. Lean and ● p≤0.01 vs. Sham. Lean: Zucker$^{fa/+}$ rats (n=12), Obese: sham-operated Zucker$^{fa/fa}$ rats (n=12), RYGB: Roux-en-Y gastric bypass surgery operated Zucker$^{fa/fa}$ obese rats (n=13 for HSP70 and n=14 for HO-1), CR: body weight matched to RYGB group with caloric restriction of Zucker$^{fa/fa}$ obese rats (n=4 for HSP70 and n=5 for HO-1).

4.1.4.3 DNA damage induction

Two different methods were used to monitor the genomic instability, alkaline comet assay and γ-H2AX antibody staining.

The comet assay was used to investigate the DNA damage in freshly isolated primary colon cells. There was no significant change in the percentage of viable cells among the groups after isolation (**Table 6**).

Table 6. Viability of the primary colon cells after isolation.

Group	Viability (%)
Lean	93.21±2.21
Obese	89.56±2.88
RYGB	84.75±2.66
CR	80.60±1.78

Data are presented as mean viability ± SEM. Lean: Zucker$^{fa/+}$ rats (n=12), Obese: sham-operated Zucker$^{fa/fa}$ rats (n=12), RYGB: Roux-en-Y gastric bypass surgery operated Zucker$^{fa/fa}$ obese rats (n=14), CR: body weight matched to RYGB group with caloric restriction of Zucker$^{fa/fa}$ obese rats (n=5).

The sham-operated Obese rats showed a slight increase compared to Lean group. Both weight reduction groups (RYGB and CR) exhibited a slight reduction in DNA damage compared to the Obese rats. However, the differences were not significant due to the high standard deviation within the groups (**Figure 38**).

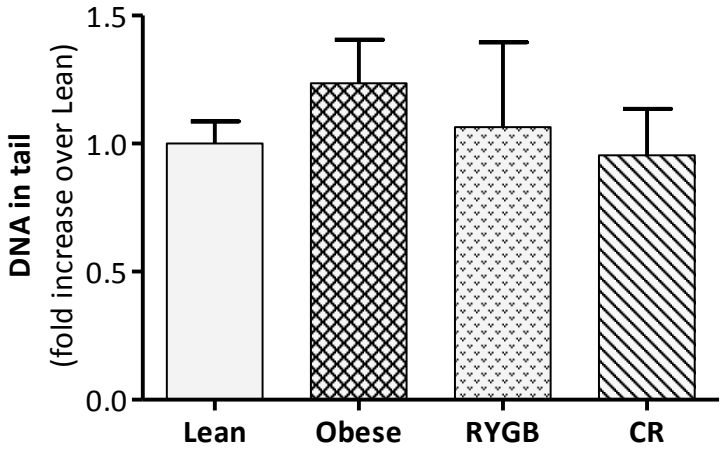

Figure 38: DNA damage in primary rat colon cells measured by comet assay. Data are presented as mean of DNA damage as percentages of DNA in tail ± SEM. Lean: Zucker$^{fa/+}$ rats (n=12), Obese: sham-operated Zucker$^{fa/fa}$ rats (n=12), RYGB: Roux-en-Y gastric bypass surgery operated Zucker$^{fa/fa}$ obese rats (n=14), CR: body weight matched to RYGB group with caloric restriction of Zucker$^{fa/fa}$ obese rats (n=5).

An antibody staining was performed against γ-H2AX to monitor DNA double strand breaks in colon tissue samples. A representative picture of a γ-H2AX antibody staining can be seen in **Figure 39**.

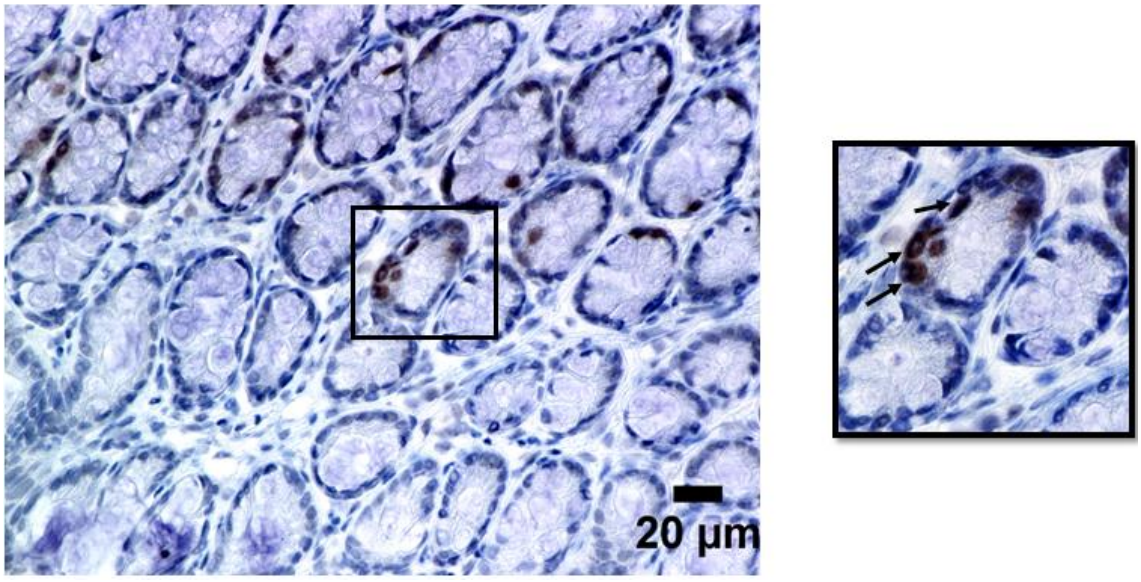

Figure 39: Representative picture of γ-H2AX antibody stained paraffin embedded colon section of sham-operated obese rat. Brown color cells, which are indicated by black arrows, represent γ-H2AX positive cells.

The amount of DNA double strand breaks in colon samples showed a significant increase in the sham-operated Obese group compared to the Lean animals and a significant reduction after the weight loss either by gastric bypass (RYGB group) or by caloric restriction (CR group) (**Figure 40**).

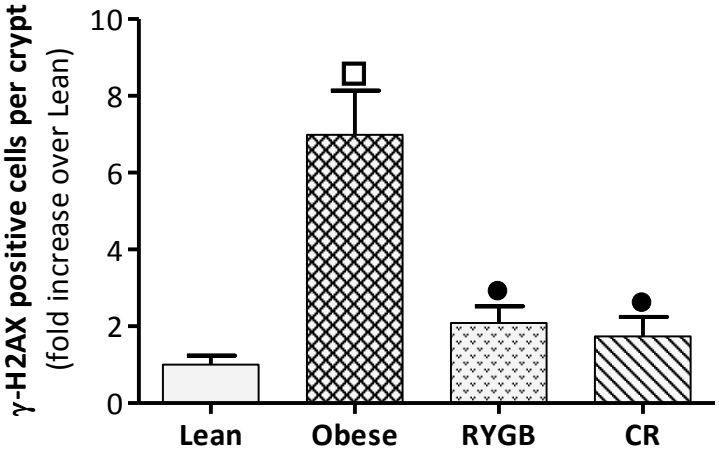

Figure 40: Detection of phosphorylated H2AX sites as DNA double strand break marker on paraffin embedded colon sections. Quantification of colon sections: 50 colon crypts were quantified per animal by image j. Data are presented as mean of γ-H2AX positive cells per crypt ± SEM. □ p≤0.01 vs. Lean and ● p≤0.01 vs. Sham. Lean: Zucker$^{fa/+}$ rats (n=11), Obese: sham-operated Zucker$^{fa/fa}$ rats (n=10), RYGB: Roux-en-Y gastric bypass surgery operated Zucker$^{fa/fa}$ obese rats (n=13) and CR: body weight matched to RYGB group with caloric restriction of Zucker$^{fa/fa}$ obese rats (n=4).

4.1.4.4 Correlation between DNA-damage and basal plasma insulin level

In the search for a possible connection between genomic damage and plasma insulin level, γ-H2AX positive cells were correlated with basal insulin levels (plasma insulin level at 120 min after beginning of OGTT, shortly before sacrificing the animals) for all Zucker$^{fa/fa}$ rats. The reason for including RYGB and CR was that even within these groups insulin levels were still higher than in healthy lean rats.

The DNA damage showed a positive correlation with the plasma insulin level (120 min of OGTT test, before sacrificing) in colon with a Spearman`s correlation coefficient of 0.634 ($p \leq 0.01$) (**Figure 41**).

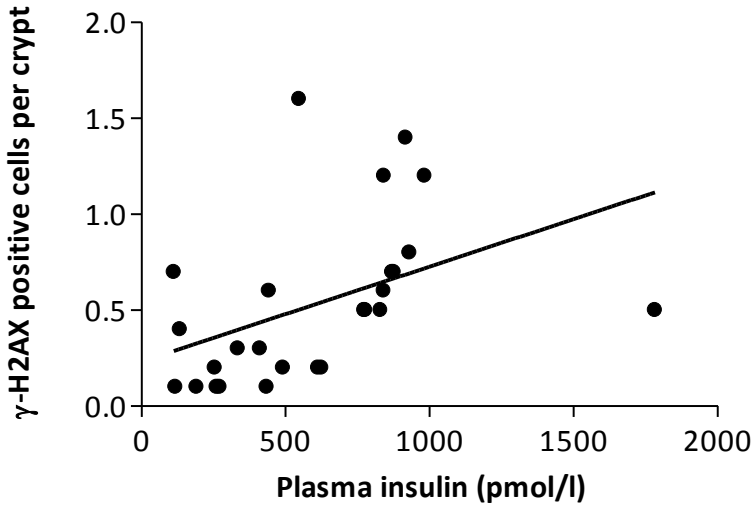

Figure 41: Correlation between the DNA damage marker γ-H2AX and basal plasma insulin level (120 min of OGTT test, before sacrificing) in colon. Data are presented as mean of γ-H2AX positive cells per crypt ± SEM across all Zucker$^{fa/fa}$ rats (9 Obese, 13 RYGB and 4 CR).

4.1.5 Urine analysis of obese Zucker$^{fa/fa}$ rats

4.1.5.1 Lipid peroxidation products

Due to the elevated ROS and the accumulation of fat tissue, lipid oxidation is one of the important concerns in obesity. Therefore, lipid peroxidation was measured in urine samples using the TBARS assay before and after the intervention (postoperative days 14, 21 and 27, after the intervention).

Before, the urinary lipid peroxidation products in Obese rats (assigned to the future sham-operated Obese, RYGB and CR groups) were elevated significantly compared to the Lean rats (**Figure 42**).

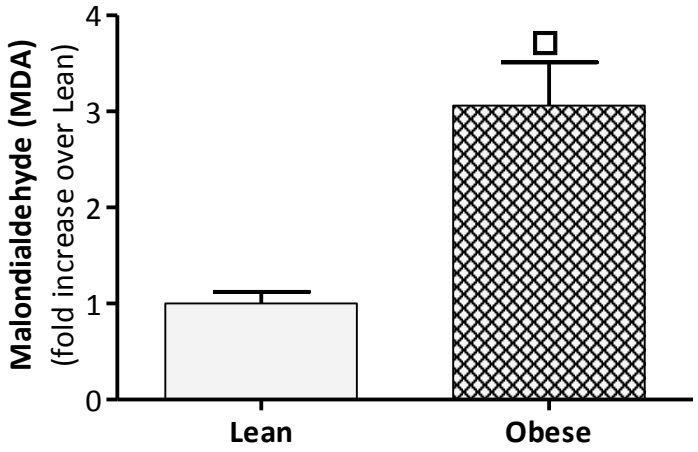

Figure 42: Detection of lipid peroxidation products by TBARS assay before the intervention. The results were normalized to the urinary creatinine concentration and displayed as malondialdehyde equivalents. Data were expressed as mean ± SEM. □ p≤0.01 vs. Lean. Lean: Zucker$^{fa/+}$ rats (n=5), Obese: 21 Zucker$^{fa/fa}$ obese rats (intended to constitute the sham-operated obese, RYGB, CR groups).

After the intervention, at three time points, the elevation of lipid peroxidation showed a similar pattern with some fluctuations.

Four week after intervention, the elevation of lipid peroxidation was still significant in the sham-operated Obese group compared to the Lean group and the weight loss reduced the lipid peroxidation in the RYGB and CR groups to the level of the Lean rats (**Figure 43a**, **b** and **c**).

Overall, lipid peroxidation products were elevated in Obese rats and were reduced by both methods of weight loss significantly.

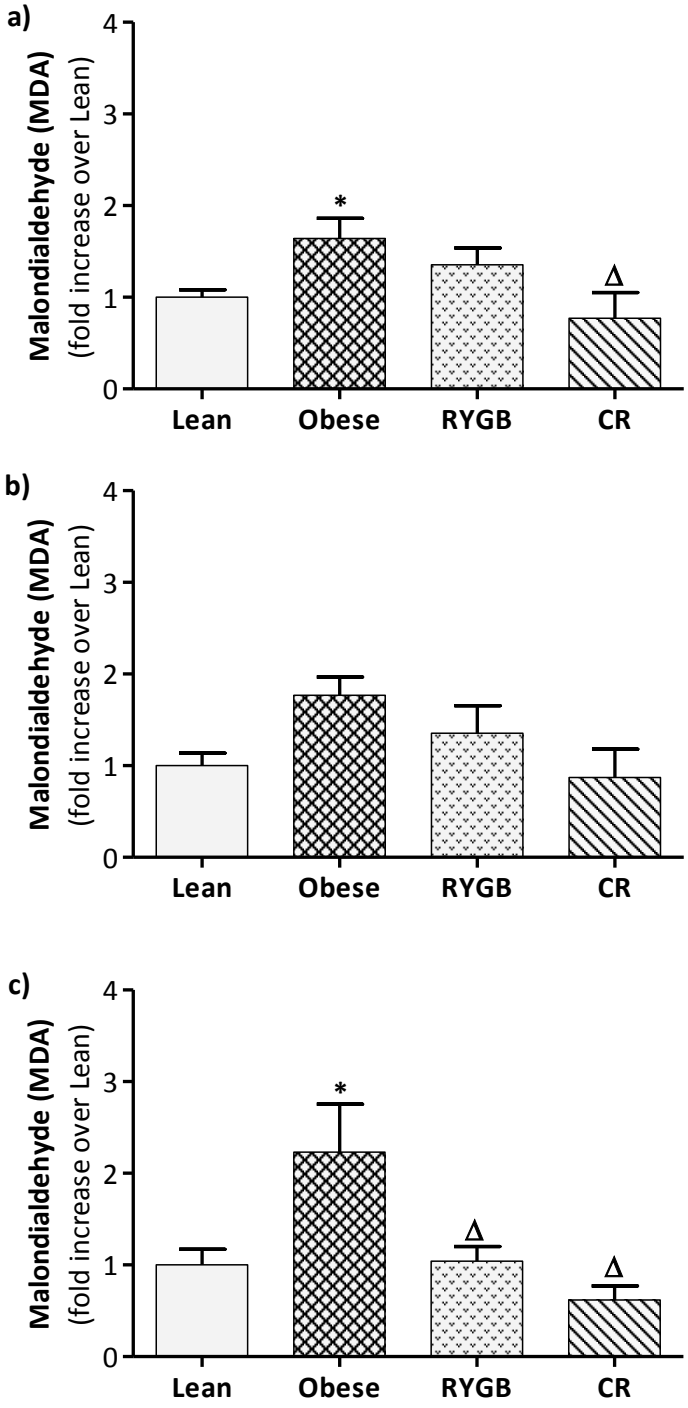

Figure 43: Detection of lipid peroxidation products by TBARS assay after the intervention. Urine samples were collected on 14th (**a**), 21st (**b**) and 27th (**c**) days during postoperative period. The results were normalized to the urinary creatinine concentration and displayed as malondialdehyde equivalents. Data were expressed as mean ± SEM. * p≤0.05 vs. Lean and Δ p≤0.05 vs. Obese. Lean: Zucker$^{fa/+}$ rats (n=12), Obese: sham-operated Zucker$^{fa/fa}$ obese rats (n=12), RYGB: Roux-en-Y gastric bypass surgery operated Zucker$^{fa/fa}$ obese rats (n=12) and CR: body weight matched to RYGB group with caloric restriction of Zucker$^{fa/fa}$ obese rats (n=5).

4.1.5.2 RNA oxidation biomarker

Oxidized RNA might impair the quality of expression of proteins and is an indicator for the oxidation of cellular nucleic acids. In this respect, the urinary excretion product 8-oxoGuo (oxidized RNA derived nucleoside) was analyzed by LC/MS/MS. Before the intervention (**Figure 44**), urinary excretion of 8-oxoGuo was significantly higher in Obese (sham-operated Obese, RYGB and CR groups) rats compared to the Lean group.

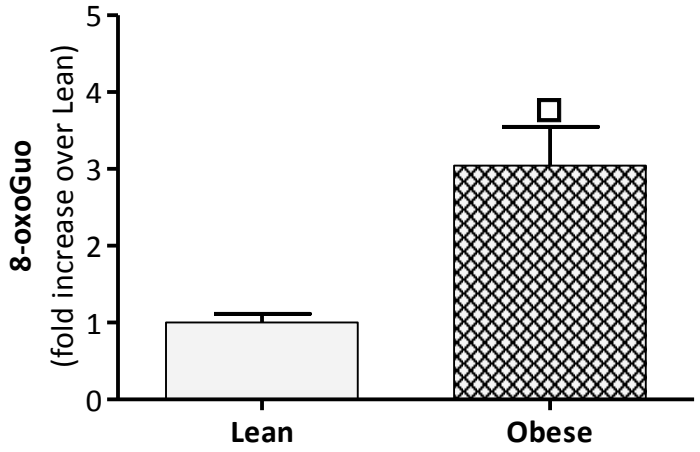

Figure 44: Urinary excretion product from RNA-oxidation (8-hydroxyguanosine; 8-oxoGuo) measured by LC/MS/MS. Urine samples were collected before the intervention and 8-oxoGuo was determined. The results were normalized to the urinary creatinine concentration. Data are presented as mean ± SEM. □ p≤0.01 vs. Lean. Lean: Zucker$^{fa/+}$ rats (n=5), Obese: 21 Zucker$^{fa/fa}$ obese rats (intended to constitute the sham-operated Obese, RYGB, CR groups).

After intervention, sham-operated Obese rats exhibited significant elevation in urinary excretion of 8-oxoGuo compared to the Lean rats. Between the 14th postoperative day and 27th day, Obese rats showed a further increase in urinary excretion of 8-oxoGuo. The elevation in the urinary excretion of 8-oxoGuo was significantly reduced after the weight loss either with gastric bypass (RYGB group) or with caloric restriction (CR group). Reduction in the urinary 8-oxoGuo excretion of caloric restriction group was already significant on the 14th post-operative day. However, RYGB group showed slight reduction in the excretion of 8-oxoGuo over the time and it was significant on the 27th post-operative day (**Figure 45a**, **b** and **c**).

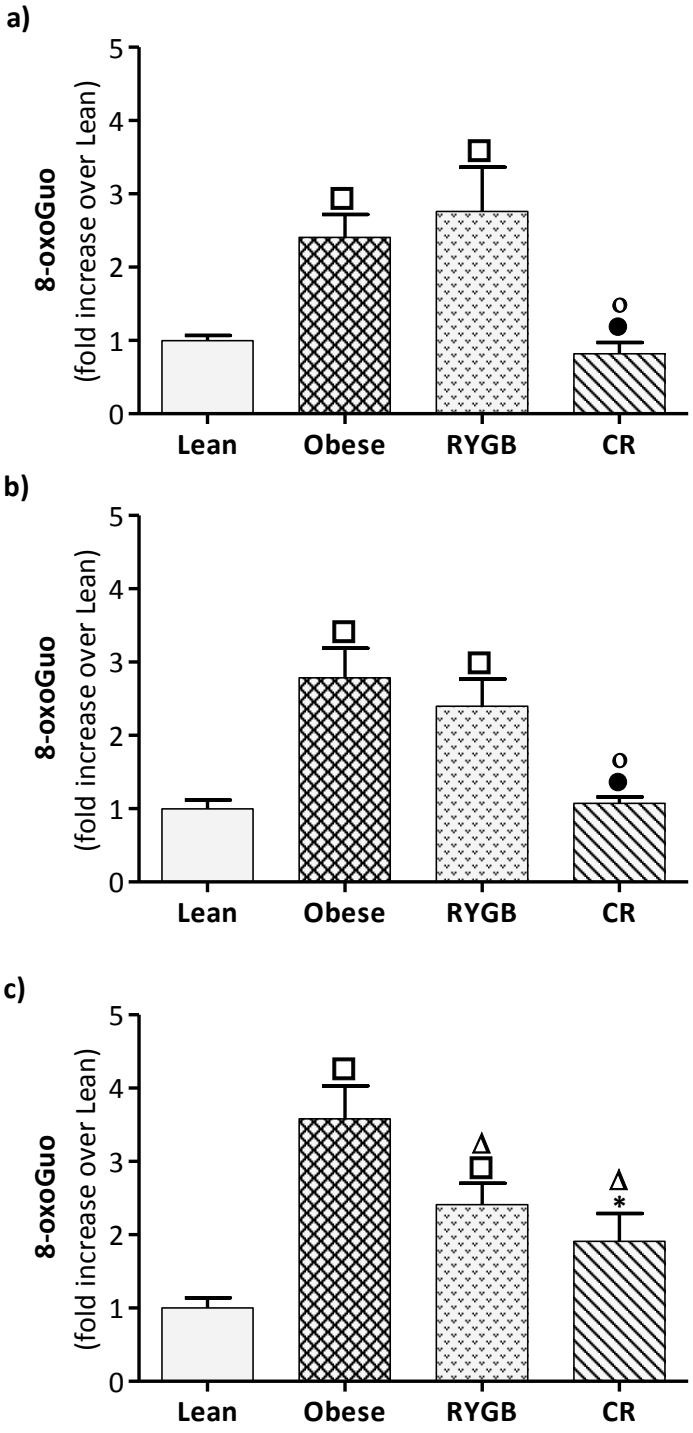

Figure 45: Urinary excretion product from RNA-oxidation (8-hydroxyguanosine; 8-oxoGuo) measured by LC/MS/MS. Urine samples were collected on 14th (**a**), 21st (**b**) and 27th (**c**) days during postoperative period. The results were normalized to the urinary creatinine concentration. Data are presented as mean ± SEM. □ p≤0.01 vs. Lean, * p≤0.05 vs. Lean, Δ p≤0.05 vs. Obese, ● p≤0.01 vs. Obese and ○ p≤0.05 vs. RYGB. Lean: Zucker$^{fa/+}$ rats (n=12), Obese: sham-operated Zucker$^{fa/fa}$ obese rats (n=12), RYGB: Roux-en-Y gastric bypass surgery operated Zucker$^{fa/fa}$ obese rats (n=13) and CR: body weight matched to RYGB group with caloric restriction of Zucker$^{fa/fa}$ obese rats (n=5).

4.1.5.3 DNA oxidation biomarkers

Oxidation of DNA is an important link between oxidative stress and cancer risk. Among the four DNA bases, guanine is more prone to oxidation than the other ones. In this respect, the urinary excretion products 8-oxoGua (oxidized DNA derived base) and 8-oxodG (oxidized DNA derived nucleoside) were analyzed by LC/MS/MS. Before the intervention (**Figure 46**), urinary excretion of 8-oxodG was increased in Obese rats compared to the Lean group, but the difference was not significant. 8-oxoGua was significantly higher in the Obese rats compared to the Lean group.

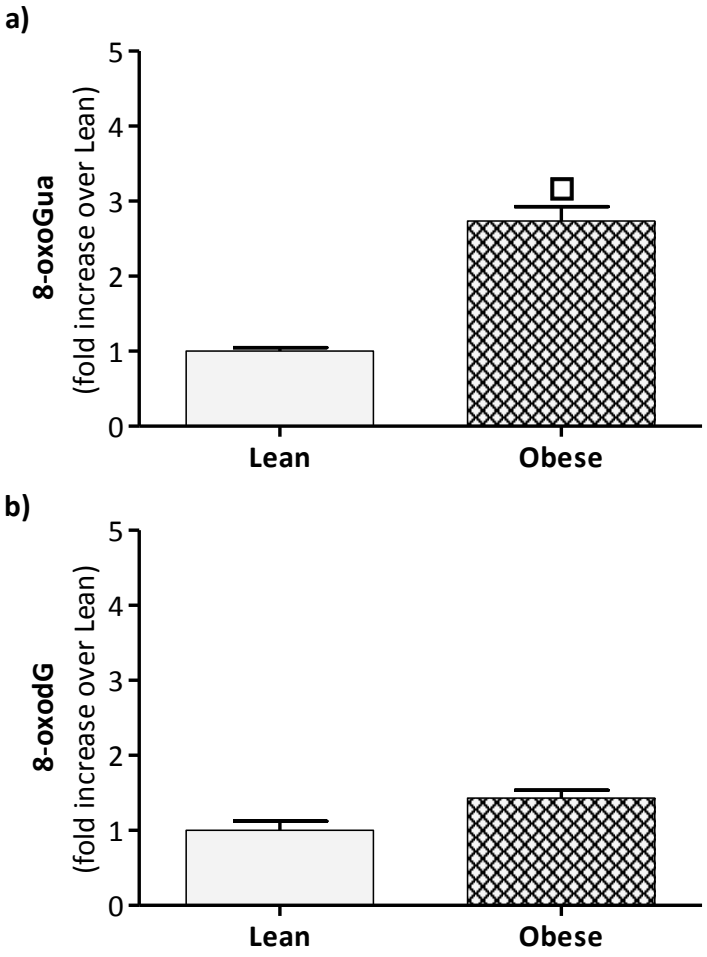

Figure 46: Urinary excretion products from DNA oxidation measured by LC/MS/MS. Urine samples were collected before the intervention. 8-hydroxyguanine (8-oxoGua) (**a**) and 8-hydroxydeoxyguanosine (8-oxodG) (**b**) were determined and the results normalized to the urinary creatinine concentration. Data are presented as mean ± SEM □ $p \leq 0.01$ vs. Lean. Lean: Zucker$^{fa/+}$ rats (n=5), Obese: 21 Zucker$^{fa/fa}$ obese rats (assigned to the later sham-operated Obese, RYGB, CR groups).

The excretion of urinary 8-oxodG in Obese rats increased slowly over time and became significant on the 14th postoperative day. On the 14th postoperative day after the intervention, CR group showed a slight, but not significant reduction in urinary 8-oxodG level. However, RYGB did not show any reduction. On the other hand, the urinary 8-oxoGua level in RYGB group showed a slight reduction on the 14th postoperative day (**Figure 47**).

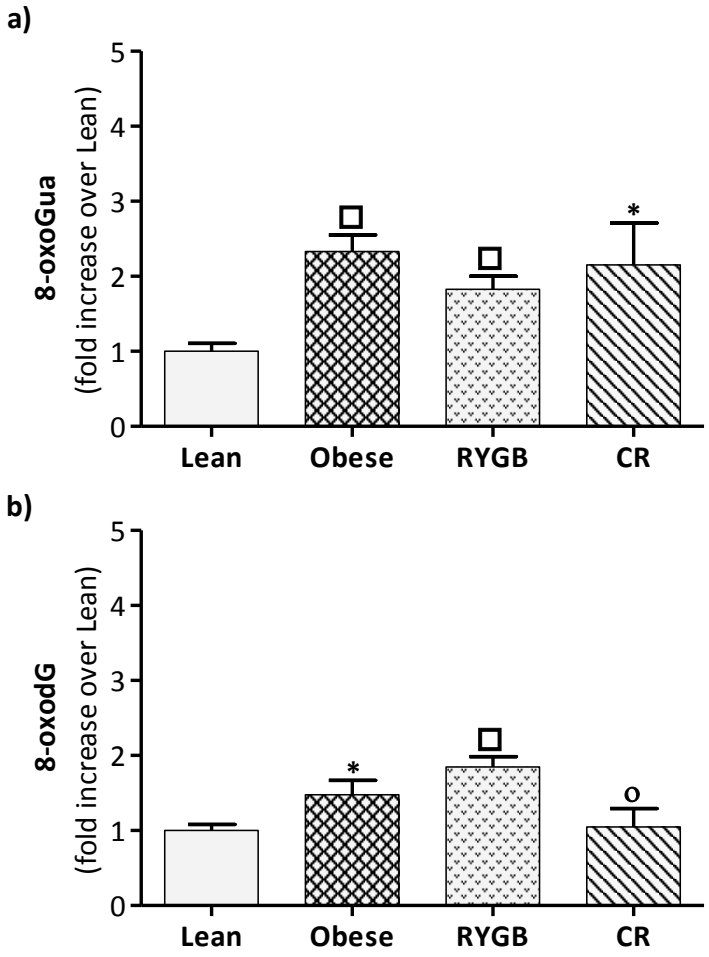

Figure 47: Urinary excretion products from DNA measured by LC/MS/MS. Urine samples were collected on 14th post-operative day. 8-hydroxyguanine (8-oxoGua) (**a**) and 8-hydroxydeoxyguanosine (8-oxodG) (**b**) were determined. The results were normalized to the urinary creatinine concentration. Data are presented as mean ± SEM. □ p≤0.01 vs. Lean, * p≤0.05 vs. Lean and ○ p≤0.05 vs. RYGB. Lean: Zucker$^{fa/+}$ rats (n=12), Obese: sham-operated Zucker$^{fa/fa}$ obese rats (n=12), RYGB: Roux-en-Y gastric bypass surgery operated Zucker$^{fa/fa}$ obese rats (n=13) and CR: body weight matched to RYGB group with caloric restriction of Zucker$^{fa/fa}$ obese rats (n=5).

On the 21st postoperative day, the increase in the urinary 8-oxoGua and 8-oxodG levels rose further in Obese rats. In RYGB and CR groups, urinary 8-oxoGua level reduced compared to the Obese group. However, weight loss (either by RYGB or by CR) did not lead to any significant reduction in urinary 8-oxodG excretion on the 21st postoperative day **Figure 48**.

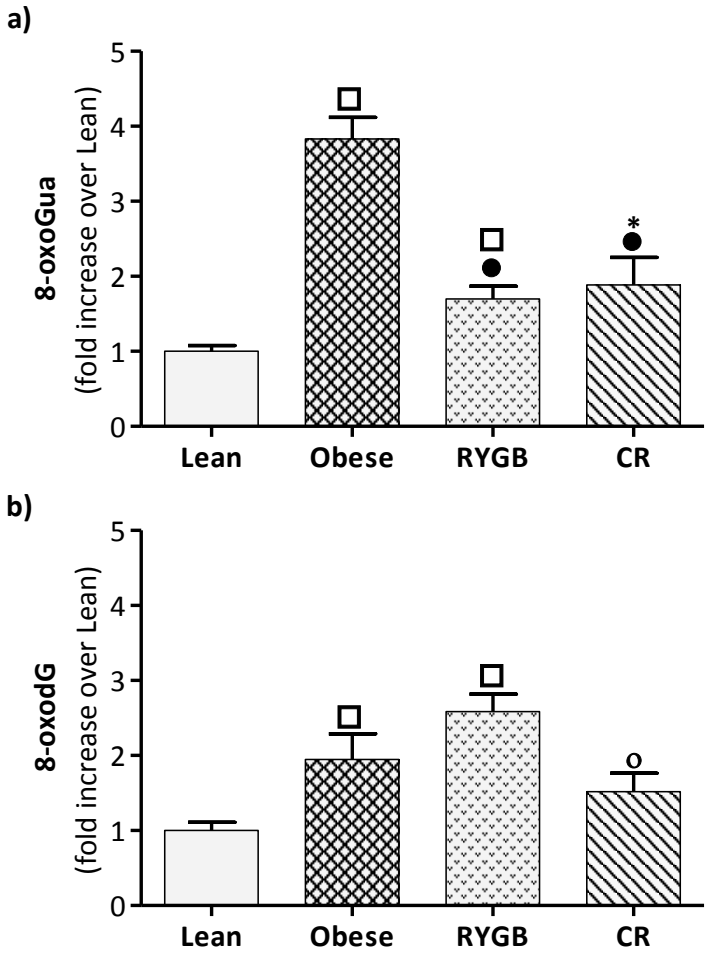

Figure 48: Urinary excretion products from DNA measured by LC/MS/MS. Urine samples were collected on 21st post-operative day. 8-hydroxyguanine (8-oxoGua) (**a**) and 8-hydroxydeoxyguanosine (8-oxodG) (**b**) were determined. The results were normalized to the urinary creatinine concentration. Data are presented as mean ± SEM. □ p≤0.01 vs. Lean, * p≤0.05 vs. Lean, ● p≤0.01 vs. Obese and ○ p≤0.05 vs. RYGB. Lean: Zucker$^{fa/+}$ rats (n=12), Obese: sham-operated Zucker$^{fa/fa}$ obese rats (n=12), RYGB: Roux-en-Y gastric bypass surgery operated Zucker$^{fa/fa}$ obese rats (n=13) and CR: body weight matched to RYGB group with caloric restriction of Zucker$^{fa/fa}$ obese rats (n=5).

At the end of the study, (**Figure 49**) Obese rats exhibited significant elevation in urinary excretion of 8-oxoGua and 8-oxodG compared to the Lean rats. The excretion of 8-oxodG in urine was raised further after the gastric bypass surgery (RYGB group). The rats in the CR group showed a significant reduction in urinary 8-oxodG compared to the rats in the Obese and RYGB groups.

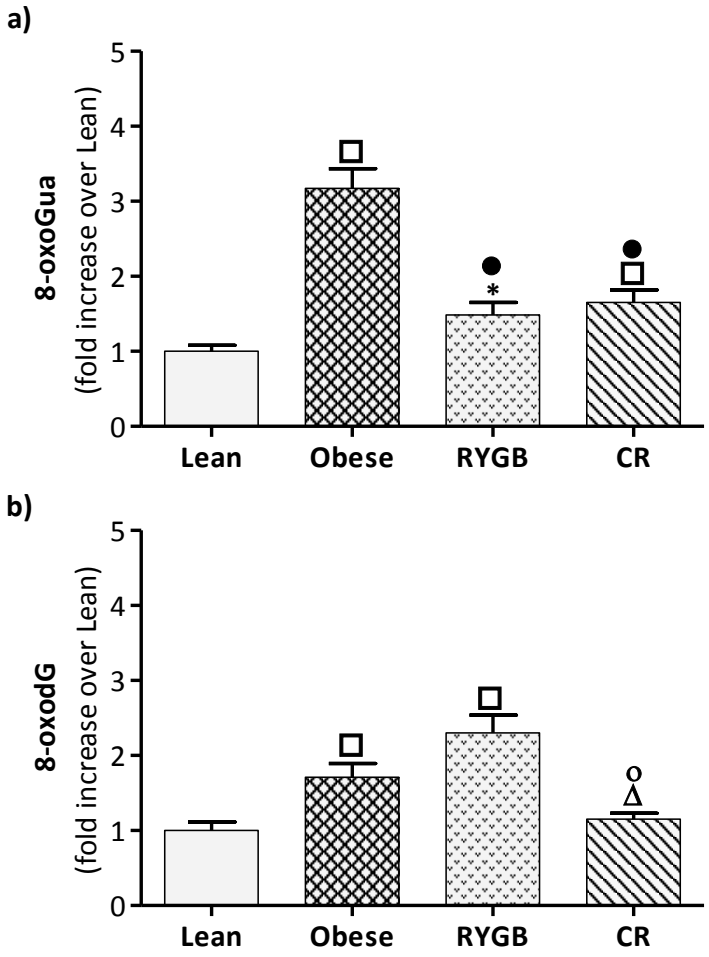

Figure 49: Urinary excretion products from DNA measured by LC/MS/MS. Urine samples were collected on 27th post-operative day. 8-hydroxyguanine (8-oxoGua) (**a**) and 8-hydroxydeoxyguanosine (8-oxodG) (**b**) were determined. The results were normalized to the urinary creatinine concentration. Data are presented as mean ± SEM. □ p≤0.01 vs. Lean, * p≤0.05 vs. Lean, ● p≤0.01 vs. Obese, Δ p≤0.05 vs. Obese and ○ p≤0.05 vs. RYGB. Lean: Zucker$^{fa/+}$ rats (n=12), Obese: sham-operated Zucker$^{fa/fa}$ obese rats (n=12), RYGB: Roux-en-Y gastric bypass surgery operated Zucker$^{fa/fa}$ obese rats (n=13) and CR: body weight matched to RYGB group with caloric restriction of Zucker$^{fa/fa}$ obese rats (n=5).

Altogether, 8-oxoGua and 8-oxodG showed elevation in the Obese group in comparison with the Lean group. The elevation in the urinary excretion of 8-oxoGua was significantly reduced after the weight loss either with gastric bypass (RYGB group) or with caloric restriction (CR group), while it was increased after RYGB.

4.2 Results of insulin-mediated oxidative stress and genomic damage

Since insulin turned out to be a possible cause for the obesity mediated genomic damage, the mechanistic pathway of insulin mediated DNA damage became of interest. A major switch in the regulation of cellular insulin mediated activity is Pten, also known as tumor suppressor gene. Physiologically, it inhibits the activation of insulin dependent reaction cascades. We therefore investigated in a cell line in vitro whether inhibition of Pten activity would result in an increased genomic damage caused by insulin.

4.2.1 Modulation of insulin mediated oxidative stress and genomic damage *in vitro*

4.2.1.1 Insulin induced oxidative stress in immortalized human hepatocytes

DHE staining was applied to monitor intracellular ROS after treating the cells with 10 and 100 nM of insulin for 30 min with and without the addition of the Pten-inhibitor VO-OHpic (50 nM). As seen in **Figure 50**, insulin treatment caused an increase in red colour intensity. The intensity was further enhanced by addition of the Pten-inhibitor. Quantification of the staining intensity is shown in **Figure 51**. Treatment with 10 and 100 nM insulin caused significant induction of ROS. The combination of the Pten inhibitor with 100 nM insulin yielded a significant increase in ROS formation compared to the 100 nM insulin treated cells.

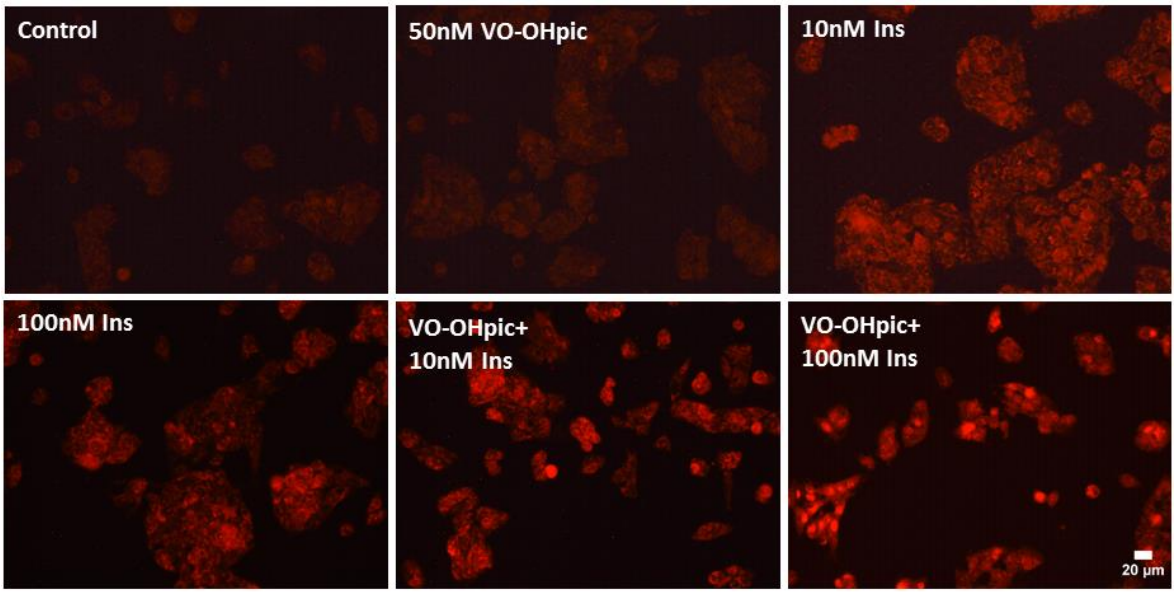

Figure 50: Representative pictures of DHE stained IHH cells. ROS formation is visualized by staining IHH cells with the dye DHE. VO-OHpic: Pten inhibitor and Ins: Insulin.

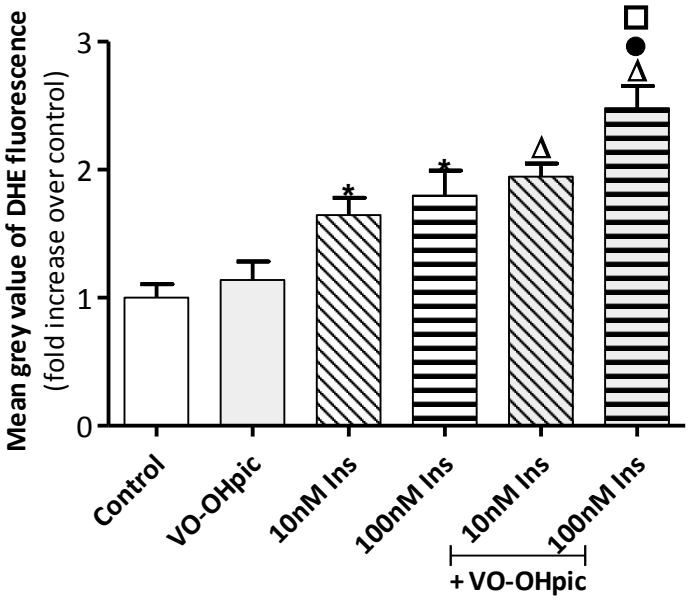

Figure 51: Intracellular oxidative stress induction by insulin treatment with or without addition of the Pten inhibitor VO-OHpic. Pten inhibition was achieved by adding the Pten inhibitor 15 min prior to the insulin treatment. ROS were measured after 30 min treatment with insulin with and without the presence of Pten inhibitor VO-OHpic. Quantification of DHE fluorescence was done by measuring the mean grey value of 250 cells using image j software. Data are presented as mean ± SEM of 5 independent experiments. * p≤0.05 vs. Control, Δ p≤0.05 vs. VO-OHpic, ○ p≤0.05 vs. 10 nM insulin, ● p≤0.05 vs. 100 nM insulin and □ p≤0.05 vs. VO-OHpic + 10 nM insulin. VO-OHpic: Pten inhibitor and Ins: Insulin.

4.2.1.2 Insulin induced genomic damage in immortalized human hepatocytes

Two different methods were used to monitor the modulation of the genotoxic potential of insulin, the alkaline comet assay and the cytokinesis block micronucleus test. Viability and proliferation were monitored in order to eliminate any interference of cytotoxicity in the determination of genotoxicity.

The alkaline comet assay was used to show single and double strand breaks of DNA. A typical comet picture can be seen in **Figure 52**. In the alkaline comet assay, IHH cells were treated for 2 hours with 10 and 100 nM insulin with or without the presence of the Pten inhibitor VO-Ohpic.

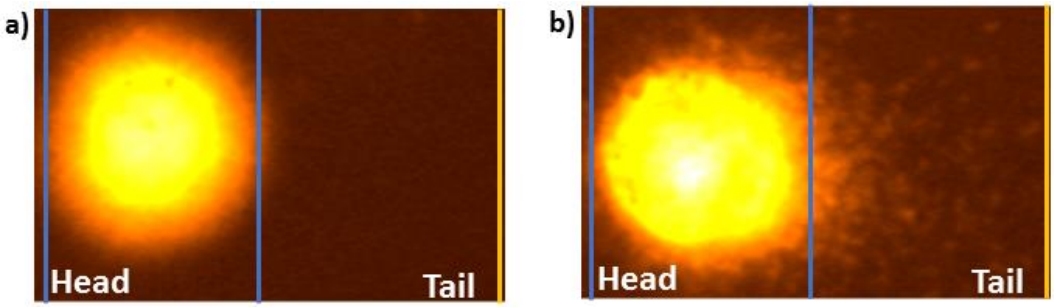

Figure 52: Representative microscopic pictures of agarose embedded IHH cells in the comet assay. Example for a cell with intact nuclear DNA (**a**) and example for a cell with DNA damage after insulin treatment group (**b**). The comet assay is based on the migration of small DNA fragments (single or double strand breaks, alkalilabile sites) in an electric field. DNA damage is quantified with a special software according to percent of DNA in tail.

As displayed in **Figure 53**, insulin treatment caused a dose dependently significant induction of DNA damage. The Pten inhibition induced a further increase in DNA damage. There was no significant change in the percentage of viable cell following 2 hours insulin treatment either with or without Pten inhibitor (**Table 7**).

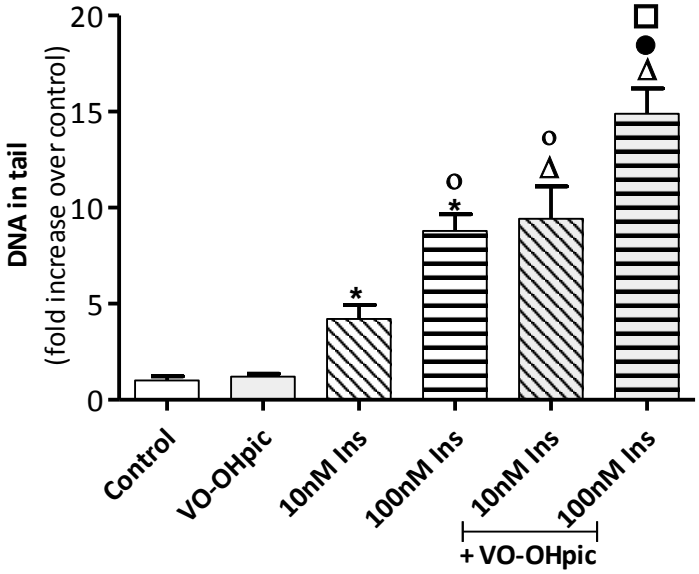

Figure 53: DNA damage induction by insulin treatment with or without Pten inhibition. DNA damage was measured after 2 hours treatment with insulin with or without the presence of Pten inhibitor. Pten inhibition was achieved by adding the Pten inhibitor 15 min prior to the insulin treatment. DNA damage was quantified with the comet assay. Quantification of comet assay results: 100 cells were evaluated per treatment group and the results were expressed as percent of DNA in tail. Data are presented as mean ± SEM of 4 independent experiments. The percentage of viable cells was assessed by counting 200 cells per treatment group, after FDA/ gel red staining was performed. * p≤0.05 vs. Control, Δ p≤0.05 vs. VO-OHpic, ○ p≤0.05 vs. 10 nM insulin, ● p≤0.05 vs. 100 nM insulin and □ p≤0.05 vs. VO-OHpic + 10 nM insulin. VO-OHpic: Pten inhibitor and Ins: Insulin.

Table 7: Viability of IHH cells following to 2 hours insulin treatment with or without Pten inhibition.

Group	Viability (%)
Control	93.88±1.60
50nM VO-OHpic	96.88±0.83
10nM Ins	97.38±0.75
100nM Ins	96.13±1.53
VO-OHpic+10 nM Ins	96.88±1.40
VO-OHpic+100nM Ins	94.38±1.25

VO-OHpic: Pten inhibitor and Ins: Insulin. Data are presented as mean viability ± SEM of 4 independent experiments.

The cytokinesis block micronucleus test was used to monitor irreversible chromosomal damage *in vitro*. A typical appearance of a micronucleus in binucleated cells can be seen in **Figure 54**.

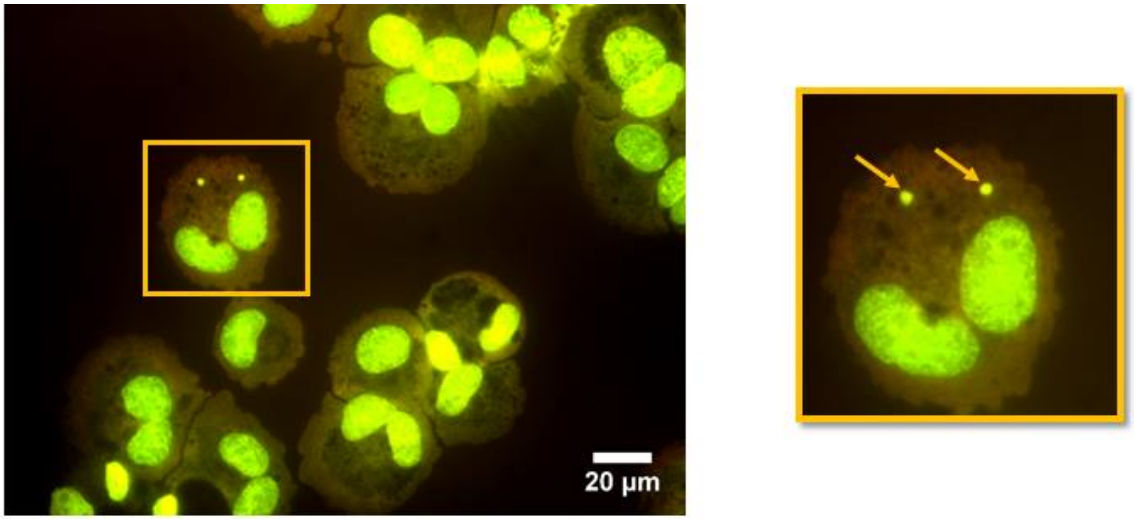

Figure 54: Representative picture of micronuclei in binucleated cells. Orange arrows indicate micronuclei in a binucleated cell.

Quantification of the cytokinesis block micronucleus test is shown in **Figure 55**. After 4 hours of treatment with 10 and 100 nM of insulin, a significant induction of micronucleus formation was observed. The combination of the Pten inhibitor VO-OHpic with insulin yielded an elevated micronucleus formation compared with insulin alone, which was significant for 10nM insulin.

The cytokinesis block proliferation index, apoptosis and mitosis were assessed in the same preparation and the results can be found in **Table 8**. There was no significant observation in apoptosis, mitosis and proliferation following 4 hours insulin treatment with or without Pten inhibitor.

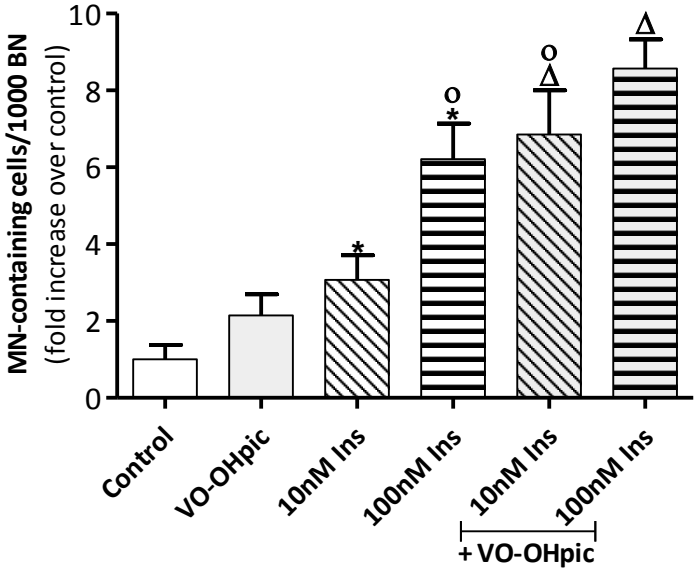

Figure 55: Micronucleus induction by insulin treatment with or without Pten inhibition by VO-OHpic. Micronucleus formation was achieved in IHH cells, treated for 4 hours with insulin with or without the presence of the Pten inhibitor, followed by 24 hours incubation with the cytokinesis blocker cytochalasin B. Data are presented as mean of MN-containing cells in 1000 binucleated cells (BN) ± SEM of 4 independent experiments. The slides prepared for micronucleus test were used as well to quantify the cytokinesis block proliferation index (CBPI: (number of mononucleated cells + 2 x no.binucleated cells + 3 x no. multinucleated cells)/(sum of mononucleated, binucleated and multinucleated cells), 1000 cells per treatment group). * p≤0.05 vs. Control, Δ p≤0.05 vs. VO-OHpic, ○ p≤0.05 vs. 10 nM insulin and ● p≤0.05 vs. 100 nM insulin. VO-OHpic: Pten inhibitor and Ins: Insulin.

Table 8: Effect of 4 hours insulin treatment with or without Pten inhibitor on apoptosis, mitosis and cytokinesis block proliferation index.

Group	Apoptosis/1000cells	Mitosis/1000 cells	CBPI
Control	1.00±0.227	1.00±0.099	1.95±0.008
VO-OHpic	0.83±0.147	1.07±0.161	1.95±0.004
10nM Ins	0.56±0.198	1.29±0.187	1.94±0.011
100nM Ins	1.14±0.184	1.18±0.137	1.96±0.004
VO-OHpic+10nM Ins	1.11±0.187	1.05±0.174	1.97±0.005
VO-OHpic+100nM Ins	1.14±0.412	1.18±0.205	1.97±0.006

CBPI: cytokinesis block proliferation index, VO-OHpic: Pten inhibitor, Ins: Insulin. Data are represented as mean±SEM of 4 independent experiments. Except CBPI, all values are given as fold increase over control.

4.2.2 Influence of deficiency of Pten, a protein in the insulin signaling, on oxidative stress and genomic damage *in vivo*

At this point, we gained access to samples from a whole-body Pten haplodeficient mouse model lacking Akt2 from the Hepatology division of the University Hospital Würzburg. Liver tissue was available to investigate whether – under physiological insulin levels – the reduction of Pten activity (by reduced expression in this model) would also lead to increased genomic damage *in vivo.* An additional group with a whole-body Pten haplodeficiency lacking Akt2 was used to answer the question whether slowing down the insulin-signaling cascade can improve the oxidative status and genomic damage. Snap-frozen liver samples and paraffin-embedded liver sections were analyzed from following groups:

Standard diet (SD) fed groups:

- **WT** (wild-type mice, $Pten^{+/+}/Akt2^{+/+}$, n=6)
- ***Pten*$^{+/-}$*/Akt2*$^{+/+}$** (whole-body Pten haplodeficient mice, n=9)
- ***Pten*$^{+/-}$*/Akt2*$^{-/-}$** (whole-body Pten haplodeficient mice lacking Akt2, n=8)

High fat diet (HFD) fed groups:

- **WT** (wild-type mice, $Pten^{+/+}/Akt2^{+/+}$, n=9)
- ***Pten*$^{+/-}$*/Akt2*$^{+/+}$** (whole-body Pten haplodeficient mice, n=9)
- ***Pten*$^{+/-}$*/Akt2*$^{-/-}$** (whole-body Pten haplodeficient mice lacking Akt2, n=9)

4.2.3 Oxidative stress and genomic damage in the liver of a whole-body Pten haplodeficient mouse model

4.2.3.1 Oxidative stress

Pten-deficient and wild type control mice were fed with standard diet (SD) or with high fat diet (HFD). Representative pictures of DHE stained cryosections from livers of WT**,** $Pten^{+/-}/Akt2^{+/+}$ and $Pten^{+/-}/Akt2^{-/-}$ mice can be found in **Figure 56**. As seen in **Figure 57**, elevation in oxidative stress was detected either with SD or with HFD in the $Pten^{+/-}/Akt2^{+/+}$ group compare to the control WT mice significantly.

The elevated oxidative stress could reduced back by knocking Akt2 out. However, the reduction was only significant in Pten$^{+/-}$/Akt2$^{-/-}$, HFD group compared to Pten$^{+/-}$/Akt2$^{+/+}$ group either fed with SD or with HFD.

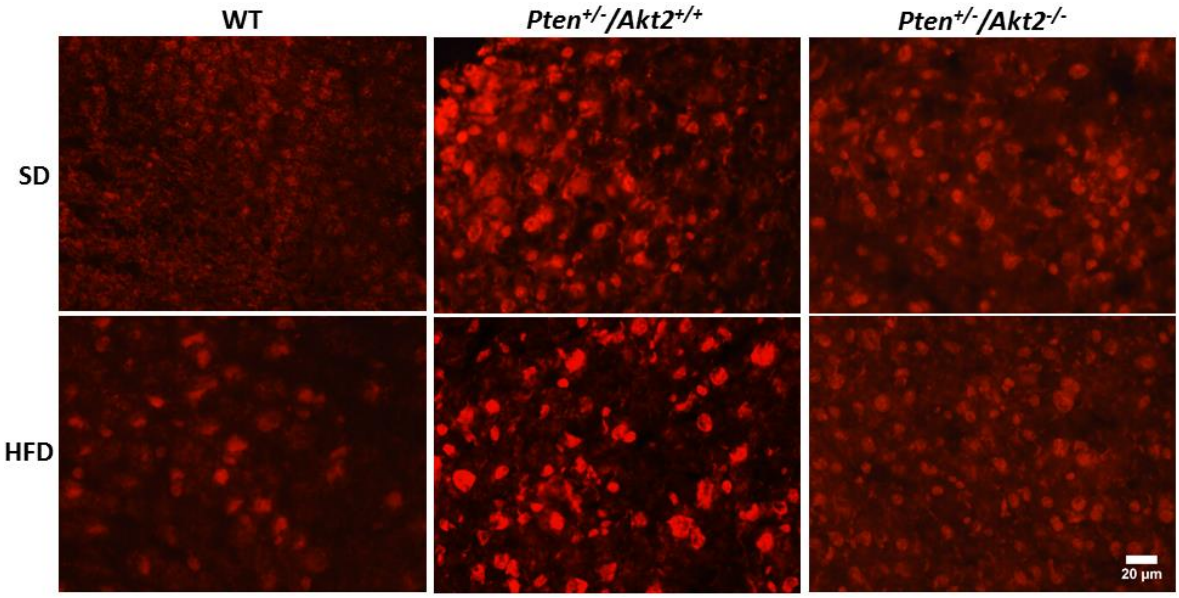

Figure 56: Representative pictures of DHE stained liver sections of wild type (WT), whole-body Pten haplodeficient (*Pten$^{+/-}$/Akt2$^{+/+}$*) and whole-body Pten haplodeficient lacking Akt2 (*Pten$^{+/-}$/Akt2$^{-/-}$*) mice after feeding with standard diet (SD) or high fat diet (HFD).

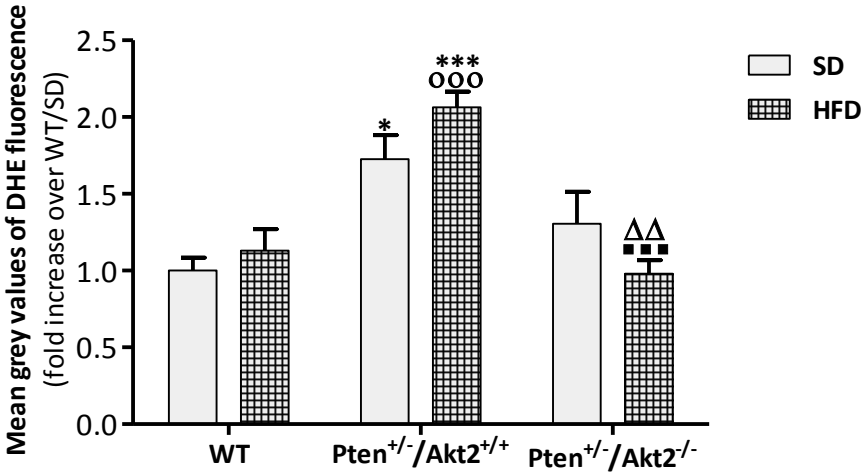

Figure 57: Detection of ROS in mouse liver by DHE staining. Quantification of ROS formation was achieved by measuring the mean grey value of 200 cells using image j software. Mice (WT (SD, n=6; HFD, n=9), *Pten$^{+/-}$/Akt2$^{+/+}$* (n=9) and *Pten$^{+/-}$/Akt2$^{-/-}$* (n=7)) had been fed with SD or HFD for 20 weeks. Data are presented as mean ± SEM. SD fed groups: * p≤0.05 vs. WT, Δ p≤0.05 vs. *Pten$^{+/-}$/Akt2$^{+/+}$* and HFD fed groups: ○ p≤0.05 vs. WT, ▪ p≤0.05 vs. *Pten$^{+/-}$/Akt2$^{+/+}$*.

4.2.3.2 Heat shock protein expression

Figure 58 a (SD) and **b** (HFD) show representative pictures of the bands from western blot analysis of HSP70 expression. The relative quantification of the HSP70 bands can be found in **Figure 59**. There was no difference in the expression of HSP70 protein among the groups under standard diet conditions. However, a slight increase in the expression of HSP70 protein was observed in WT fed with high fat diet compared to the standard diet and a significant increase was observed between *Pten*$^{+/-}$*/Akt2*$^{+/+}$ mice fed with high fat diet compared to the standard diet fed group. There was no statistically significant difference within the high fat diet group, but a trend was monitored. The whole body Pten-haplodeficiency caused elevation in the expression of HSP70 protein with a combination of HFD compared to the mice in WT/SD and *Pten*$^{+/-}$*/Akt2*$^{+/+}$/SD groups. Akt2 knockout showed a slight reduction compared to the just Pten haplodeficient mice in both diet conditions.

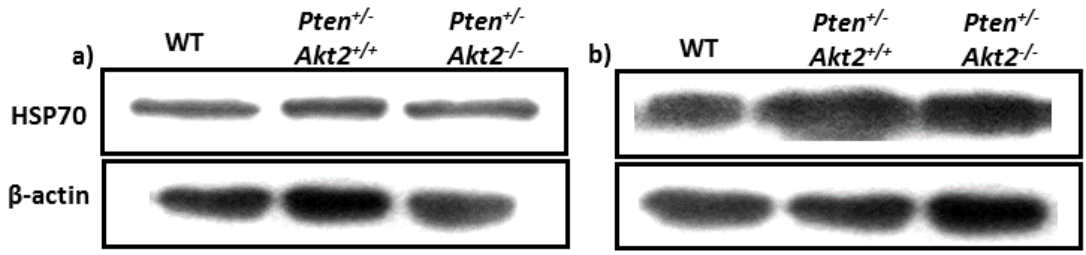

Figure 58: Photographs of representative western blots from HSP70 (**a**: SD and **b:** HFD).

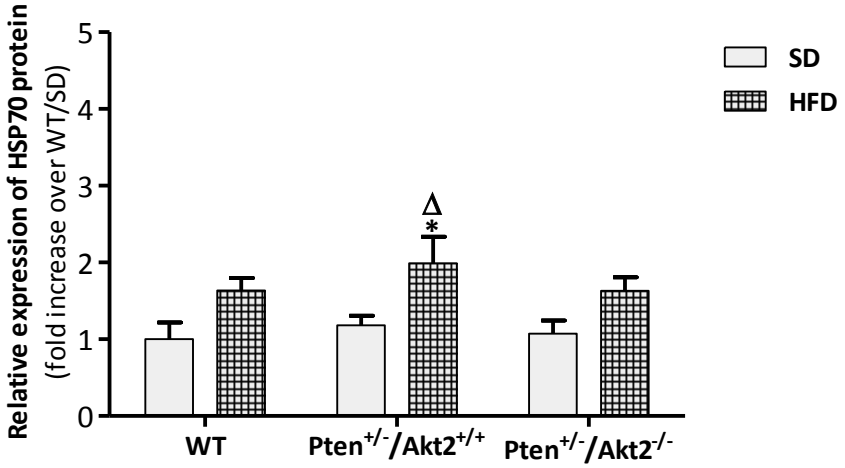

Figure 59: Relative expression of heat-shock protein 70 (HSP70) in mouse liver. Quantification: The band intensity of HSP70 from liver tissue of mice (WT (SD, n=6; HFD, n=8), *Pten*$^{+/-}$*/Akt2*$^{+/+}$ (SD, n=9; HFD, n=8) and *Pten*$^{+/-}$*/Akt2*$^{-/-}$ (SD, n=8; HFD, n=9)) that had been fed with SD or HFD for 20 weeks was quantified by image j and adjusted to equal loading using the endogenous control of β-actin. Data are presented as mean ± SEM. SD fed groups: * p≤0.05 vs. WT and Δ p≤0.05 vs. *Pten*$^{+/-}$*/Akt2*$^{+/+}$.

Figure 60 a (SD) and **b** (HFD) show representative pictures of the bands from western blot analysis of HO-1 expression. Quantification of the relative expression of HO-1 protein is represented in **Figure 61**. Within the standard diet groups, there was a significant increase in the expression of HO-1 in the Pten haplodeficient group (*Pten*$^{+/-}$*/Akt2*$^{+/+}$) compared to the WT group. Within the high fat diet groups, the expression of HO-1 from mice in the *Pten*$^{+/-}$*/Akt2*$^{+/+}$ group was elevated significantly compared to the mice in the WT group fed with SD and HFD. Furthermore, a significant increase in the expression of HO-1 was observed in the mice fed with *Pten*$^{+/-}$*/Akt2*$^{+/+}$ (HFD) compared to the *Pten*$^{+/-}$*/Akt2*$^{+/+}$ (SD) group. This increase in the HO-1 expression level could be reduced back to the control level in *Pten*$^{+/-}$*/Akt2*$^{-/-}$ mice (HFD).

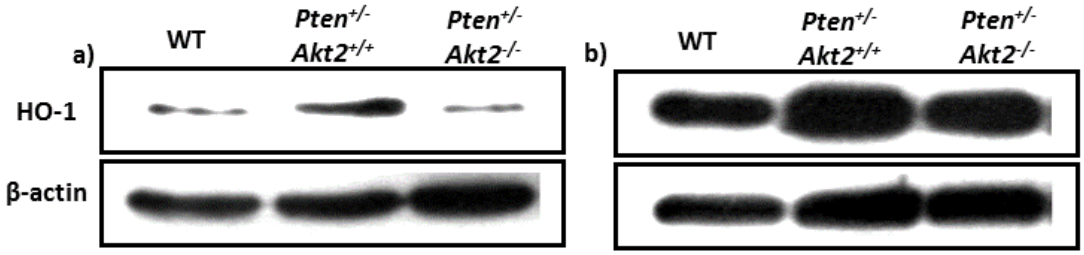

Figure 60: Photographs of representative western blots from HO-1 (**a:** SD and **b:** HFD).

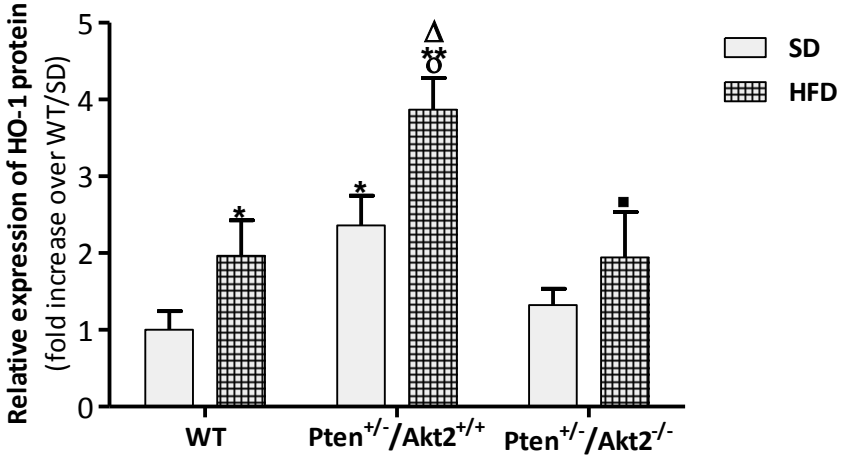

Figure 61: Relative expression of heme oxygenase 1 (HO-1) in mouse liver. Quantification: The band intensity of HO-1 from liver tissue of mice (WT (SD, n=5; HFD, n=6), *Pten*$^{+/-}$*/Akt2*$^{+/+}$ (SD, n=6; HFD, n=8) and *Pten*$^{+/-}$*/Akt2*$^{-/-}$ (SD, n=6; HFD, n=6)) that fed with SD or HFD for 20 weeks was quantified by image j and normalized to the endogenous control β-actin. Data are presented as mean ± SEM. SD fed groups: * p≤0.05 vs. WT, ** p≤0.01 vs. WT, Δ p≤0.05 vs. *Pten*$^{+/-}$*/Akt2*$^{+/+}$ and HFD groups: ○ p≤0.05 vs. WT, ▪ p≤0.05 vs. *Pten*$^{+/-}$*/Akt2*$^{+/+}$.

4.2.3.3 DNA damage induction in the liver of whole-body Pten haplodeficient mice

Genomic instability was monitored by an antibody staining against γ-H2AX in liver tissue. A representative picture of γ-H2AX antibody staining can be seen in **Figure 62**.

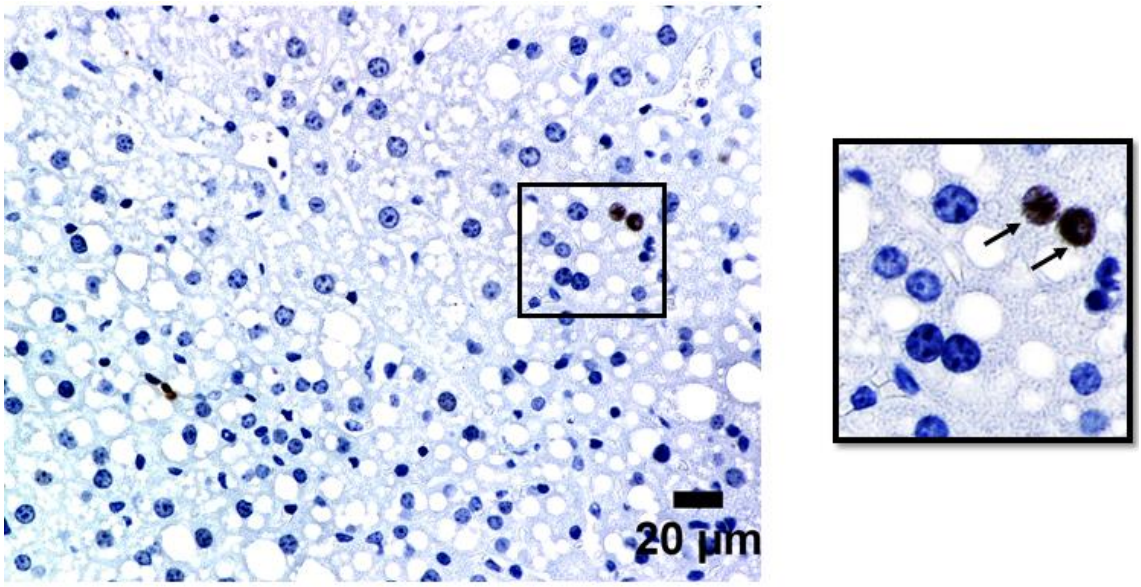

Figure 62: Representative picture of γ-H2AX antibody stained paraffin embedded liver section of sham-operated obese rat. Brown colored cells, which are indicated by black arrows, represent γ-H2AX positive cells.

In the liver of the whole-body Pten haplodeficient mice, a slight, but not significant elevation of DNA double strand breaks was observed compared to WT and a reduction back to the WT level in the mice group lacking Akt2. The genomic stability in the liver samples was reduced in all groups with HFD and a significant increase in the DNA damage was monitored in HFD fed WT mice compared to SD fed WT mice. Pten haplodeficiency gave a further rise to DNA damage in *Pten*$^{+/-}$*/Akt2*$^{+/+}$ mice fed with HFD and the knockout of Akt2 was enough to reduce the DNA damage significantly (**Figure 63**).

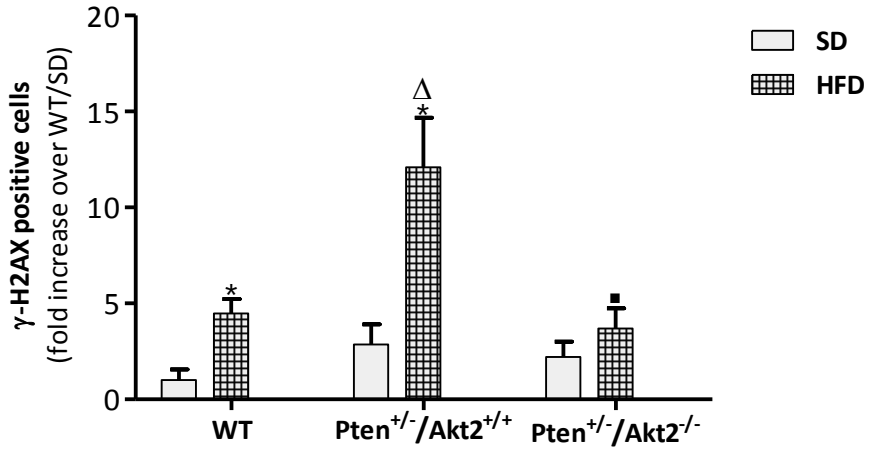

Figure 63: Detection of phosphorylated H2AX sites as DNA double strand break marker on paraffin embedded liver section. Quantification of liver sections: 12 to 15 photos per animal were quantified by image j (WT (SD, n=3; HFD, n=8), *Pten*$^{+/-}$*/Akt2*$^{+/+}$ (SD, n=8; HFD, n=8) and *Pten*$^{+/-}$*/Akt2*$^{-/-}$ (SD, n=7; HFD, n=8)). Data are presented as mean of γ-H2AX positive cell percentage ± SEM. SD fed groups: * p≤0.05 vs. WT, Δ p≤0.05 vs. *Pten*$^{+/-}$*/Akt2*$^{+/+}$ and HFD fed groups: ▪ p≤0.05 vs. *Pten*$^{+/-}$*/Akt2*$^{+/+}$.

5 DISCUSSION

5.1 Oxidative stress and genomic damage induction in obese Zucker$^{fa/fa}$ rats

In this study, we investigated the link between obesity, increased oxidative stress and DNA damage in the kidney, liver and colon of obese Zucker$^{fa/fa}$ rats. Furthermore, we demonstrated the influence of the same amount of weight loss induction either by gastric bypass surgery (RYGB) or by caloric restriction on oxidative stress status and genomic damage in these tissues. The rationale behind this study was the association between obesity and cancer incidence of the kidney, liver and colon [122-124].

The association among overweight, type 2 diabetes mellitus, cardiovascular disease and hypertension is well established. Despite that, the relationship between cancer and overweight has not been clearly defined. Epidemiological studies manifest that adiposity is linked with increased risk of cancers such as kidney, liver, colon and colorectal cancer. Cancer is a more prevalent reason of death in overweight and obese individuals than in people with normal weight. An unanswered question is the influence of weight loss on the risk of cancer in adiposity [122-124]. There are no studies that focused on the effects of weight reduction methods such as caloric restriction and/or physical exercise and cancer risk reduction. Although lower body weight clearly seems beneficial, it might be too superficial to claim that a reduction of body weight is also always beneficial concerning the cancer risk. For example, it is known that weight loss does not improve mortality in all patient groups. Logue et al., [125] demonstrated a U-shape relationship between BMI and mortality rate in T2DM patients. T2DM patients with normal weight and obese patients showed a higher mortality rate than the overweight group. Similarly, for the association of BMI with mortality in dialysis patients. Jialin et al., [126] showed in a meta-analysis that a BMI ≥ 25 correlated with lower mortality rates in hemodialysis patients. Even if altering body weight to an ideal amount could be preventive against further damage, previously fixed genomic damage might not be reversible by weight reduction.

According to the findings of this study, obesity caused elevation in oxidative stress in kidney, liver and colon tissue of rats and weight loss helped to achieve and maintain oxidative balance within the body, independent from the weight loss method.

The expression of the stress response protein HSP70 and the antioxidant enzyme HO-1 in the kidney of the Obese rats was increased significantly compared to the Lean group. The expressions of HSP70 and HO-1 in the kidney of the RYGB and the CR group were reduced significantly after weight loss compared to the Obese group. While alterations of the expression of HSP70 in liver tissue as well as in colon tissue did not reach statistical significance, HO-1 expression in the liver and colon of the Obese animals was elevated significantly compared to the Lean group and was reduced significantly by weight loss with either by gastric bypass surgery or by caloric restriction. Urinary measurements of indirect oxidative stress markers such as oxidation products of lipids, DNA and RNA supported the findings of elevation in oxidative stress further. Here, we found a correlation between body weight and oxidative stress markers using an obesity rat model. Weight loss, whether achieved by RYGB or caloric restriction, helped to re-establish oxidative homeostasis.

It was shown in the present studies that obesity might induce systemic oxidative stress. However, the question of how oxidative stress is induced has not been answered yet. There are at least five major hypothetical reasons that might contribute to the oxidative stress in adiposity, which are mitochondrial dysfunction, over-expression or -activity of NADPH oxidase enzymes, chronic hyperinsulinemia, dysregulation of adipocytes and chronic inflammation [50, 127, 128]. The adipose tissue is an endocrine organ, which plays an important role in various physiological processes. Tumor necrosis factor-alpha (TNFα), leptin, and interleukin-6 (IL-6) are some of the key adipokines, which are secreted by adipose tissue. Obesity can be defined as excessive fat accumulation, which means an expanded fat deposit because of hyperplasia and hypertrophy of adipocytes. These alterations cause major changes in adipocyte pathophysiology. The hypertrophic-hyperplastic adipocytes display less insulin receptor, release more TNFα, IL-6 and free fatty acids (FFA). Dysregulation in the production of these bioactive molecules cooperate with the pathogenesis of obesity and oxidative stress [19]. Furukawa et al, [127], found elevation in the mRNA level of NADPH oxidase subunits ($p22^{phox}$, $gp91^{phox}$, $p47^{phox}$, $p40^{phox}$ and $p67^{phox}$) in white adipose tissue (WAT) of obese KKAy mice as well as reduced anti-oxidant enzyme activity. They suggested that this might be due to macrophage infiltration and/ or high expression of NOX4 in WAT. Their results point not only to the NOX proteins as a cause of oxidative stress, but also to the WAT as source of the oxidative stress [127].

Adipose tissue plays an important role in insulin sensitivity. As a response to other endocrine organs, adipose tissue releases adiponectins and free fatty acids (FFA), which take a part in the insulin-signaling cascade. In the course of obesity, the release of FFA and TNFα from adipose tissue increases, while on the other hand the release of adiponectin is reduced. This situation gives rise to insulin resistance and hyperinsulinemia. Elevation of the insulin level leads to an increased level of free IGF-1. Insulin and IGF-1 are both known to induce proliferation and to inhibit apoptosis [50, 128]. Moreover, it has been shown that insulin induce ROS production and genomic damage in vitro via mitochondria and NADPH oxidase [129]. The association between oxidative stress, insulin resistance and obesity is intricate as each can be a cause for or the result of the other. However, the findings in this study demonstrate that elevated oxidative stress is a part of the pathophysiology of obesity and that it induces oxidation of lipids, DNA and RNA.

Novel findings suggested that RNA takes on an important part in the pathology of various diseases. In this regard, oxidative RNA modifications have become a new focus of research in addition to oxidative DNA modifications. Broedbaek et al., [130], found an association between mortality and elevated urinary 8-oxoGuo level in diabetic patients and suggested that RNA oxidation might have impact on diabetes complications. We analyzed the RNA oxidation marker, 8-oxoGuo, simultaneously with the DNA oxidation markers 8-oxoGua and 8-oxodG. Our findings showed that obese rats had a significant elevation in urinary 8-oxoGuo level in comparison to Lean rats and the weight loss either by caloric restriction or by RYGB surgery led to a significant reduction in urinary 8-oxoGuo level. DNA and RNA have variations in their synthesis and maintenance mechanisms. Considering that maintenance of DNA mainly depends on repair mechanism and RNA more on breakdown, urinary 8-oxoGua and 8-oxodG markers represent the repair rate as well as the oxidation status. Since the 8-oxoGuo marker comes from the breakdown of RNA, it is possible to regard 8-oxoGuo more as an oxidative stress status marker than as a marker for the repair rate. Hence, we can observe the significant elevation and the reduction in urinary 8-oxoGuo before and after intervention [131].

Among the many possible DNA oxidation products, the modified guanine base is the most investigated one. Another reason for the focused attention on the modified guanine base

is its mutagenic potential. Oxidative modifications of the guanine base may cause a loss of its base pairing specificity and lead to GC to AT transversion in case of inefficient repair [27]. In this sense, we analyzed urinary 8-oxoGua and 8-oxodG as DNA oxidation marker in addition to the RNA oxidation marker 8-oxoGuo. Before the intervention, the Obese rats showed a significant increase in urinary 8-oxoGua in comparison to the Lean rats. However, 8-oxodG elevation in the Obese rats was not significant. After the intervention, the increase in urinary 8-oxodG of Obese rats was significant as well as the urinary 8-oxoGua increase, compared with the Lean rats. The elevation in urinary 8-oxoGua was significantly reduced after weight loss either by caloric restriction or by gastric bypass surgery. Moreover, the caloric restriction provided a significant reduction of urinary 8-oxodG compared with the Obese rats. Nevertheless, rats that were subjected to RYGB, showed further elevation in urinary 8-oxodG.

At this point, it is necessary to discuss the possible differences between excretion of urinary 8-oxoGua and 8-oxodG. The measurement of urinary 8-oxoGua and 8-oxodG is a non-invasive approach that may supply a good monitoring option for oxidative status and risk for mutagenicity in vivo. However, interpretation of the source of oxidation products in urine might be complex due to the contribution of repair mechanisms. The data from the urinary DNA oxidation markers 8-oxoGua and 8-oxodG might represent more than one finding. The base excision repair pathway (BER) is mainly responsible for the repair of non-bulky base adducts. In the BER system, there are two human 8-oxoGua repair enzymes: the one is 8-oxoGua glycosylase and the second one is 8-oxoGua endonuclease. The repair by 8-oxoGua glycosylase generates the release of modified guanine bases, while the activity of 8-oxoGua endonuclease produces 3', 5', 8-oxodGDP, which might further hydrolyze to 8-oxodG. Recent findings suggested that nucleotide excision repair (NER) plays a role in the repair of oxidative DNA damage too. The oxidative DNA modifications cause conformational changes and base mismatches may become a target for the NER mechanism and result in the release of 8-oxodG to urine [20, 27]. In order to investigate the role of the human ogg1 enzyme, Klungland et al. used an $ogg1^{-/-}$ null mouse model and showed that the repair of oxidized guanine bases was slow but significant. This suggested that NER may be a back-up for the removal of oxidative DNA modifications [132]. Another possible source of urinary 8-oxodG is the nucleotide pool.

Because the oxidation of free deoxynucleotide is easier than of polynucleotides, the nucleotide pool is one of the important resources for oxidative base modifications. The oxidized free deoxynucleotide triphosphates from the nucleotide pool might then be converted into 8-oxodG due to the activity of repair enzymes (sanitation of the nucleotide pool by hydrolization of oxidized triphosphate to monophosphate) and excreted into urine. By virtue of this sanitation mechanism in the nucleotide pool, a misincorporation of oxidized triphosphates into DNA can be prevented too. A further possibility for 8-oxodG excretion into urine is the cell death. 8-oxodG might evolve from dead cells as a result of the activity of unspecific nucleases and phosphatases [133]. Although diet is mentioned as potential source for 8-oxodG in the literature, recent findings showed that it does not have a significant effect on urinary 8-oxodG [27, 134]. Nevertheless, it has to be considered that in our experiments a serious change in the gastric tract of the RYGB rats was introduced. This change in the digestive system might induce an artefactual elevation of urinary 8-oxodG.

Since the genomic integrity is very important for an organism, stability of DNA is sustained by complicated DNA repair mechanisms and DNA damage checkpoints. Under extreme conditions such as disease or impairment of repair mechanism, DNA damage may accumulate and lead to mutagenesis. Depending on the location of the damage, it might lead to the loss of tumor suppressors, triggering un-controlled proliferation and increase the risk of cancer [74, 135]. Here, DNA damage in the primary cells of kidney, liver and colon was investigated by application of the alkaline comet assay. We observed a small increase in the DNA damage of obese rats and a small reduction following the weight loss (RYGB and CR groups) in kidney, liver and colon, but no significant differences. The alkaline comet assay results can be affected by several factors like position of the slide in the electrophoresis chamber, temperature, and cell isolation. It is very difficult to combine analyses of different electrophoresis runs, but impossible to run all samples together, because the procedure has to be performed with fresh material immediately after animal sacrifice, and the sample number that fits into the electrophoresis chamber is limited. Sample preparation is tedious and can only be performed for a limited number of animals at the same time. Even though we always chose samples in a way to have at least one representative from each group of animals run together and always used the same

chamber and overall kept conditions as much the same as possible, experimental variability is unavoidable in this type of assay, possibly reducing the sensitivity of the assay. Besides, viability of the cells is an important factor for the quality of the comet assay. Unfortunately, we could not sustain vitality at a desired level and increased numbers of nonviable cells may have had an impact on the background quality of the slides, which may have added to an overall loss of sensitivity and detection quality.

Therefore, in addition to the alkaline comet assay, another marker for DNA damage was applied. Immunohistochemical detection of γ-H2AX, a DNA double strand break (DSBs) marker, was performed in sections of kidney, liver and colon of the rats. DNA DSBs are highly mutagenic lesions, which may lead to chromosomal aberrations and genome rearrangements. DNA DSBs are considered as major risk factor for cancer [136, 137]. Our findings demonstrated an elevation in γ-H2AX positive cell number in Obese rats in comparison with Lean rats. This increase could be reduced after the intervention either by caloric restriction or by gastric bypass surgery. The increases of γ-H2AX positive cell number in kidney and colon of Obese rats were significant. Since the development of cancer can take decades, surrogate markers such as DNA-damage are useful for fast gain of knowledge. Othman et al., [129, 138], showed that insulin induced oxidative stress and DNA damage in vitro and in vivo. Hyperinsulinemia is one of the key factors in this rodent model and we showed that the insulin response pattern was improved by weight reduction in the RYGB and CR groups. Therefore, we tested whether the basal insulin level was correlated with DNA damage (γ-H2AX positive cells percent) across all groups except for the Lean, which have a different genetic background. The Spearman test indicated a positive correlation between the basal insulin levels and DNA-damage in kidney, liver and colon across all groups.

Although hyperinsulinemia is an important aspect of this rodent model, there are other factors that may have contributed too. For example, obesity is usually associated with high blood pressure. The elevation of oxidative stress and genomic damage has been described for rodent models with the hypertension regulating hormones angiotensin II and aldosterone [139-141]. Insulin [129, 138], angiotensin II [141, 142] and aldosterone [143, 144] have been reported to induce formation of ROS via activation of mitochondria and of

NADPH oxidases. Mitochondria are one of the main sources of intracellular ROS. Electrons constantly leak from the respiratory chain and lead to the production of superoxide [145, 146]. Mitochondria play a crucial role in energy expenditure, and excessive energy consumption causes mitochondrial dysfunction, increasing the superoxide output [147]. The family of NOX is another important source of cellular ROS [44]. Phagocyte NADPH oxidase (NOX2) was the first identified isoform, and generates ROS in the context of host defense. In the following years, homologs of NADPH oxidase such as NOX1, NOX3, NOX4, NOX5, DUOX1 and DUOX2 were found and are now considered as NOX family. Members of this enzyme family exist almost in every tissue and produce ROS for host defence and/or signaling purposes [46]. Overexpression of any NOX family member might induce genomic instability due to elevation in ROS generation. In turn, adipose tissue plays an important role in insulin sensitivity. As a response to other endocrine organs, adipose tissue releases adiponectins and free fatty acids (FFA), which take part in the insulin-signaling cascade. Therefore, ROS generation, insulin signaling and obesity are linked in complex ways and vicious cycles of mutual enhancement may exist between them.

An increased cancer risk in obese individuals has been show in meta-analysis studies for the organs investigated here (kidney, liver and colon) [148, 149]. Our findings suggested that weight loss (either by RYGB or by caloric restriction) helps to reduce DNA damage. Since genomic instability and DNA damage are linked to mutagenesis and carcinogenesis, weight loss might help to reduce the elevated cancer risk.

Although bariatric surgery may reduce the overall cancer risk [95, 150] RYGB may increase the risk for the development of CRC [151]. Derogar et al., [152] found an increased colorectal cancer (CRC) risk after obesity surgery (RYGB, gastric banding and vertical banded gastroplasty). On the other hand, Raptis et al., [151], criticized the study due to methodological problems. Criticism was directed towards the following issues: CRC risk in the nonsurgical obese group did not show any elevation as expected during the observation period. Furthermore, mortality data were not shown. Therefore, it was not clear whether the surgery groups lived longer and had more time to develop cancer or whether - due to an increase in early mortality in the nonsurgical group - cancer development could not be observed. Interestingly, three different surgery types, which have very different anatomy

and physiological mechanisms, did not show any difference in CRC risk. For instance, altered bile flow, which was suggested as a reason for increased CRC, is only caused by RYGB. Our results did not indicate any increased DNA damage in the colon after RYGB surgery in our rat model. However, tumor promoting mechanisms, like increased cell death and compensatory proliferation might enhance the CRC risk without inducing DNA damage.

In conclusion, we have shown that obesity is a state of increased oxidative stress and DNA damage, and for the first time that weight loss by RYGB or caloric restriction can help normalize the oxidative stress level and the degree of DNA damage in kidney, liver and colon. Thus, weight loss may reduce the elevated risk of mutagenesis and carcinogenesis in the context of obesity.

5.2 Role of Pten in insulin-mediated oxidative stress and DNA damage

Because we had observed a correlation between basal insulin level and genomic damage in the rat obesity model, we emphasized this aspect with a study involving cultured liver cells and liver tissue from a knockdown mouse model. Some steps in the genotoxic mechanism of insulin-action had been described [129, 138, 153], but the very important inhibitory activity of Pten had not been investigated in this context. Therefore, we investigated the role of Pten loss in insulin-mediated oxidative stress and genomic damage *in vitro* in a non-malignant immortalized human hepatocyte (IHH) cell line and *in vivo* in a whole-body Pten haplodeficient mouse model.

Pten (Phosphatase and Tensin homolog) is a tumour suppressor gene, which is located on chromosome 10q23 region. Pten is among the most commonly mutated genes in cancer. The Pten protein dephosphorylates phosphatidylinositol (3, 4, 5)-triphosphate (PIP3) to phosphatidylinositol(4, 5)-bi-phosphate (PIP2) and plays a critical role as a negative regulator of PI3K by dephosphorylation of PIP3 [154]. In order to investigate the role of Pten in insulin-mediated genomic damage in vitro, we used a vanadium complex to inhibit Pten. The applied inhibitor VO-OHpic is known as a specific Pten inhibitor, which is active in nanomolar concentrations (IC_{50}, 46±10 nM) [155]. We used the conditions suggested in Mak et al., [155], for reversible inhibition of the Pten protein.

In vitro, insulin caused an elevation of oxidative stress and Pten inhibition with the pharmacological inhibitor VO-OHpic enhanced the effect of insulin. IHH cells showed significant elevation of genomic damage in the comet assay and micronucleus test and Pten inhibition led a further dose dependent increased in genomic damage. Othman et al., [129, 138, 153], demonstrated insulin-mediated oxidative stress and genomic damage in kidney and colon cells, which could be reduced by the inhibition of mitochondria or NADPH oxidase. Our results in a non-malignant hepatocyte cell line are complementary to these data regarding the genotoxicity of insulin in various tissues. Insulin can bind to both insulin receptor and IGF1 receptor to activate the PI3K/Akt pathway, which can be negatively regulate by Pten. Activation of the PI3K/Akt pathway leads to elevated ROS formation through mitochondria and NADPH oxidase [153, 156].

In our *in vitro* model, it is therefore most likely that Pten inhibition enhanced the insulin-mediated activation of the PI3K/Akt pathway and caused elevated ROS formation, which induced increased genomic damage. Even though, we did not observe any increase in proliferation *in vitro*, the PI3K/Akt pathway is also involved in the regulation of cell proliferation and enhanced stimulation of proliferation might also contribute to an increased genomic instability by compromising cell cycle checkpoint accuracy.

In *in vitro* systems, it is easier to investigate specific mechanisms. However, *in vivo* there are usually many connected or overlapping pathways and factors that might contribute. In order to investigate the *in vivo* relevance of our *in vitro* findings concerning Pten inhibition, a whole-body Pten haplodeficient mouse model with an additional mouse group, which lacked Akt2 was used. Because liver tissue was available for us through a collaboration and because liver has important functions in energy homeostasis [157] and is one of the organs affected by increased cancer risk in obesity, we investigated the mutagenic effect of insulin and the role of Pten in liver tissue. To gain a better understanding of insulin signaling in oxidative stress and genomic damage, we used the additional group of mice with the whole-body Pten haplodeficiency lacking Akt2. Akt2 is one of three Akt isoform that is mainly expressed in liver [158]. Especially in mouse liver Akt2 is 84% of the total Akt protein [159]. Besides, insulin responsive tissues like muscle, fat and liver are rich in Akt2 isoform [67]. Cho et al., [67], demonstrated in a mouse model the importance of Akt2 in hepatic insulin signaling to maintain glucose homeostasis.

The liver tissue from whole-body Pten haplodeficient mice showed a significant increase in oxidative stress compared to wild type mice in standard diet (SD) groups. High fat diet (HFD) feeding in WT mice induced significant oxidative stress itself. Pten deficiency gave a further rise to oxidative stress in HFD mice compared to WT mice both fed with SD and with HFD as well as $Pten^{+/-}/Akt2^{+/+}$ mice fed with SD. Akt2 knockout in HFD fed mice group helped to reduce the oxidative stress significantly. Whole-body Pten haplodeficiency alone as well as high fat diet alone were sufficient to cause significant elevation in oxidative stress. Nevertheless, combination of these two factors caused a further significant increase of the oxidative stress level, which could reduced back by Akt2 knockout.

HSP70 expression can be induced by several stress factors such as infection, hyperthermia and oxidative stress. It is known that high-energy expenditure causes the expression HSP70 and vice versa, elevated HSP70 expression alters the metabolism to the direction of anaerobic glycolysis [160]. According to our data, HSP70 expression was not altered between WT and $Pten^{+/-}/Akt2^{+/+}$ mice in the standard diet group. HFD fed $Pten^{+/-}/Akt2^{+/+}$ mice demonstrated elevated expression of HSP70 compared to the WT and $Pten^{+/-}/Akt2^{+/+}$ mice in the SD group. However, the $Pten^{+/-}/Akt2^{-/-}$ group did not show significant reduction, but just a slight trend.

The expression of HO-1 responded slightly different from HSP70. The HO-1 expression in the liver of $Pten^{+/-}/Akt2^{+/+}$ mice was significantly higher than in the WT mice among the SD groups. HFD alone caused a significant increase in the HO-1 expression in WT mice. Besides, a significant increase was observed in the HO-1 expression of $Pten^{+/-}/Akt2^{+/+}$ mice, which were fed with HFD compared to WT mice in both diet groups and $Pten^{+/-}/Akt2^{+/+}$ mice in SD group. In whole-body Pten haplodeficent mice lacking Akt2 fed with HFD, the expression of HO-1 was reduced to control level. HO-1 is an enzyme, which helps to reduce oxidative stress and inflammatory response. Under normal conditions, HO-1 expression is low in cells. However, it can be stimulated by various stress conditions like oxidative stress, elevated cytokines, growth factor and hypoxia [161, 162]. Brunt et al., [163], demonstrated the co-dependence of Akt and HO-1 expression on a translational and post-translational level. This might partly explain the further induction of HO-1 expression in the Pten haplodeficient groups. Alaoui-Jamali et al., [164], showed *in vivo* and *in vitro* elevated HO-1 expression in prostate cancer cells and that the inhibition of HO-1 helped to reduce invasive features of the cancer cells. In our study, HSP70 and HO-1 were investigated as oxidative stress markers and their association with Pten and insulin signaling was not the main focus. However, this might be an interesting aspect for future works.

The whole-body Pten haplodefiency independent from the diet could induce a significant increase in ROS formation. Among WT, $Pten^{+/-}/Akt2^{+/+}$ and $Pten^{+/-}/Akt2^{-/-}$ mice under standard diet condition showed a clear trend in the oxidative status. However, the whole-body Pten haplodeficient mice lacking Akt2 showed only a significant reduction in the HFD fed group. This might be due to the role of Akt in hepatic *de novo lipogenesis*.

In various studies, the mouse models with lacking Akt isoforms showed that the Akt2 isoform is necessary for hepatic lipid accumulation [165]. In our mouse model, Pten deficiency caused sensitization of Akt signaling and HFD led to hyperactivation of Akt2. In this sense, the impact of the Akt2 knockout became more obvious in HFD fed mice.

The DSBs marker γ-H2AX was increased significantly in HFD fed mice compared to the SD group. Especially HFD fed $Pten^{+/-}/Akt2^{+/+}$ mice showed significant induction of DNA DSBs compared to SD fed $Pten^{+/-}/Akt2^{+/+}$ mice. Opposite to the oxidative stress markers, Pten haplodeficiency alone did not cause any significant increase in γ-H2AX in the SD groups. Nonetheless, there was an elevation in γ-H2AX positive cell number in HFD fed $Pten^{+/-}/Akt2^{+/+}$ mice compared to SD fed $Pten^{+/-}/Akt2^{+/+}$ mice and Akt2 knockout could reduce the DNA damage significantly. Our data showed that high fat diet alone was capable of inducing a significant amount DNA damage in liver. Since insulin has a key role in hepatic metabolism, HFD could lead to imbalance in hepatic insulin signaling. Pten deficiency reinforced the impact of HFD on insulin signaling and caused further induction of DNA damage. The mouse group lacking Akt2 with improved DNA integrity proved the role of insulin signaling in DNA damage.

Pten deficiency alone was capable to induce a significant amount oxidative stress, but not DNA damage. High fat diet with combination of Pten deficiency caused a further increase of oxidative stress and DNA damage, which could be prevented by Akt2 knockout. In the SD group, Pten haplodeficiency induced ROS formation might not be sufficient to enable radicals to pass through the nuclear membrane. Apart from this, high fat diet feeding caused a significant further increase in ROS formation, which could enhance the chance for radicals to reach the DNA. However, another possibility is that HFD diet induced hyperactivation of Akt2 may have caused DNA damage by a different mechanism in addition to the oxidation.

It has been shown that in a concentration and time dependent manner H_2O_2 can inactivate Pten by oxidation of cysteine residue [22, 23]. In this sense, HFD induced excessive ROS might lead to a further reduction in Pten activity in $Pten^{+/-}/Akt2^{+/+}$ mice fed with HFD and increase the DNA damage.

HFD has an impact on liver metabolism and mitochondrial function. Garnol et al., [166], showed that isolated hepatocytes from male albino Wistar rats have a reduced mitochondrial complex 1 activity following to 6 weeks HFD (71% energy fat) compared to a SD group (10% energy fat). Our findings demonstrated that HFD caused elevated ROS formation and DNA damage in mice. HFD further enhanced the impact of Pten haplodeficiency, which itself showed as well a slight induction in the SD group. High fat diet can stimulate hyperinsulinemia and enhance impaired glucose tolerance. Marshall et al., [167], published a diabetes study investigating the mutual dependency of high fat diet and T2DM in impaired glucose tolerance subjects and found that the fat composition of the diet is a determining factor in the development of T2DM. Vial et al. [168], investigated the effect of HFD on rat liver metabolism and ROS production. Following 8 weeks of HFD, they showed increased mitochondrial ROS production and decreased fatty acid oxidation in rat liver. Increased fat intake means increased energy intake. However, in the human body the response to increased fat consumption by elevated fat oxidation is limited and ends with fat accumulation in the body [169]. Since fatty acids are vulnerable to oxidation, they give rise to the formation of lipid radicals and lead to further damage in the organism. Especially the accumulation of fatty acids in mitochondria, which is one of the main sources of ROS in cells, increases the risk even more. Fatty acids can access the mitochondria by flip-flop mechanism through the mitochondrial membrane lipids. During this passive flip-flop mechanism, fatty acids are converted to fatty acid anions, which cannot cross the mitochondrial membrane again and undergo β-oxidation [169]. Especially the altered fatty acid oxidation and accumulation of fatty acids in mitochondria might lead to lipotoxicity and impaired metabolism [170, 171]. Regarding this point, high fat consumption, elevated caloric intake, and hepatic fat accumulation are links to mitochondrial activity and insulin signaling. Mitochondria might have an important role in the development of insulin resistance. Houstis et al. [172] used two different cellular insulin resistance models in vitro and showed that insulin resistance co-exists with oxidative stress and an antioxidant treatment could improve the insulin resistance.

In our model system, we demonstrated the impact of systemically disturbed haplodeficiency of Pten and the role of Akt2 in the elevation of oxidative stress and genomic damage in liver tissue.

In summary, our findings supported the idea that hyperactivation of Akt2 (as downstream mediator of PI3K signaling) caused increased oxidative stress and DNA damage. Although oxidative stress might not be the only factor for elevated DNA damage, it seems to be a main contributor. This suggests that antioxidants might be therapeutic candidates for reduction of cancer risk and other pathologies in obesity and related syndromes such as non-alcoholic fatty liver disease and T2DM.

6 CONCLUSION

Here, we show that obesity is linked to oxidative stress and genomic damage and weight loss either by caloric restriction or by gastric bypass surgery can help to reduce oxidative stress and genomic damage. Elevated insulin levels and hyperactivation of PI3K/Akt signaling is one of the major contributor in obesity and related disease (such as NAFLD and T2DM). Pten as a negative regulator of PI3K/Akt signaling has a key role. In obese subjects, weight loss might be a therapeutic option to improve insulin tolerance as well as to reduce oxidative stress and DNA damage. Additionally, antioxidant supplements might be an alternative to supply redox balance, reduce DNA damage and improve the insulin tolerance in metabolic syndrome.

7 SUMMARY

Several cohort studies showed that obesity increases the risk of chronic disease such as T2DM, hypertension and non-alcoholic fatty liver disease and various types of cancer. Different factors were described that might be involving in these diseases in obesity. Some of these suggested factors were chronic infection, elevated free fatty acids, increased ROS formation, mitochondrial dysfunction and raised NAPDH oxidase activity. Obesity is a multifactorial disease and it is very hard to distinguish between all of these factors. In this study, we wanted to focus on the association between obesity, oxidative stress and genomic damage in kidney, liver and colon, which are the most relevant organs for cancer risk according to the cohort studies. Our findings indicated elevated oxidative stress in kidney, liver and colon together with elevated lipid, RNA and DNA oxidation in the whole body. Additionally, we were able to show increased DNA damage in kidney, liver and colon.

Since obesity has become an epidemic all over the world, possible therapeutic applications such as life style changes (diet and sport), pharmacological supplements and various type of surgeries are increasing. As a second question, we focused on the effect of weight loss, which is supplied either by Roux-en-Y gastric bypass surgery or by caloric restriction designed in a way to provide the same extent of weight loss, on oxidative stress and genomic damage. Our results indicated that weight loss either by gastric bypass surgery or by caloric restriction led to reduced oxidative stress and genomic damage in kidney, liver and colon. We could not find any difference between the weight loss methods, except the DNA oxidation and repair marker urinary 8-oxodG, which was still elevated after RYGB, but not after caloric restriction.

It is known that hyperinsulinemia and in the long term T2DM are among the biggest concerns in obese individuals. Since we know the mutagenic potential of elevated insulin levels from previous data in our working group, the correlation between the highly mutagenic DNA DBSs marker, γ-H2AX and the plasma insulin level was tested and the findings indicated a positive correlation. In order to demonstrate the association between insulin-related oxidative stress and genomic damage, we used *in vitro* and *in vivo* models with Pten deficiency. In this part of study, the work was focused on liver.

Pten is a known negative regulator of the PI3K/Akt pathway, which is responsible for the elevated NADPH oxidase activity and mitochondrial dysfunction through elevated insulin levels. Pten inhibition or deficiency were used to sensitize the system to insulin. Non-transformed immortalized human hepatocytes were used to show the mutagenic potential of elevated insulin and these i*n vitro* data revealed once more the link between insulin signaling, elevated oxidative stress and genomic damage. Since the metabolic function of the liver is not only due to the extent of the hepatic insulin response but is also affected by systemic interactions, a whole-body Pten haplodeficient mouse model with an additional $Pten^{+/-}/Akt2^{-/-}$ group was utilized for *in vivo* investigation of insulin-mediated toxicity. Our findings in this model suggested that Pten deficiency alone can cause an increase in oxidative stress. HFD alone was sufficient to increase the expression of HO-1 and genomic damage significantly. Moreover, the combination (whole-body Pten haplodeficient mice fed with HFD) showed significantly elevated oxidative stress and genomic damage in mouse liver. However, Akt2 knockout could only reduce the oxidative stress and DNA damage in high fat diet fed mice significantly.

All these findings demonstrated that obesity can induce oxidative stress and genomic damage. Elevated insulin levels are associated with obesity-mediated oxidative stress and genomic damage. However, the underlying mechanisms are surely multifaceted and complicated. For example, Pten as oncogene might also induce other mechanisms besides the elevation of the PI3K/Akt pathway activity.

In conclusion, it is clear that oxidative stress and DNA damage are linked to obesity and that weight loss can reduce these two factors. Since DNA-damage is associated with an elevated cancer risk, it might be logical to use an antioxidant therapy in obese individuals to reduce the side effects and oxidative stress dependent mutagenicity and cancer risk in these individuals. However, much more research will be needed to support this idea experimentally.

8 ZUSAMMENFASSUNG

Mehrere Kohorten-studien zeigten, dass Adipositas das Risiko chronischer Erkrankungen wie Diabetes Mellitus Typ 2 (T2DM), Bluthochdruck, nicht-alkoholische Fettleber sowie das Risiko für unterschiedliche Krebsarten erhöht. Verschiedene Faktoren, die in Zusammenhang mit den Erkrankungen stehen, die Adipositas verursachen wurden bereits beschrieben. Einige dieser möglichen Faktoren sind chronische Infektionen, gesteigerte freie Fettsäuren, sowie reaktive Sauerstoffradikale, mitochondriale Dysfunktion und erhöhte Aktivität von NADPH-Oxidase. Adipositas ist eine multifaktorielle Erkrankung und unter von diesen Faktoren schwierig zu trennen. In dieser Studie wurde der Schwerpunkt auf den Zusammenhang von Adipositas, oxidativem Stress und Genomschäden in der Niere, Leber und dem Darm gelegt. Diese Organe sind gemäß der Kohortenstudien die anfälligsten hinsichtlich des Krebsrisikos. Unsere Befunde zeigten einen erhöhten oxidativen Stress in Niere, Leber und Darm, zusammen mit gesteigerter systemischer RNA-, DNA- und Fettoxidation, detektierbar anhand von Urinmarkern. Zusätzlich konnte eine Zunahme von DNA-Schäden in Niere, Leber und Darm aufgezeigt werden.

Da Adipositas weltweit eine Epidemie geworden ist, nehmen mögliche therapeutische Anwendungen sowie eine Änderung des Lebensstils (Diät und Sport), pharmazeutische Ergänzungsmittel und verschiedene Arten von chirurgischen Behandlungen zu. Hier wurde der Fokus auf die Wirkung des Gewichtsverlustes, der durch Roux-en-Y Magen-Bypass-Chirurgie oder durch Kalorienreduzierung mit der Vorgabe eines gleichen Ausmaßes an Gewichtsverlust vorgegeben war, auf die Intensität des oxidativen Stress und des Genomschadens gerichtet. Unsere Befunde zeigten, dass der Gewichtsverlust sowohl durch Magen-Bypass-Chirurgie als auch durch Kalorienreduzierung zu einem reduzierten oxidativem Stress und Genomschaden in der Niere, der Leber und im Darm führten. Es konnte kein Unterschied zwischen den Methoden zur Reduzierung des Gewichtes gefunden werden, außer bei der DNA-Oxidation und dem Reparaturmarker 8-oxodG im Urin, der nach der RYGB immer noch erhöht war, aber nicht nach der Kalorienreduzierung.

Es ist bekannt, dass Hyperinsulinämie bzw. Diabetes Mellitus Typ 2 eines der häufigsten Probleme bei übergewichtigen Patienten ist. Da wir das mutagene Potenzial von erhöhten

Insulinspiegeln aus vorherigen Daten unserer Arbeitsgruppe kannten, wurde der Zusammenhang zwischen dem hoch mutagenen DNA-DSBs-Marker γ-H2AX und dem Plasma-Insulinspiegel analysiert. Die Befunde wiesen eine positive Korrelation auf. Um die Beziehung zwischen Insulin-verursachtem oxidativem Stress und Genomschaden aufzuzeigen, wurden in-vitro und in-vivo-Modelle mit Pten-Mangel benutzt. In diesem Teil der Studie wurde das Augenmerk auf die Leber gelegt.

Das Protein Pten ist als negativer Regulator des PI3K/Akt Signalwegs bekannt, der unter anderem für die erhöhte Aktivität von NADPH Oxidase und mitochondrielle Dysfunktion durch erhöhten Insulinspiegel verantwortlich ist. Pten-Hemmung oder Pten-Mangel wurde genutzt, um unsere Versuchsmodelle für Insulin zu sensibilisieren. Nicht transformierbare immortalisierte menschliche Hepatozyten wurden verwendet, um das mutagene Potenzial von erhöhtem Insulin zu untersuchen, und die damit erzielten in -vitro-Daten wiesen wiederum auf die Beziehung zwischen Insulin-Signalwegen, oxidativem Stress und Genomschaden hin. Da die metabolische Funktion der Leber nicht nur dem Ausmaß der hepatischen Insulin-Reaktion geschuldet ist, sondern auch von systemischen Interaktionen beeinflusst wird, wurde ein Mausmodell für eine in-vivo-Untersuchung eingesetzt, das neben einem haploiden Pten-Mangel ($Pten^{+/-}$) in einer Tiergruppe mit einer zusätzlichen $Akt2^{-/-}$ Defizienz ($Pten^{+/-}/Akt2^{-/-}$). Defizienz ausgestattet war. Unsere Befunde in diesem Modell zeigten, der Pten-Mangel alleine bereits erhöhten oxidativen-Stress verursachen kann. HFD war ebenfalls alleine bereits ausreichend, um die Expression von HO-1 und Genomschäden signifikant zu steigern. Darüber hinaus zeigte die Kombination (Pten-Mangel gefüttert mit HFD) eine signifikante Erhöhung des oxidativen Stresses und der Genomschäden in der Mäuseleber. Allerdings konnte das Fehlen von Akt2 den oxidativen Stress und Genomschaden nur in den mit HFD gefütterte Tieren signifikant verringern.

Alle diese Befunde wiesen darauf hin, dass Adipositas oxidativen Stress und Genomschaden hervorrufen kann. Erhöhte Insulinspiegel sind mit Insulin-verursachtem oxidativem Stress und Genomschaden assoziiert. Allerdings sind die zugrunde liegenden Mechanismen sicherlich vielfältig und kompliziert. Zum Beispiel könnte Pten als Onkogen auch andere Mechanismen außer dem Anstieg der Aktivität des PI3K/Akt-Signalwegs- herbeiführen.

Zusammenfassend ist es klar, dass oxidativer Stress und DNA-Schäden mit Adipositas zusammenhängen, und dass Gewichtsreduzierung diese zwei Faktoren verringern kann. Da DNA-Schäden mit erhöhtem Krebsrisiko assoziiert sind, könnte es folglich eine logische Konsequenz sein, Antioxidantien therapeutisch bei adipösen Patienten anzuwenden, um die Nebenwirkungen und die auf oxidativem Stress beruhende Mutagenität und das Krebsrisiko dieser Patienten zu verringern. Allerdings wird weitere intensive Forschung nötig sein, um dies mit experimentellen Daten zu untermauern.

9 REFERENCES

[1] I. Savini, M.V. Catani, D. Evangelista, V. Gasperi, L. Avigliano, Obesity-associated oxidative stress: strategies finalized to improve redox state, Int J Mol Sci, 14 (2013) 10497-10538.

[2] O. Sirin, M.G. Kolonin, Treatment of obesity as a potential complementary approach to cancer therapy, Drug Discovery Today, 18 (2013) 567-573.

[3] P.T. James, Obesity: The worldwide epidemic, Clinics in Dermatology, 22 (2004) 276-280.

[4] W.H.O.e. consultation, Appropriate body-mass index for Asian populations and its implications for policy and intervention strategies, The Lancet, 363 (2004) 157-163.

[5] T. Kelly, W. Yang, C.S. Chen, K. Reynolds, J. He, Global burden of obesity in 2005 and projections to 2030, Int J Obes (Lond), 32 (2008) 1431-1437.

[6] Obesity and Overweight, Fact sheet N°311. World Health Organization; 2015 (http://www.who.int/mediacentre/factsheets/fs311/en/, accessed 17 March 2016).

[7] Prevalence of obesity, ages 18+, 2014 (age standardized estimate), Female. Geneva: World Health Organization; 2014 (http://gamapserver.who.int/mapLibrary/Files/Maps/Global_Obesity_2014_Female.png, accessed 17 March 2016).

[8] Prevalence of obesity, ages 18+, 2014 (age standardized estimate), Male. Geneva: World Health Organization; 2014 (http://gamapserver.who.int/mapLibrary/Files/Maps/Global_Obesity_2014_Male.png, accessed 17 March 2016).

[9] T. Lobstein, L. Baur, R. Uauy, Obesity in children and young people: a crisis in public health, Obesity reviews : an official journal of the International Association for the Study of Obesity, 5 Suppl 1 (2004) 4-104.

[10] J.J. Reilly, J. Kelly, Long-term impact of overweight and obesity in childhood and adolescence on morbidity and premature mortality in adulthood: systematic review, Int J Obes, 35 (2011) 891-898.

[11] S.E. Kahn, R.L. Hull, K.M. Utzschneider, Mechanisms linking obesity to insulin resistance and type 2 diabetes, Nature, 444 (2006) 840-846.

[12] A. Abdullah, A. Peeters, M. de Courten, J. Stoelwinder, The magnitude of association between overweight and obesity and the risk of diabetes: A meta-analysis of prospective cohort studies, Diabetes Research and Clinical Practice, 89 (2010) 309-319.

[13] Do You Know Some of the Health Risks of Being Overweight? National Institute of Diabetes and Digestive and Kidney Diseases; 2012 (http://www.niddk.nih.gov/health-

information/health-topics/weight-control/health_risks_being_overweight/Pages/health-risks-being-overweight.aspx, accessed 17 March 2016).

[14] C.K. Roberts, K.K. Sindhu, Oxidative stress and metabolic syndrome, Life sciences, 84 (2009) 705-712.

[15] C. Nathan, A. Cunningham-Bussel, Beyond oxidative stress: an immunologist's guide to reactive oxygen species, Nat Rev Immunol, 13 (2013) 349-361.

[16] M. Valko, D. Leibfritz, J. Moncol, M.T. Cronin, M. Mazur, J. Telser, Free radicals and antioxidants in normal physiological functions and human disease, Int J Biochem Cell Biol, 39 (2007) 44-84.

[17] A.I. Ruperez, A. Gil, C.M. Aguilera, Genetics of oxidative stress in obesity, Int J Mol Sci, 15 (2014) 3118-3144.

[18] Y. Taniyama, K.K. Griendling, Reactive oxygen species in the vasculature: molecular and cellular mechanisms, Hypertension, 42 (2003) 1075-1081.

[19] A. Fernandez-Sanchez, E. Madrigal-Santillan, M. Bautista, J. Esquivel-Soto, A. Morales-Gonzalez, C. Esquivel-Chirino, I. Durante-Montiel, G. Sanchez-Rivera, C. Valadez-Vega, J.A. Morales-Gonzalez, Inflammation, oxidative stress, and obesity, Int J Mol Sci, 12 (2011) 3117-3132.

[20] J. Lunec, K.A. Holloway, M.S. Cooke, S. Faux, H.R. Griffiths, M.D. Evans, Urinary 8-oxo-2’-deoxyguanosine: redox regulation of DNA repair in vivo?1, Free Radical Biology and Medicine, 33 (2002) 875-885.

[21] J.E. Klaunig, L.M. Kamendulis, B.A. Hocevar, Oxidative stress and oxidative damage in carcinogenesis, Toxicol Pathol, 38 (2010) 96-109.

[22] J. Kwon, S.-R. Lee, K.-S. Yang, Y. Ahn, Y.J. Kim, E.R. Stadtman, S.G. Rhee, Reversible oxidation and inactivation of the tumor suppressor PTEN in cells stimulated with peptide growth factors, Proceedings of the National Academy of Sciences of the United States of America, 101 (2004) 16419-16424.

[23] S.R. Lee, K.S. Yang, J. Kwon, C. Lee, W. Jeong, S.G. Rhee, Reversible inactivation of the tumor suppressor PTEN by H2O2, The Journal of biological chemistry, 277 (2002) 20336-20342.

[24] J.A. Petros, A.K. Baumann, E. Ruiz-Pesini, M.B. Amin, C.Q. Sun, J. Hall, S. Lim, M.M. Issa, W.D. Flanders, S.H. Hosseini, F.F. Marshall, D.C. Wallace, mtDNA mutations increase tumorigenicity in prostate cancer, Proceedings of the National Academy of Sciences of the United States of America, 102 (2005) 719-724.

[25] H.K. Vincent, K.R. Vincent, C. Bourguignon, R.W. Braith, Obesity and postexercise oxidative stress in older women, Medicine and science in sports and exercise, 37 (2005) 213-219.

[26] T.B. Kryston, A.B. Georgiev, P. Pissis, A.G. Georgakilas, Role of oxidative stress and DNA damage in human carcinogenesis, Mutat Res, 711 (2011) 193-201.

[27] M.S. Cooke, M.D. Evans, K.E. Herbert, J. Lunec, Urinary 8-oxo-2'-deoxyguanosine--source, significance and supplements, Free Radic Res, 32 (2000) 381-397.

[28] S. Jiranusornkul, C.A. Laughton, Destabilization of DNA duplexes by oxidative damage at guanine: implications for lesion recognition and repair, Journal of the Royal Society, Interface / the Royal Society, 5 Suppl 3 (2008) S191-198.

[29] H.A. Al-Aubaidy, H.F. Jelinek, Oxidative DNA damage and obesity in type 2 diabetes mellitus, European journal of endocrinology / European Federation of Endocrine Societies, 164 (2011) 899-904.

[30] K.M. Holmstrom, T. Finkel, Cellular mechanisms and physiological consequences of redox-dependent signalling, Nature reviews. Molecular cell biology, 15 (2014) 411-421.

[31] S.S. Sabharwal, P.T. Schumacker, Mitochondrial ROS in cancer: initiators, amplifiers or an Achilles' heel?, Nat Rev Cancer, 14 (2014) 709-721.

[32] I. Bratic, A. Trifunovic, Mitochondrial energy metabolism and ageing, Biochimica et biophysica acta, 1797 (2010) 961-967.

[33] F. Diaz, H. Kotarsky, V. Fellman, C.T. Moraes, Mitochondrial disorders caused by mutations in respiratory chain assembly factors, Seminars in fetal & neonatal medicine, 16 (2011) 197-204.

[34] J. Nunnari, A. Suomalainen, Mitochondria: In Sickness and in Health, Cell, 148 (2012) 1145-1159.

[35] P. Schrauwen, V. Schrauwen-Hinderling, J. Hoeks, M.K. Hesselink, Mitochondrial dysfunction and lipotoxicity, Biochimica et biophysica acta, 1801 (2010) 266-271.

[36] M. Alexeyev, I. Shokolenko, G. Wilson, S. LeDoux, The maintenance of mitochondrial DNA integrity--critical analysis and update, Cold Spring Harbor perspectives in biology, 5 (2013) a012641.

[37] E. Samper, D.G. Nicholls, S. Melov, Mitochondrial oxidative stress causes chromosomal instability of mouse embryonic fibroblasts, Aging cell, 2 (2003) 277-285.

[38] Michael P. Murphy, How mitochondria produce reactive oxygen species, Biochemical Journal, 417 (2009) 1-13.

[39] E. Cadenas, K.J.A. Davies, Mitochondrial free radical generation, oxidative stress, and aging1, Free Radical Biology and Medicine, 29 (2000) 222-230.

[40] A.M. James, Y. Collins, A. Logan, M.P. Murphy, Mitochondrial oxidative stress and the metabolic syndrome, Trends in endocrinology and metabolism: TEM, 23 (2012) 429-434.

[41] J.D. Lambeth, NOX enzymes and the biology of reactive oxygen, Nat Rev Immunol, 4 (2004) 181-189.

[42] J.M. Li, A.M. Shah, ROS generation by nonphagocytic NADPH oxidase: potential relevance in diabetic nephropathy, Journal of the American Society of Nephrology : JASN, 14 (2003) S221-226.

[43] K.H. Krause, Tissue distribution and putative physiological function of NOX family NADPH oxidases, Japanese journal of infectious diseases, 57 (2004) S28-29.

[44] C. Guichard, R. Moreau, D. Pessayre, T.K. Epperson, K.H. Krause, NOX family NADPH oxidases in liver and in pancreatic islets: a role in the metabolic syndrome and diabetes?, Biochem Soc Trans, 36 (2008) 920-929.

[45] L. Serrander, L. Cartier, K. Bedard, B. Banfi, B. Lardy, O. Plastre, A. Sienkiewicz, L. Fórró, W. Schlegel, K.-H. Krause, NOX4 activity is determined by mRNA levels and reveals a unique pattern of ROS generation, The Biochemical Journal, 406 (2007) 105-114.

[46] K. Bedard, K.-H. Krause, The NOX Family of ROS-Generating NADPH Oxidases: Physiology and Pathophysiology, 2007.

[47] B.J. Goldstein, M. Kalyankar, X. Wu, Redox Paradox: Insulin Action Is Facilitated by Insulin-Stimulated Reactive Oxygen Species With Multiple Potential Signaling Targets, Diabetes, 54 (2005) 311-321.

[48] K. Mahadev, H. Motoshima, X. Wu, J.M. Ruddy, R.S. Arnold, G. Cheng, J.D. Lambeth, B.J. Goldstein, The NAD(P)H oxidase homolog Nox4 modulates insulin-stimulated generation of H2O2 and plays an integral role in insulin signal transduction, Molecular and cellular biology, 24 (2004) 1844-1854.

[49] World Cancer Research Fund/American Institute for Cancer Research, Food, Nutrition, Physical Activity, and the Prevention of Cancer: A Global Perspective., AICR. Washington, DC, 2007.

[50] E.E. Calle, R. Kaaks, Overweight, obesity and cancer: epidemiological evidence and proposed mechanisms, Nat Rev Cancer, 4 (2004) 579-591.

[51] W. Zhang, X. Bai, H.e. Ge, H. Cui, Z. Wei, G. Han, Meta-analysis in the association between obesity and risk of thyroid cancer, International Journal of Clinical and Experimental Medicine, 7 (2014) 5268-5274.

[52] G. De Pergola, F. Silvestris, Obesity as a major risk factor for cancer, J Obes, 2013 (2013) 291546.

[53] S.K. Garg, H. Maurer, K. Reed, R. Selagamsetty, Diabetes and cancer: two diseases with obesity as a common risk factor, Diabetes, obesity & metabolism, 16 (2014) 97-110.

[54] J. Incio, D. McManus, P. Suboj, N. Rahbari, S.M. Chin, S. Babycutty, T. Vardan-Kaur, Y. Huang, K. Jung, D. Duda, R. Soares, D. Fukumura, R.K. Jain, Abstract LB-203: Obesity

promotes resistance to anti-VEGF therapy in breast cancer via pro-inflammatory and angiogenic pathways, Cancer research, 75 (2015) LB-203.

[55] I. Vucenik, J.P. Stains, Obesity and cancer risk: evidence, mechanisms, and recommendations, Annals of the New York Academy of Sciences, 1271 (2012) 37-43.

[56] S.M. Louie, L.S. Roberts, D.K. Nomura, Mechanisms linking obesity and cancer, Biochimica et Biophysica Acta (BBA) - Molecular and Cell Biology of Lipids, 1831 (2013) 1499-1508.

[57] C.A. Gilbert, J.M. Slingerland, Cytokines, obesity, and cancer: new insights on mechanisms linking obesity to cancer risk and progression, Annual review of medicine, 64 (2013) 45-57.

[58] J. Chen, Multiple signal pathways in obesity-associated cancer, Obesity reviews : an official journal of the International Association for the Study of Obesity, 12 (2011) 1063-1070.

[59] M. Cargnello, P.P. Roux, Activation and Function of the MAPKs and Their Substrates, the MAPK-Activated Protein Kinases, Microbiology and Molecular Biology Reviews : MMBR, 75 (2011) 50-83.

[60] K.S. Siveen, S. Sikka, R. Surana, X. Dai, J. Zhang, A.P. Kumar, B.K.H. Tan, G. Sethi, A. Bishayee, Targeting the STAT3 signaling pathway in cancer: Role of synthetic and natural inhibitors, Biochimica et Biophysica Acta (BBA) - Reviews on Cancer, 1845 (2014) 136-154.

[61] M. Pollak, Insulin and insulin-like growth factor signalling in neoplasia, Nat Rev Cancer, 8 (2008) 915-928.

[62] N. Mu, Y. Zhu, Y. Wang, H. Zhang, F. Xue, Insulin resistance: A significant risk factor of endometrial cancer, Gynecologic oncology, 125 (2012) 751-757.

[63] R. Zoncu, A. Efeyan, D.M. Sabatini, mTOR: from growth signal integration to cancer, diabetes and ageing, Nature reviews. Molecular cell biology, 12 (2011) 21-35.

[64] V.T. Samuel, G.I. Shulman, Mechanisms for insulin resistance: common threads and missing links, Cell, 148 (2012) 852-871.

[65] G. Wilcox, Insulin and Insulin Resistance, Clinical Biochemist Reviews, 26 (2005) 19-39.

[66] J.E. Pessin, A.R. Saltiel, Signaling pathways in insulin action: molecular targets of insulin resistance, J Clin Invest, 106 (2000) 165-169.

[67] H. Cho, J. Mu, J.K. Kim, J.L. Thorvaldsen, Q. Chu, E.B. Crenshaw, 3rd, K.H. Kaestner, M.S. Bartolomei, G.I. Shulman, M.J. Birnbaum, Insulin resistance and a diabetes mellitus-like syndrome in mice lacking the protein kinase Akt2 (PKB beta), Science, 292 (2001) 1728-1731.

[68] S.M. Schultze, B.A. Hemmings, M. Niessen, O. Tschopp, PI3K/AKT, MAPK and AMPK signalling: protein kinases in glucose homeostasis, Expert reviews in molecular medicine, 14 (2012) e1.

[69] L. Bozulic, B.A. Hemmings, PIKKing on PKB: regulation of PKB activity by phosphorylation, Current opinion in cell biology, 21 (2009) 256-261.

[70] K.D. Copps, M.F. White, Regulation of insulin sensitivity by serine/threonine phosphorylation of insulin receptor substrate proteins IRS1 and IRS2, Diabetologia, 55 (2012) 2565-2582.

[71] O.T. Hardy, M.P. Czech, S. Corvera, What causes the insulin resistance underlying obesity?, Current opinion in endocrinology, diabetes, and obesity, 19 (2012) 81-87.

[72] G.I. Shulman, Cellular mechanisms of insulin resistance, J Clin Invest, 106 (2000) 171-176.

[73] M.J. Khandekar, P. Cohen, B.M. Spiegelman, Molecular mechanisms of cancer development in obesity, Nat Rev Cancer, 11 (2011) 886-895.

[74] J.H.J. Hoeijmakers, DNA Damage, Aging, and Cancer, New England Journal of Medicine, 361 (2009) 1475-1485.

[75] J. Bartek, J. Bartkova, J. Lukas, DNA damage signalling guards against activated oncogenes and tumour progression, Oncogene, 26 (2007) 7773-7779.

[76] A.R.P. Carol Bernstein, Valentine Nfonsam and Harris Bernstein, DNA Damage, DNA Repair and Cancer, in: P.C. Chen (Ed.) DNA Damage, DNA Repair and Cancer, New Research Directions in DNA Repair

InTech2013.

[77] J.H.J. Hoeijmakers, Genome maintenance mechanisms for preventing cancer, Nature, 411 (2001) 366-374.

[78] C.J. Lord, A. Ashworth, The DNA damage response and cancer therapy, Nature, 481 (2012) 287-294.

[79] D. Trachootham, W. Lu, M.A. Ogasawara, N.R.-D. Valle, P. Huang, Redox Regulation of Cell Survival, Antioxidants & redox signaling, 10 (2008) 1343-1374.

[80] N. Hosoya, K. Miyagawa, Targeting DNA damage response in cancer therapy, Cancer Science, 105 (2014) 370-388.

[81] V.G. Gorgoulis, L.-V.F. Vassiliou, P. Karakaidos, P. Zacharatos, A. Kotsinas, T. Liloglou, M. Venere, R.A. DiTullio, N.G. Kastrinakis, B. Levy, D. Kletsas, A. Yoneta, M. Herlyn, C. Kittas, T.D. Halazonetis, Activation of the DNA damage checkpoint and genomic instability in human precancerous lesions, Nature, 434 (2005) 907-913.

[82] F. Tort, J. Bartkova, M. Sehested, T. Orntoft, J. Lukas, J. Bartek, Retinoblastoma pathway defects show differential ability to activate the constitutive DNA damage response in human tumorigenesis, Cancer research, 66 (2006) 10258-10263.

[83] J. Bartkova, Z. Horejsi, K. Koed, A. Kramer, F. Tort, K. Zieger, P. Guldberg, M. Sehested, J.M. Nesland, C. Lukas, T. Orntoft, J. Lukas, J. Bartek, DNA damage response as a candidate anti-cancer barrier in early human tumorigenesis, Nature, 434 (2005) 864-870.

[84] R. Di Micco, M. Fumagalli, A. Cicalese, S. Piccinin, P. Gasparini, C. Luise, C. Schurra, M. Garre, P. Giovanni Nuciforo, A. Bensimon, R. Maestro, P. Giuseppe Pelicci, F. d/'Adda di Fagagna, Oncogene-induced senescence is a DNA damage response triggered by DNA hyper-replication, Nature, 444 (2006) 638-642.

[85] R. Pallavi, M. Giorgio, P.G. Pelicci, Insights into the beneficial effect of caloric/ dietary restriction for a healthy and prolonged life, Frontiers in physiology, 3 (2012) 318.

[86] S.R. Spindler, Rapid and reversible induction of the longevity, anticancer and genomic effects of caloric restriction, Mechanisms of Ageing and Development, 126 (2005) 960-966.

[87] X. Qiu, K. Brown, M.D. Hirschey, E. Verdin, D. Chen, Calorie restriction reduces oxidative stress by SIRT3-mediated SOD2 activation, Cell Metab, 12 (2010) 662-667.

[88] Y. Li, M. Daniel, T.O. Tollefsbol, Epigenetic regulation of caloric restriction in aging, BMC Medicine, 9 (2011) 98-98.

[89] B.J. Willcox, D.C. Willcox, H. Todoriki, A. Fujiyoshi, K. Yano, Q. He, J.D. Curb, M. Suzuki, Caloric restriction, the traditional Okinawan diet, and healthy aging: the diet of the world's longest-lived people and its potential impact on morbidity and life span, Ann N Y Acad Sci, 1114 (2007) 434-455.

[90] P.E. O'Brien, Bariatric surgery: Mechanisms, indications and outcomes, Journal of Gastroenterology and Hepatology, 25 (2010) 1358-1365.

[91] V.L. Gloy, M. Briel, D.L. Bhatt, S.R. Kashyap, P.R. Schauer, G. Mingrone, H.C. Bucher, A.J. Nordmann, Bariatric surgery versus non-surgical treatment for obesity: a systematic review and meta-analysis of randomised controlled trials, 2013.

[92] J.O. Hill, Can a small-changes approach help address the obesity epidemic? A report of the Joint Task Force of the American Society for Nutrition, Institute of Food Technologists, and International Food Information Council, Am J Clin Nutr, 89 (2009) 477-484.

[93] The National Institute of Health, Bariatric Surgery for Severe Obesity, in: U.S.D.o.H.a.H. Services (Ed.)2011.

[94] H. Buchwald, Y. Avidor, E. Braunwald, et al., Bariatric surgery: A systematic review and meta-analysis, Jama, 292 (2004) 1724-1737.

[95] D.S. Casagrande, D.D. Rosa, D. Umpierre, R.A. Sarmento, C.G. Rodrigues, B.D. Schaan, Incidence of cancer following bariatric surgery: systematic review and meta-analysis, OBES SURG, 24 (2014) 1499-1509.

[96] J.L. Colquitt, J. Picot, E. Loveman, A.J. Clegg, Surgery for obesity, The Cochrane database of systematic reviews, (2009) Cd003641.

[97] F. Seyfried, J.V. Li, A.D. Miras, N.L. Cluny, M. Lannoo, W.K. Fenske, K.A. Sharkey, J.K. Nicholson, C.W. le Roux, E. Holmes, Urinary Phenotyping Indicates Weight Loss-Independent Metabolic Effects of Roux-en-Y Gastric Bypass in Mice, Journal of proteome research, 12 (2013) 1245-1253.

[98] J.V. Li, H. Ashrafian, M. Bueter, J. Kinross, C. Sands, C.W. le Roux, S.R. Bloom, A. Darzi, T. Athanasiou, J.R. Marchesi, J.K. Nicholson, E. Holmes, Metabolic surgery profoundly influences gut microbial-host metabolic cross-talk, Gut, 60 (2011) 1214-1223.

[99] R.E. Brolin, BAriatric surgery and long-term control of morbid obesity, Jama, 288 (2002) 2793-2796.

[100] D.E. Cummings, J. Overduin, K.E. Foster-Schubert, Gastric bypass for obesity: mechanisms of weight loss and diabetes resolution, The Journal of clinical endocrinology and metabolism, 89 (2004) 2608-2615.

[101] E.J. DeMaria, Bariatric Surgery for Morbid Obesity, New England Journal of Medicine, 356 (2007) 2176-2183.

[102] J.A. Tadross, C.W. le Roux, The mechanisms of weight loss after bariatric surgery, Int J Obes (Lond), 33 Suppl 1 (2009) S28-32.

[103] K.K. Ryan, V. Tremaroli, C. Clemmensen, P. Kovatcheva-Datchary, A. Myronovych, R. Karns, H.E. Wilson-Perez, D.A. Sandoval, R. Kohli, F. Backhed, R.J. Seeley, FXR is a molecular target for the effects of vertical sleeve gastrectomy, Nature, 509 (2014) 183-188.

[104] G. Mingrone, S. Panunzi, A. De Gaetano, C. Guidone, A. Iaconelli, L. Leccesi, G. Nanni, A. Pomp, M. Castagneto, G. Ghirlanda, F. Rubino, Bariatric Surgery versus Conventional Medical Therapy for Type 2 Diabetes, New England Journal of Medicine, 366 (2012) 1577-1585.

[105] N. Stylopoulos, A.G. Hoppin, L.M. Kaplan, Roux-en-Y gastric bypass enhances energy expenditure and extends lifespan in diet-induced obese rats, Obesity, 17 (2009) 1839-1847.

[106] P.S. Griffith, D.W. Birch, A.M. Sharma, S. Karmali, Managing complications associated with laparoscopic Roux-en-Y gastric bypass for morbid obesity, Canadian Journal of Surgery, 55 (2012) 329-336.

[107] Q. Wu, J.V. Li, F. Seyfried, C.W. le Roux, H. Ashrafian, T. Athanasiou, W. Fenske, A. Darzi, J.K. Nicholson, E. Holmes, N.J. Gooderham, Metabolic phenotype-microRNA data fusion analysis of the systemic consequences of Roux-en-Y gastric bypass surgery, Int J Obes (Lond), (2015).

[108] M. Bueter, K. Abegg, F. Seyfried, T.A. Lutz, C.W. le Roux, Roux-en-Y gastric bypass operation in rats, Journal of visualized experiments : JoVE, (2012) e3940.

[109] A.R. Collins, The comet assay for DNA damage and repair: principles, applications, and limitations, Molecular biotechnology, 26 (2004) 249-261.

[110] D.J. Smart, H.D. Halicka, G. Schmuck, F. Traganos, Z. Darzynkiewicz, G.M. Williams, Assessment of DNA double-strand breaks and gammaH2AX induced by the topoisomerase II poisons etoposide and mitoxantrone, Mutat Res, 641 (2008) 43-47.

[111] L.J. Kuo, L.X. Yang, Gamma-H2AX - a novel biomarker for DNA double-strand breaks, In vivo (Athens, Greece), 22 (2008) 305-309.

[112] E. Niki, Do antioxidants impair signaling by reactive oxygen species and lipid oxidation products?, FEBS letters, 586 (2012) 3767-3770.

[113] H. Ohkawa, N. Ohishi, K. Yagi, Assay for lipid peroxides in animal tissues by thiobarbituric acid reaction, Analytical biochemistry, 95 (1979) 351-358.

[114] H.H. Draper, E.J. Squires, H. Mahmoodi, J. Wu, S. Agarwal, M. Hadley, A comparative evaluation of thiobarbituric acid methods for the determination of malondialdehyde in biological materials, Free Radical Biology and Medicine, 15 (1993) 353-363.

[115] M. Dizdaroglu, Oxidatively induced DNA damage: mechanisms, repair and disease, Cancer letters, 327 (2012) 26-47.

[116] A. Weimann, D. Belling, H.E. Poulsen, Quantification of 8-oxo-guanine and guanine as the nucleobase, nucleoside and deoxynucleoside forms in human urine by high-performance liquid chromatography-electrospray tandem mass spectrometry, Nucleic acids research, 30 (2002) E7.

[117] H.E. Poulsen, E. Specht, K. Broedbaek, T. Henriksen, C. Ellervik, T. Mandrup-Poulsen, M. Tonnesen, P.E. Nielsen, H.U. Andersen, A. Weimann, RNA modifications by oxidation: A novel disease mechanism?, Free Radical Biology and Medicine, 52 (2012) 1353-1361.

[118] A.D. Cristofano, B. Pesce, C. Cordon-Cardo, P.P. Pandolfi, Pten is essential for embryonic development and tumour suppression, Nat Genet, 19 (1998) 348-355.

[119] B. Dummler, O. Tschopp, D. Hynx, Z.-Z. Yang, S. Dirnhofer, B.A. Hemmings, Life with a Single Isoform of Akt: Mice Lacking Akt2 and Akt3 Are Viable but Display Impaired Glucose Homeostasis and Growth Deficiencies, Molecular and Cellular Biology, 26 (2006) 8042-8051.

[120] B. Rotman, B.W. Papermaster, Membrane properties of living mammalian cells as studied by enzymatic hydrolysis of fluorogenic esters, Proceedings of the National Academy of Sciences of the United States of America, 55 (1966) 134-141.

[121] M. Fenech, The in vitro micronucleus technique, Mutation Research/Fundamental and Molecular Mechanisms of Mutagenesis, 455 (2000) 81-95.

[122] E.E. Calle, C. Rodriguez, K. Walker-Thurmond, M.J. Thun, Overweight, obesity, and mortality from cancer in a prospectively studied cohort of U.S. adults, N Engl J Med, 348 (2003) 1625-1638.

[123] J. Peto, Cancer epidemiology in the last century and the next decade, Nature, 411 (2001) 390-395.

[124] P.G. Kopelman, Obesity as a medical problem, Nature, 404 (2000) 635-643.

[125] J. Logue, J.J. Walker, G. Leese, R. Lindsay, J. McKnight, A. Morris, S. Philip, S. Wild, N. Sattar, Association between BMI measured within a year after diagnosis of type 2 diabetes and mortality, Diabetes care, 36 (2013) 887-893.

[126] W. Jialin, Z. Yi, Y. Weijie, Relationship between body mass index and mortality in hemodialysis patients: a meta-analysis, Nephron Clin Pract, 121 (2012) c102-111.

[127] S. Furukawa, T. Fujita, M. Shimabukuro, M. Iwaki, Y. Yamada, Y. Nakajima, O. Nakayama, M. Makishima, M. Matsuda, I. Shimomura, Increased oxidative stress in obesity and its impact on metabolic syndrome, J Clin Invest, 114 (2004) 1752-1761.

[128] J.L. Evans, B.A. Maddux, I.D. Goldfine, The molecular basis for oxidative stress-induced insulin resistance, Antioxidants & redox signaling, 7 (2005) 1040-1052.

[129] E.M. Othman, A. Leyh, H. Stopper, Insulin mediated DNA damage in mammalian colon cells and human lymphocytes in vitro, Mutation Research/Fundamental and Molecular Mechanisms of Mutagenesis, 745–746 (2013) 34-39.

[130] K. Broedbaek, V. Siersma, T. Henriksen, A. Weimann, M. Petersen, J.T. Andersen, E. Jimenez-Solem, L.J. Hansen, J.E. Henriksen, S.J. Bonnema, N. de Fine Olivarius, H.E. Poulsen, Association between urinary markers of nucleic acid oxidation and mortality in type 2 diabetes: a population-based cohort study, Diabetes care, 36 (2013) 669-676.

[131] H.E. Poulsen, L.L. Nadal, K. Broedbaek, P.E. Nielsen, A. Weimann, Detection and interpretation of 8-oxodG and 8-oxoGua in urine, plasma and cerebrospinal fluid, Biochimica et Biophysica Acta (BBA) - General Subjects, 1840 (2014) 801-808.

[132] A. Klungland, I. Rosewell, S. Hollenbach, E. Larsen, G. Daly, B. Epe, E. Seeberg, T. Lindahl, D.E. Barnes, Accumulation of premutagenic DNA lesions in mice defective in removal of oxidative base damage, Proceedings of the National Academy of Sciences of the United States of America, 96 (1999) 13300-13305.

[133] R. Rozalski, D. Gackowski, K. Roszkowski, M. Foksinski, R. Olinski, The level of 8-hydroxyguanine, a possible repair product of oxidative DNA damage, is higher in urine of cancer patients than in control subjects, Cancer Epidemiol Biomarkers Prev, 11 (2002) 1072-1075.

[134] K. Roszkowski, W. Jozwicki, P. Blaszczyk, A. Mucha-Malecka, A. Siomek, Oxidative damage DNA: 8-oxoGua and 8-oxodG as molecular markers of cancer, Medical Science

Monitor : International Medical Journal of Experimental and Clinical Research, 17 (2011) CR329-CR333.

[135] R. Hakem, DNA-damage repair; the good, the bad, and the ugly, The EMBO Journal, 27 (2008) 589-605.

[136] J.R. Chapman, Martin R.G. Taylor, Simon J. Boulton, Playing the End Game: DNA Double-Strand Break Repair Pathway Choice, Molecular Cell, 47 (2012) 497-510.

[137] P. Pfeiffer, W. Goedecke, G. Obe, Mechanisms of DNA double-strand break repair and their potential to induce chromosomal aberrations, Mutagenesis, 15 (2000) 289-302.

[138] E.M. Othman, M.C. Kreissl, F.R. Kaiser, P.A. Arias-Loza, H. Stopper, Insulin-mediated oxidative stress and DNA damage in LLC-PK1 pig kidney cell line, female rat primary kidney cells, and male ZDF rat kidneys in vivo, Endocrinology, 154 (2013) 1434-1443.

[139] N. Queisser, K. Happ, S. Link, D. Jahn, A. Zimnol, A. Geier, N. Schupp, Aldosterone induces fibrosis, oxidative stress and DNA damage in livers of male rats independent of blood pressure changes, Toxicol Appl Pharmacol, 280 (2014) 399-407.

[140] S. Brand, K. Amann, P. Mandel, A. Zimnol, N. Schupp, Oxidative DNA damage in kidneys and heart of hypertensive mice is prevented by blocking angiotensin II and aldosterone receptors, PloS one, 9 (2014) e115715.

[141] S. Brand, K. Amann, N. Schupp, Angiotensin II-induced hypertension dose-dependently leads to oxidative stress and DNA damage in mouse kidneys and hearts, J Hypertens, 31 (2013) 333-344.

[142] G. Fazeli, H. Stopper, R. Schinzel, C.W. Ni, H. Jo, N. Schupp, Angiotensin II induces DNA damage via AT1 receptor and NADPH oxidase isoform Nox4, Mutagenesis, 27 (2012) 673-681.

[143] N. Queisser, N. Schupp, H. Stopper, R. Schinzel, P.I. Oteiza, Aldosterone increases kidney tubule cell oxidants through calcium-mediated activation of NADPH oxidase and nitric oxide synthase, Free Radical Biology and Medicine, 51 (2011) 1996-2006.

[144] G. Shi, Y. Fu, W. Jiang, A. Yin, M. Feng, Y. Wu, Y. Kawai, I. Miyamori, C. Fan, Activation of Src-ATF1 pathway is involved in upregulation of Nox1, a catalytic subunit of NADPH oxidase, by aldosterone, Endocr J, 58 (2011) 491-499.

[145] V.N. Kotiadis, M.R. Duchen, L.D. Osellame, Mitochondrial quality control and communications with the nucleus are important in maintaining mitochondrial function and cell health, Biochimica et Biophysica Acta (BBA) - General Subjects, 1840 (2014) 1254-1265.

[146] M.D. Brand, C. Affourtit, T.C. Esteves, K. Green, A.J. Lambert, S. Miwa, J.L. Pakay, N. Parker, Mitochondrial superoxide: production, biological effects, and activation of uncoupling proteins, Free Radical Biology and Medicine, 37 (2004) 755-767.

[147] J.C. Bournat, C.W. Brown, Mitochondrial dysfunction in obesity, Curr Opin Endocrinol Diabetes Obes, 17 (2010) 446-452.

[148] S.C. Larsson, A. Wolk, Obesity and colon and rectal cancer risk: a meta-analysis of prospective studies, Am J Clin Nutr, 86 (2007) 556-565.

[149] L. Li, K. Kalantar-Zadeh, Obesity that makes kidney cancer more likely but helps fight it more strongly, J Natl Cancer Inst, 105 (2013) 1848-1849.

[150] A. Maestro, M. Rigla, A. Caixàs, Does bariatric surgery reduce cancer risk? A review of the literature, Endocrinología y Nutrición (English Edition), 62 (2015) 138-143.

[151] D.A. Raptis, T. Bachler, A. Nocito, M. Bueter, Obesity Surgery and the Risk of Colorectal Carcinoma-Searching for the Fly in the Ointment?, Ann Surg, (2013).

[152] M. Derogar, M.A. Hull, P. Kant, M. Ostlund, Y. Lu, J. Lagergren, Increased risk of colorectal cancer after obesity surgery, Ann Surg, 258 (2013) 983-988.

[153] E.M. Othman, H. Hintzsche, H. Stopper, Signaling steps in the induction of genomic damage by insulin in colon and kidney cells, Free Radic Biol Med, 68 (2014) 247-257.

[154] M. Keniry, R. Parsons, The role of PTEN signaling perturbations in cancer and in targeted therapy, Oncogene, 27 (2008) 5477-5485.

[155] L.H. Mak, R. Vilar, R. Woscholski, Characterisation of the PTEN inhibitor VO-OHpic, Journal of Chemical Biology, 3 (2010) 157-163.

[156] M.C. Hollander, G.M. Blumenthal, P.A. Dennis, PTEN loss in the continuum of common cancers, rare syndromes and mouse models, Nat Rev Cancer, 11 (2011) 289-301.

[157] C. Koliaki, J. Szendroedi, K. Kaul, T. Jelenik, P. Nowotny, F. Jankowiak, C. Herder, M. Carstensen, M. Krausch, Wolfram T. Knoefel, M. Schlensak, M. Roden, Adaptation of Hepatic Mitochondrial Function in Humans with Non-Alcoholic Fatty Liver Is Lost in Steatohepatitis, Cell Metabolism, 21 (2015) 739-746.

[158] L. He, X. Hou, G. Kanel, N. Zeng, V. Galicia, Y. Wang, J. Yang, H. Wu, M.J. Birnbaum, B.L. Stiles, The Critical Role of AKT2 in Hepatic Steatosis Induced by PTEN Loss, The American Journal of Pathology, 176 (2010) 2302-2308.

[159] M. Lu, M. Wan, K.F. Leavens, Q. Chu, B.R. Monks, S. Fernandez, R.S. Ahima, K. Ueki, C.R. Kahn, M.J. Birnbaum, Insulin regulates liver metabolism in vivo in the absence of hepatic Akt and Foxo1, Nature medicine, 18 (2012) 388-395.

[160] L. Wang, U. Schumann, Y. Liu, O. Prokopchuk, J.M. Steinacker, Heat shock protein 70 (Hsp70) inhibits oxidative phosphorylation and compensates ATP balance through enhanced glycolytic activity, Journal of applied physiology (Bethesda, Md. : 1985), 113 (2012) 1669-1676.

[161] Y. Li, J. Su, X. DingZhang, J. Zhang, M. Yoshimoto, S. Liu, K. Bijian, A. Gupta, J.A. Squire, M.A. Alaoui Jamali, T.A. Bismar, PTEN deletion and heme oxygenase-1 overexpression cooperate in prostate cancer progression and are associated with adverse clinical outcome, The Journal of pathology, 224 (2011) 90-100.

[162] R. Motterlini, R. Foresti, R. Bassi, V. Calabrese, J.E. Clark, C.J. Green, Endothelial heme oxygenase-1 induction by hypoxia. Modulation by inducible nitric-oxide synthase and S-nitrosothiols, The Journal of biological chemistry, 275 (2000) 13613-13620.

[163] K.R. Brunt, K.K. Fenrich, G. Kiani, M.Y. Tse, S.C. Pang, C.A. Ward, L.G. Melo, Protection of human vascular smooth muscle cells from H2O2-induced apoptosis through functional codependence between HO-1 and AKT, Arteriosclerosis, thrombosis, and vascular biology, 26 (2006) 2027-2034.

[164] M.A. Alaoui-Jamali, T.A. Bismar, A. Gupta, W.A. Szarek, J. Su, W. Song, Y. Xu, B. Xu, G. Liu, J.Z. Vlahakis, G. Roman, J. Jiao, H.M. Schipper, A Novel Experimental Heme Oxygenase-1–Targeted Therapy for Hormone-Refractory Prostate Cancer, Cancer research, 69 (2009) 8017-8024.

[165] S.M. Schultze, J. Jensen, B.A. Hemmings, O. Tschopp, M. Niessen, Promiscuous affairs of PKB/AKT isoforms in metabolism, Archives of physiology and biochemistry, 117 (2011) 70-77.

[166] T. Garnol, R. Endlicher, O. Kucera, Z. Drahota, Z. Cervinkova, Impairment of mitochondrial function of rat hepatocytes by high fat diet and oxidative stress, Physiological research / Academia Scientiarum Bohemoslovaca, 63 (2014) 271-274.

[167] J.A. Marshall, S. Hoag, S. Shetterly, R.F. Hamman, Dietary fat predicts conversion from impaired glucose tolerance to NIDDM. The San Luis Valley Diabetes Study, Diabetes care, 17 (1994) 50-56.

[168] G. Vial, H. Dubouchaud, K. Couturier, C. Cottet-Rousselle, N. Taleux, A. Athias, A. Galinier, L. Casteilla, X.M. Leverve, Effects of a high-fat diet on energy metabolism and ROS production in rat liver, Journal of hepatology, 54 (2011) 348-356.

[169] P. Schrauwen, High-fat diet, muscular lipotoxicity and insulin resistance, The Proceedings of the Nutrition Society, 66 (2007) 33-41.

[170] J. Szendroedi, E. Phielix, M. Roden, The role of mitochondria in insulin resistance and type 2 diabetes mellitus, Nat Rev Endocrinol, 8 (2012) 92-103.

[171] B.H. Goodpaster, Mitochondrial deficiency is associated with insulin resistance, Diabetes, 62 (2013) 1032-1035.

[172] N. Houstis, E.D. Rosen, E.S. Lander, Reactive oxygen species have a causal role in multiple forms of insulin resistance, Nature, 440 (2006) 944-948.

10 ACKNOWLEDGEMENTS

Special thanks to Prof. Dr. Helga Stopper for giving me the opportunity to work on my PhD project and also for her valuable support.

I would like to thank Prof. Dr. Tscholpon Djuzenova, Prof. Dr. Ute Hentschel-Humeida and Prof. Dr. Jörg Vienken due to their supervision, helpful advice and interesting discussions during my PhD.

Many thanks to Dr. Florian Seyfried for excellent collaboration in obese rodent model and to Prof. Dr. Andreas Geier for supplying the immortilized human hepatocyte cell line and the liver tissue from whole-body Pten haplodeficient mouse model.

I am very thankful to Janina Dix for her excellent technical assistance and great teamwork and to Gaby Wolz for her technical support and encouraging me to speak German. I also thank all of the students and interns (Theresa Arnaudov, Philipp Burkard, Meike Hack, and Nanet Cirkel), who helped me to perform some experiments, for all their contribution to my work.

I am grateful to all my colleagues, who made me feel at home and supported me to learn German.

My special thanks to Dr. Robert Blum for his guidance and support.

Thanks to the Graduate School of Life Sciences, University of Würzburg for giving me the opportunity to develop myself further through their special programs and workshops, as well as supplying financial support to attend several conferences.

I wish to thank to Barbara & Gregor Kuttenkeuller, who became a family to me and supported me whenever I needed.

Special thanks to my dear friends Esin Candemir, Katharina Taichrib and Nina Glaser for support, encouragement and for the great times that we spent together.

Last but not least, I thank all of my family for their emotional support, patience and encouragement throughout my PhD.

12 AFFIDAVIT

I hereby confirmed that my thesis entitled “Oxidative status and genomic damage in an obesity model” is the result of my own work. I did not receive any help or support from commercial consultants. All sources and / or materials applied are listed and specified in the thesis.

Furthermore, I confirm that this thesis has not yet been submitted as part of another examination process neither in identical nor in similar form.

Würzburg, 2016

Ezgi Eylül Bankoglu